Nitric Oxide and miRNAs - Modulators of glaucoma relevant genes in the outflow tissues

Dissertation

Zur Erlangung des Doktorgrades der Naturwissenschaften
Dr. rer. nat.
der Fakultät für Biologie und Vorklinische Medizin
der Universität Regensburg.

Durchgeführt am
Lehrstuhl für Humananatomie und Embryologie
der Universität Regensburg.

Vorgelegt von
Franziska Frömel, geborene Scherl,
aus Schwandorf
im Jahr 2020.

Das Promotionsgesuch wurde eingereicht am:

09.10.2020

Die Arbeit wurde angeleitet von:

Prof. Dr. Rudolf Fuchshofer

Unterschrift:

Meinem Mann.

Table of content

1 Abstract

Glaucoma is one of the leading causes of blindness in the western world (Quigley 1996; Resnikoff et al. 2004). Its pathogenesis is characterized by a chronic degenerative neuropathy leading to the loss of axons of the retinal ganglion cells (Allingham et al. 2009; Kwon et al. 2009) and Primary Open Angle Glaucoma (POAG) is its most prevalent form. Patients suffer from visual field loss, ending in total blindness if not appropriately treated.

Intraocular pressure (IOP) has been found to be a main risk factor for POAG (Gordon et al. 2002; Higginbotham et al. 2004). During the pathogenesis of POAG, the outflow of aqueous humor (AH) is reduced due to an increased outflow resistance in the JCT of the TM (Grant 1963; Johnson 2006). Even if molecular mechanisms causing this increase are still unclear, changes in amount and quality of extracellular matrix (ECM) are likely to be involved (Lütjen-Drecoll et al. 1986; Rohen et al. 1993). Connective Tissue Growth Factor (CTGF) has been found to be elevated in the AH (Browne et al. 2011; Fahmy et al. 2008) as well as in SC cells of POAG patients (Overby et al. 2014), and potent to induce ECM expression in TM cells (Junglas et al. 2009). A CTGF overexpressing mouse model, developing elevated IOP and axon loss over time, underlined the role of CTGF in the pathogenesis of POAG (Junglas et al. 2012). Next to changes in the composition of the ECM in the JCT, endothelial cells of Schlemm's Canal (SC) inner wall seem to have the potential to modulate outflow resistance (Stamer et al. 2015). A negative correlation of pore forming ability and SC cell stiffness was found (Overby et al. 2014). If that pore forming ability becomes disrupted in POAG, it would lead to impaired AH outflow and IOP elevation.

When IOP increases, it results in increased fluid shear stress for the affected cells of the outflow pathway (Ethier et al. 2004; Stamer et al. 2011). Under healthy conditions, increasing IOP leads to increasing NO signaling and - by its cell relaxing effect - to an increased outflow facility (Buys et al. 2014). Under glaucomatous conditions, SC cells stiffen (Overby et al. 2014; Vahabikashi et al. 2019) and a dysregulation of NO release is suggested to result in ocular hypertension (Emam et al. 2014). Reducing cell stiffness trough cell relaxation is therefore an optional aim to treat POAG. Therefore, DETA-NO was chosen as exogenous NO donor in this study to investigate its effect on outflow cells *in vitro*.

Micro ribonucleic acids (miRNAs) have emerged as key regulators of gene expression by post-transcriptionally binding target messenger RNA (mRNA) according to their nucleotide sequences (Wienholds and Plasterk 2005; Krol et al. 2010; Huntzinger and Izaurralde 2011). Alterations in miRNAs have been implicated in many different diseases (Esteller 2011; Gutschner and Diederichs 2012) and it just started to investigate its role in the pathogenesis of POAG. In the present study, the premise was that aberrant biomechanical behavior of outflow cells might be due to altered expression of miRNAs that are associated to the NO regulatory system.

The present study investigated a glaucoma mouse model overexpressing CTGF. It was found that macroglia activation and IOP increase are specific for the transgenic βB1-CTGF mice, independent on their genetic background. A potential antagonist of the CTGF effects was investigated by treating SC cells with exogenous NO. There, DETA-NO treatment not only reduced the expression of CTGF and ECM components but also caused a significant reduction of cell stiffness. Furthermore, *in vitro* flow conditions induced NO production.

By a miRNA-microarray, 39 miRNAs associated to the NO signaling pathway were found to be differentially expressed in healthy and glaucomatous SC cell strains. By correlation analysis, four of them were found to have a positive correlation of miRNA abundance and cell stiffness. For miR-222-3p and miR-455-3p, the increase was confirmed and miRNA alteration by transfection experiments led to significant impact on CTGF expression. To further investigate a potential delivery system for miRNAs towards outflow tissue, the distribution of gold-core nanoparticles (AuNPs) within the anterior chamber was assessed after *ex vivo* perfusion of porcine eyes and gold content of ciliary body, cornea, iris, lens, and the TM was analyzed. ICP-MS analysis exhibited that independent on AuNP size and surface, most gold was targeted to the TM. Therefore, NPs can be used as delivery system to specifically target therapeutic agents to outflow tissue.

By revealing the effect of alterations in NO signaling and miRNA abundance on glaucoma-associated factors, the molecular mechanisms underlying glaucoma could be better understood.

2 Introduction

2.1 Primary Open Angle Glaucoma

Glaucoma is the second leading cause of blindness worldwide (Quigley 1996; Resnikoff et al. 2004; Quigley 2011) with a number of affected people increasing from 76.0 million in 2020 to 111.8 million in 2040 (Tham et al. 2014). Primary Open Angle Glaucoma (POAG) is its most prevalent form and is characterized by a chronic degenerative neuropathy leading to the loss of axons of retinal ganglion cells (RGCs) (Allingham et al. 2009; Kwon et al. 2009). This degeneration becomes visible at the papilla, the area where the optic nerve axons leave the eye (**Figure 1**). As a result, patients suffer from visual field loss, ending in total blindness if not treated appropriately.

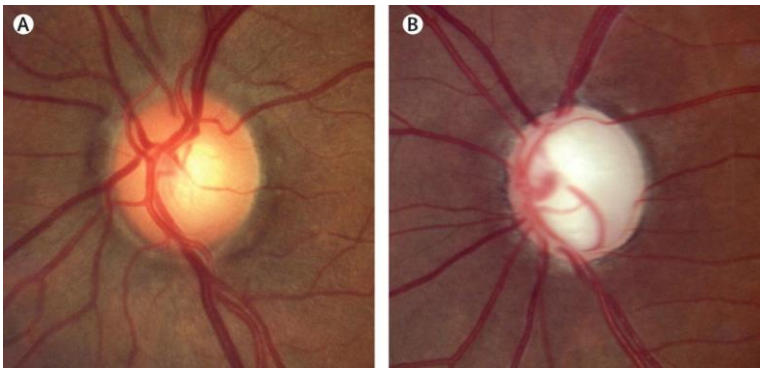

Figure 1: Ophthalmoscopic images of A) a normal and B) a glaucomatous papilla (Quigley 2011).

Beside age, sex, race and a positive family anamnesis, many prospective randomized clinical multi-centre studies have revealed that intraocular pressure (IOP) is a main risk factor for POAG (Collaborative Normal-Tension Glaucoma Study Group 1998a, 1998b; Gordon et al. 2002; Higginbotham et al. 2004). Therefore, IOP reduction is a major goal in POAG therapy.

2.2 Aqueous humor and outflow tissue

Aqueous humor (AH) is a transparent fluid filling the anterior chamber of the eye. It works as structural stabilator as well as supplier for the bradytroph tissues. AH is produced by the epithelium of the ciliary body and gets drained mainly via the conventional outflow pathway built up by the trabecular meshwork (TM) and Schlemm's Canal (SC) and from there into episcleral veins (**Figure 2**). By a homeostasis of production, circulation, and drainage of AH, IOP is generated. While

AH production is unaffected, pathological changes of POAG occur within the conventional AH outflow pathway.

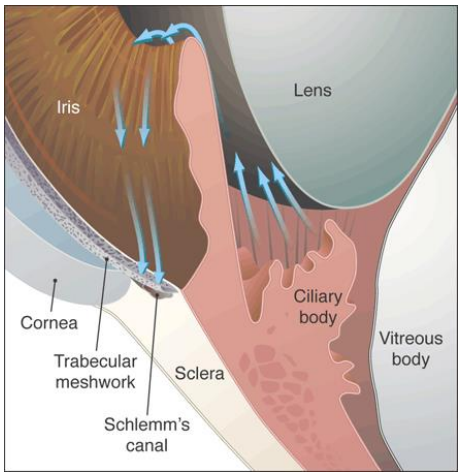

Figure 2: Circulation of Aqueous Humor (Alward 2003).

Anterior segment of the eye showing the circulation of the aqueous humor (AH), indicated by blue arrows. From the ciliary body and through the pupil, it fills the anterior chamber. AH then passes through the trabecular meshwork into Schlemm's Canal and from there into the episcleral venous system.

The TM is a filter-like structure of a series of fenestrated beams, located in the iridocorneal angle. It is differentiated into outer zones of uveal and corneoscleral TM as well as an inner zone of juxtacanalicular tissue (JCT, **Figure 3**). The JCT is immediately followed by the inner wall of SC, an endothelial cell layer that lines the SC lumen. There, the AH outflow resistance is generated. (Keller and Acott 2013)

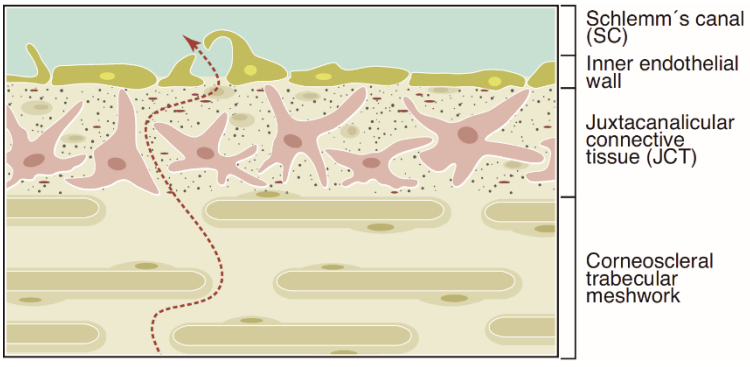

Figure 3: Schematic drawing of the trabecular outflow pathway (Mietzner and Breunig 2019).

Aqueous humor (AH) flow (indicated by the dashed arrow) through the layers of the uveal (not shown), corneoscleral und juxtacanalicular (JCT) regions of the trabecular meshwork and the inner endothelial wall of Schlemm's Canal (SC). The dense structure of the JCT and its close relation to the inner wall endothelium of SC becomes obvious. There, the main AH outflow resistance is generated.

The inner wall of SC is a unique endothelium which synergizes endothelial and lymphatic characteristics (Stamer et al. 2015). The AH passes through trans- and paracellular pores (Johnson 2006). The formation of an intracellular pore is a

sequential process, where the SC cell experiences a basal-to-apical pressure gradient and forms a giant vacuole, ending in the formation of a transcellular canal (**Figure 4**). According to these data, SC endothelial cells seems to have the potential to be a modulator of outflow resistance (Stamer et al. 2015). The correlation of pore forming ability and SC cell stiffness was investigated by perfusion as well as atomic force microscopy experiments. Thereby, a negative correlation of subcortical cell stiffness and porosity was found (Overby et al. 2014). If that pore forming ability becomes disrupted in POAG by altered SC stiffness, it would lead to impaired AH outflow and IOP elevation (Vahabikashi et al. 2019).

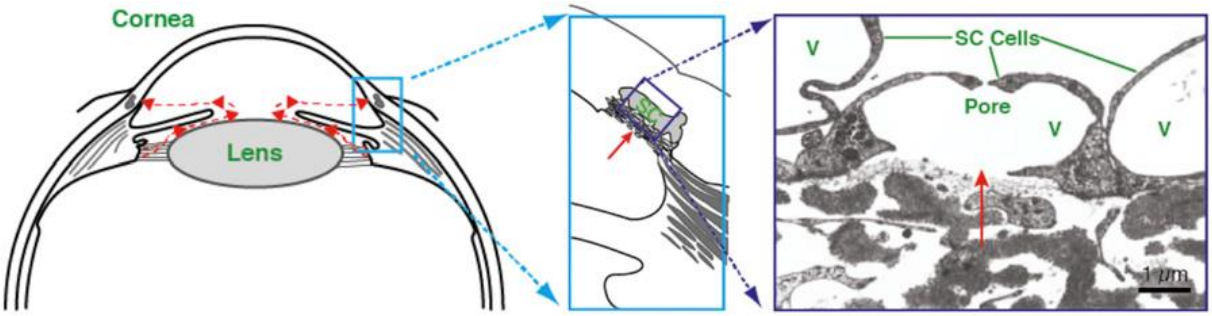

Figure 4: Aqueous humor outflow pathway (Overby et al. 2014).

Left) Schematic drawing of the anterior segment of the human eye. Red arrows indicate the direction of aqueous humor (AH) flow.

Center) Enlargement of the iridocorneal angle, highlighting the conventional AH outflow pathway.

Right) Transmission electron micrograph of endothelial cells forming the inner wall of Schlemm's Canal (SC). AH crosses the endothelium through giant vacuoles (V) and pores to enter the lumen of SC.

2.3 Pathology of POAG

During the pathology of POAG, the outflow of AH is reduced due to an increased outflow resistance in the JCT of the TM (Grant 1963; Johnson 2006). Even if molecular mechanisms causing this increase are still unclear, changes in amount and quality of extracellular matrix (ECM) are likely to be involved (Lütjen-Drecoll et al. 1986; Rohen et al. 1993).

Furthermore, not only JCT but also contractility and stiffness of inner wall endothelial cells of the SC are affected by glaucomatous changes. Comparing SC cells derived from healthy and glaucomatous eyes (Stamer et al. 1998), significant differences were found. Overby et al. had shown that glaucomatous SC cells have a reduced pore density as well as elevated cell stiffness compared to SC cells derived from healthy donors. They are more sensitive to increasing substratum stiffness, which is

accompanied by an increased expression of transforming growth factor-β2 (TGF-β2) and connective tissue growth factor (CTGF) (Overby et al. 2014).

2.4 TGF-β2 and CTGF

TGF-β signaling is likely a key regulator of the pathology of POAG. In human, three isoforms of TGF-βs are described while TGF-β2 is the most dominant form in the eye (Jampel et al. 1990). Many studies had reported significantly higher amounts of TGF-β2 in the AH of POAG eyes (Tripathi et al. 1994; Inatani et al. 2001; Picht et al. 2001; Ochiai and Ochiai 2002; Ozcan et al. 2004; Min et al. 2006; Trivedi et al. 2011; Agarwal et al. 2015; Guo et al. 2019). By perfusion experiments of anterior eye segments, TGF-β2 has been shown to increase IOP (Fleenor et al. 2006; Bhattacharya et al. 2009) and decrease outflow facility (Gottanka et al. 2004; Bachmann et al. 2006). Furthermore, TGF-β2 has been shown to induce fibronectin (FN) and plasminogen activator inhibitor-1 (PAI-1) (Fuchshofer et al. 2003; Bachmann et al. 2006; Fleenor et al. 2006) as well as the contraction of TM cells (Fuchshofer et al. 2007).

CTGF, a downstream mediator of TGF-β signaling (Ihn 2002; Leask and Abraham 2004), has been shown to be as potent as TGF-β2 to induce ECM expression and cell contractility in TM cells (Junglas et al. 2009; Junglas et al. 2012). Other diseases, associated with an increase of ECM, have also been reported to be associated with increased CTGF expression (Ito et al. 1998; Cicha et al. 2005; Yamamoto et al. 2005). In POAG, glaucomatous SC cells have a significantly increased expression of CTGF mRNA compared to cells derived from healthy donors (Overby et al. 2014). Furthermore, a CTGF overexpressing mouse model, developing elevated IOP as well as axon loss over time but no other obvious impairments, underlined the role of CTGF in the pathogenesis of POAG (Junglas et al. 2012).

2.5 Nitric Oxide

When IOP increases, it results in increased fluid shear stress for the affected cells of the outflow pathway (Ethier et al. 2004; Stamer et al. 2011). Consequently, the glycocalyx activates endothelial nitric oxide synthase (eNOS) to increase nitric oxide (NO) release. NO is synthesized from L-arginine and functions as a signaling molecule for neighboring cells since it can diffuse via cell membranes. There, it activates a signal cascade leading to cell relaxation (Overby et al. 2014). Via contraction assay, it has

been shown that the relaxation of human TM cells increases after exogenous NO treatment (Dismuke et al. 2014).

Under healthy conditions, increasing IOP causes an higher NO release and thereby reduced outflow resistance (Buys et al. 2014). Under glaucomatous conditions, a dysregulation of NO release is suggested to result in ocular hypertension (Emam et al. 2014). Regarding POAG, a case-control study identified decreased NO_x plasma levels in POAG patients (Emam et al. 2014) while other studies could not confirm these findings (Chang et al. 2000; Tsai et al. 2002). Studies investigating NO level in the AH are also not consistent which might be due to NO's volatile character (Chang et al. 2000; Tsai et al. 2002; Kosior-Jarecka et al. 2004). Regardless, animal models prove the role of eNOS as overexpression of eNOS caused an increased outflow facility while eNOS inhibition via L-NAME reduced outflow facility in comparison to wildtype littermates (Stamer et al. 2011). In addition, *ex vivo* mouse eye perfusion with an exogenous NO donor increased outflow facility (Chang et al. 2015).

Furthermore, SC cells respond to pharmacological agents that are known to modulate outflow resistance. Outflow resistance increasing substrates led to a stiffening of SC cells while drugs reducing resistance caused a softening (Zhou et al. 2012). Reducing cell stiffness trough cell relaxation might therefore be an optional aim to treat POAG. Therefore, DETA-NO was chosen as exogenous NO donor in the present study to investigate its effect on outflow cells *in vitro*.

2.6 Non-coding RNAs

Micro RNAs (miRNAs) have emerged as key regulators of gene expression. They are a large family of highly conserved, non-coding RNAs with a size of about 22 nucleotides. After transcription, a pre-miRNA is exported form the nucleus to the cytoplasm and gets incorporated into the RNA-induced silencing complex (RISC). Hereby, mature miRNAs can bind target messenger RNA (mRNA) according to their nucleotide sequences. Near-perfect complementarity leads to mRNA cleavage while partial complementarity leads to translational repression. (Wienholds and Plasterk 2005; Krol et al. 2010; Huntzinger and Izaurralde 2011) Interestingly, miRNAs have been found to often be co-expressed with their target genes (Baskerville and Bartel 2005).

MiRNAs have been implicated in many different diseases (Esteller 2011; Gutschner and Diederichs 2012) and it just started to investigate its role in the pathogenesis of POAG. Since the miRNA expression within the AH of POAG patients differs from that of age-matched controls (Jayaram et al. 2017), miRNA could be used as potential biomarker of POAG. As an example, miR-29 is down-regulated by TGF-β2. That mechanism has been shown to contribute to the induction of several ECM components in TM cells (Luna et al. 2011).

In the present study, the premise was that aberrant biomechanical behavior of outflow cells might be due to altered expression of miRNAs that are associated to the NO regulatory system.

2.7 Aims of the study

The present study was divided into several projects.

Aim 1: Analysis of a glaucoma mouse model overexpressing CTGF

Our work group established a glaucoma mouse model, overexpressing CTGF under a lens-specific promotor (Junglas et al. 2012; Reinehr et al. 2019). To support the likelihood of CTGF to play a key role during the pathology of POAG independently of the genetic background, mice were bred into different mouse strains. Investigations of glaucomatous changes in the retina as well as the analysis of the CTGF-induced increase in IOP were made *in vivo*.

Aim 2: Investigations on the effect of NO on biomechanical behavior and expression profile of SC cells

Since POAG is associated with increased AH outflow resistance due to increased cell stiffness of TM and SC cells, DETA-NO as exogenous NO donor was used in this study to induce cell relaxation *in vitro*. Thereafter, investigations on the actin cytoskeleton and cell stiffness were made. Furthermore, the expression of genes affecting the NO pathway as well as of glaucoma relevant genes was investigated.

Aim 3: Revealing the role of miRNA in glaucomatous outflow resistance dysregulation

MiRNAs became apparent as key regulators of gene expression in numerous cellular signaling pathways. They have also been implicated in the development of many

diseases. Preliminary investigations have shown changes in various miRNAs in glaucomatous SC cells compared to healthy controls. By transfection experiments with selected miRNAs, their effect on the expression profile of glaucoma-associated genes was investigated.

Aim 4: Studying the intracameral distribution of gold nanoparticles as potential delivery system for miRNA to outflow tissue

Finally, the distribution of gold nanoparticles (AuNPs) within the anterior chamber was investigated after *ex vivo* perfusion of porcine eyes. Using layer-by-layer coated NPs with miRNA or other small interfering RNA (siRNA) could provide an intracameral delivery system for glaucoma therapy. Functionalization of the NPs surface with hyaluronan acid (HA) has been shown to support NPs mobility within the ECM of outflow tissue and by interacting with the CD44 receptor directing them towards target tissue (Dillinger et al. 2018).

3 Material and Methods

3.1 Material

3.1.1 Reagents

In **Table 1**, all reagents used in this study are listed alphabetically.

reagent	source of supply
1,4-Diazabicyclo[2.2.2]octan (DABCO)	Roth, Karlsruhe, Germany
4',6-Diamidin-2-phenylindol (DAPI)	Vector Laboratories Inc., CA, USA
agarose	VWR International GmbH, Darmstadt, Germany
ammonium persulfate (APS)	Roth, Karlsruhe, Germany
β-mercaptoethanol	Serva Electrophoresis GmbH, Heidelberg, Germany
bovine serum albumin (BSA)	Roth, Karlsruhe, Germany
bromophenol blue	Serva Electrophoresis GmbH, Heidelberg, Germany
Calcein-AM	Thermo Fisher Scientific, PA, USA
Calcium dihydrogen phosphate KH_2PO_4	Roth, Karlsruhe, Germany
CDP-Star, developer for AP	Roche, Penzberg, Germany
chloroform $CHCl_3$	Roth, Karlsruhe, Germany
deoxynucleotide triphosphates (dNTPs)	Thermo Fisher Scientific, Waltham, MA, USA
DETA-NO	Sigma-Aldrich, St. Louis, MO, USA
Dinatriumhydrogenphosphat Na_2HPO_4	Merck, Darmstadt, Germany
dithiothreitol (DTT), 1 M	Merck, Darmstadt, Germany
ethanol C_2H_6O	Roth, Karlsruhe, Germany
ethidium bromide	Serva Electrophoresis GmbH, Heidelberg, Germany
fetal bovine serum (FBS)	PPA Laboratories, Pasching, Austria
fluorescent mounting medium (Mowiol)	Vector Laboratories Inc., CA, USA
glucose	Sigma-Aldrich, St. Louis, MO, USA
glycerol, 87% p. a.	AppliChem, Darmstadt, Germany
guanidine hydrochloride	Roth, Karlsruhe, Germany
heparin sodium, 5,000 I.E./ml	Braun, Melsungen, Germany
isoflurane®	Abbott Laboratories Ltd, Berkshire, UK
isopropanol, 100%	Fluka Chemie, Buchs, Switzerland
Ketamine, 10%	WDT, Garbsen, Germany
Luminata, developer for HRP	Millipore Corporation, MA, USA
magnesium dichloride $MgCl_2$,25 mM	New England Biolabs GmbH, Frankfurt am Main, Germany
methanol CH_3OH	Thermo Fisher Scientific, PA, USA
milk powder	Roth, Karlsruhe, Germany
paraformaldehyde (PFA)	Merck, Darmstadt, Germany
Penicillin/Streptomycin	PAA Laboratories, Pasching, Austria
peqGold TriFast™	PeqLab, Erlangen, Germany
Phalloidin	Sigma-Aldrich, St. Louis, MO, USA
phosphatase inhibitor cocktail	Merck, Darmstadt, Germany
phosphate buffered saline (PBS)	PAN Biotech GmbH, Aidenbach, Germany
potassium chloride KCl	Merck, Darmstadt, Germany
protease inhibitor cocktail plus	Roth, Karlsruhe, Germany
Re-blot Plus	Millipore Corporation, MA, USA

Roti® Quant universal	Roth, Karlsruhe, Germany
sodium dichloride $NaCl_2$	VWR International GmbH, Darmstadt, Germany
sodium dodecyl sulfate (SDS)	Roth, Karlsruhe, Germany
tetramethylethylendiamin (TEMED)	Roth, Karlsruhe, Germany
Tissue-Tek	Sakura Finetek, Alphen aan den Rijn, Netherlands
Tris/HCl	Roth, Karlsruhe, Germany
Triton X-100	Merck, Darmstadt, Germany
Trypsin/EDTA, 0.05%	PAA Laboratories, Pasching, Austria
Tween 20	Roth, Karlsruhe, Germany
water H_2O, RNase free	Roth, Karlsruhe, Germany
Xylazine, 2%	Serumwerk Bernberg AG, Bernberg, Germany

Table 1: Overview of reagents used for molecular and histological studies.

3.1.2 Enzymes and Kits

For molecular studies, in **Table 2** listed enzymes and kits were used.

enzyme/kit	order number	source of supply
DuoSet® Ancillary Reagent Kit 2 for ELISA	DY008	R&D Systems by biotechne, Minneapolis, MN, USA
eNOS ELISA	DY950-05	R&D Systems by biotechne, Minneapolis, MN, USA
Griess Reagent Kit for Nitrite Determination	G-7921	Molecular Probes by Thermo Fisher Scientific, Waltham, MA, USA
mirVana™ miRNA Isolation Kit	AM1560	Thermo Fisher Scientific, Waltham, MA, USA
proteinase K, 10 mg/ml	E00492	Fermentas by Thermo Fisher Scientific, Waltham, MA, USA
qScript™ cDNA Synthesis Kit	95047-100	Quanta Biosciences Inc., Beverly, MA, USA
RNeasy® Plus Mini Kit	74134	Qiagen, Hilden, Germany
taq polymerase	“A taq”	selfmade by Angelika Pach
TaqMan® Advanced miRNA cDNA Synthesis Kit	A28007	Thermo Fisher Scientific, Waltham, MA, USA

Table 2: Overview of enzymes and kits used for molecular studies.

3.1.3 Oligonucleotide primer

To genotype mice, polymerase chain reaction (PCR) was performed. The thereby used primer are listed in **Table 3**. As standard, the 100 bp Gene Ruler from Thermo Fisher Scientific was used. Thereby, the size of the generated DNA fragments, separated by the help of agarose gel electrophoresis, was determined.

gene	orientation	5’ - 3’ sequence
βB1	forward	GGA AGT GCC AGC TCA TCA GT
	reverse	GTG CGG GAC AGA AAC CTG
SV40	forward	GTG AAG GAA CCT TAC TTC TGT GGT G
	reverse	GTC CTT GGG GTC TTC TAC CTT TCTC
DCN	forward	CTG AAG ATG ACA CTG GCA TCG G
	reverse	CCT TCT GGC ACA AGT CTC TTG G

Table 3: Overview of oligonucleotide primer for genotyping PCR.

All oligonucleotide primer for quantitative, real-time PCR (RT-qPCR) are listed in **Table 4**. They are all species-specific for human and designed to span intron-exon boundaries. They were generated with the help of the Universal Probe Library Assay Design Center from Roche and obtained by Invitrogen.

gene	orientation	5' - 3' sequence
α-SMA	forward	CTG AAG TAC CCG ATA GAA CAT GG
	reverse	TTG TAG AAA GAG TGG TGC CAG AT
CALM-1	forward	TCA GCT GAC CGA AGA ACA GA
	reverse	GTG CCA TCG CCA TCT TTA TC
CAV-1	forward	TCT TCC AAC ACG TAG CTG CCC
	reverse	GGA TGG GAA CGG TGT AGA GA
CD44	forward	GAC ACA TTC CAC CCC AGT G
	reverse	TGG AAT TTG GGGTGT CCT TA
COL4A2	forward	CCA GGA CAG AAA GGA GAC CA
	reverse	GGT GTG ATG CCT GGG AAC
CTGF	forward	CTC CTG CAG GCT AGA GAA GC
	reverse	GAT GCA CTT TTT GCC CTT CTT
DCN	forward	TGG ACA ACA ACA AGC TTA CCA
	reverse	GAA GTC ACT TGA TCC AAC TAC AGA GA
eNOS	forward	CAG ATG ATC CCC CAG AAC TC
	reverse	CAG GGC TGC AAA CCA CTC
FN	forward	GGG AAG ACA TAC CAC GTA GGA G
	reverse	AGG TCT GCG GCA GTT GTC
GNB2L	forward	CCT AAC CGC TAC TGG CTG TG
	reverse	CTA GAA TGAT CTT TCC CTC TAA ATC C
HO-1	forward	TTC AGA AGG GCC AGG TGA
	reverse	TGT TGC GCT CAA TCT CCT C
HSP-90	forward	CGG AGA ATT CTA TAA GAG CTT GAC C
	reverse	AGG GCT CTG AAT TCC AAC TG
iNOS	forward	GTC CAG CGC TAC AAC ATC CT
	reverse	CAG CTT GTG CGT TTC CAG
NID-1	forward	CCA GAC CAG AAA GGC AAG AG
	reverse	GGA AAA TGG CAT AGG AGC TG
nNOS	forward	CTG TGA CAA CTC CCG CTA CA
	reverse	ACG TCT TCC TCA TGT CTA AGT TCA
PAI-1	forward	AAG GCA CCT CTG AGA ACT TCA
	reverse	CCC AGG ACT AGG CAG GTG
RPL32	forward	GAA GTT CCT GGT CCA CAA CG
	reverse	GCG ATC TCG GCA CAG TAA G
TGF-β2	forward	CCA AAG GGT ACA ATG CCA AC
	reverse	CAG ATG CTT CTG GAT TTA TGG TAT T

Table 4: Overview of oligonucleotide primer for real-time PCR.

3.1.4 TaqMan probes

TaqMan probes were used as additional approach to assess mRNA expression (**Table 5**). They are species-specific for human and obtained from applied biosystems by Thermo Fisher Scientific.

gene	order number
eNOS	Hs01574665_m1
RPL32	Hs00851655_g1

Table 5: Overview of TaqMan probes for TaqMan technique.

3.1.5 Transfection reagents

Transfection reagents were purchased by Dharmacon™ (GE Healthcare, Horizon Discovery, Cambridge, UK) and are listed in **Table 6**. They are species-specific for human and were used with DharmaFECT™ 4 transfection reagent that was optimized for small RNA delivery and formula 4 was recommended for endothelial cells.

reagent	order number	function
miR222-3p	C-300579-07-0005	miRNA mimic
	IH-300579-08-0005	miRNA hairpin inhibitor
miR455-3p	C-301172-01-0005	miRNA mimic
	IH-301172-02-0005	miRNA hairpin inhibitor
miRIDIAN microRNA Mimic Negative Control #1	CN-001000-01-05	mimic negative control
miRIDIAN microRNA Hairpin Inhibitor Negative Control #1	IN-001005-01-05	hairpin inhibitor negative control
DharmaFECT™ 4	T-2004-02	transfection reagent

Table 6: Overview of miRNA mimics and inhibitors as well as their appropriate controls.

With miRNA mimics, gain-of-function experiments were performed. Supplier stated that their products have the same sequence as the MIMAT code of the mature miRNA. **Table 7** lists the corresponding codes and sequences for miRNAs investigated in this study.

miRNA mimic	MIMAT code	mature sequence
hsa-miR-222-3p	MIMAT0000279	AGC UAC AUC UGG CUA CUG GGU
hsa-miR-455-3p	MIMAT0004784	GCA GUC CAU GGG CAU AUA CAC

Table 7: Overview of miRNA mimics and their mature sequence.

For miRNA inhibitors, the supplier did not provide sequence. According to manufacturer, the inhibitor was designed to build a hairpin shape and was said to be specific for the corresponding miRNA. With the use of these inhibitors, loss-of-function experiments were performed.

Since inhibitor were designed different to mimics, it was necessary to use two controls for miRNA mimics and inhibitors. According to the supplier, controls have non-targeting sequences that are listed in **Table 8**.

miRNA control	sequence
mimic negative control	CUA CCA ACA CUG ACC AAU AAU U
hairpin inhibitor negative control	UCA CAA CCU CCU AGA AAG AGU AGA

Table 8: Overview of mimic and hairpin inhibitor negative controls and their sequence.

3.1.6 Antibodies

All primary antibodies are listed in **Table 9** and are polyclonal antibodies gained by the immunization of host animals, which are specific for the corresponding human or murine protein.

protein	primary antibody	order number	source of supply
α-tubulin	rabbit anti α-tubulin	600-401-880	Rockland Immunoche micals, Gilbertsville, PA, USA
CTGF	rabbit anti CTGF	MAB91901	R&D Systems by biotechne, Minneapolis, MN, USA
eNOS	rabbit anti eNOS	9572S	Cell Signaling, Cambridge, UK
GFAP	chicken anti GFAP	LS-B4775	LifeSpan Biosciences, Seattle, WA, USA
glutamine synthetase	goat anti GS	sc-6640	Santa Cruz Biotechnology, Dallas, TX, USA
vimentin	goat anti VIM	V4630-.2ML	Sigma-Aldrich, St. Louis, MO, USA

Table 9: Overview of primary antibodies for Western Blot analyses and histological investigations.

To detect protein bands on Western Blot membranes, in **Table 10** listed secondary antibodies were used. They were either linked to horseradish peroxidase (HRP) or alkaline phosphatase (AP), which develop detectable chemiluminescence when in contact with the corresponding developer reagent.

secondary antibody	linked to	order number	source of supply
goat anti rabbit	AP	7054S	Cell Signaling, Cambridge, UK
goat anti rabbit	HRP	7074S	Cell Signaling, Cambridge, UK

Table 10: Overview of secondary antibodies for Western Blot analyses.

As molecular weight standard for proteins separated by electrophoresis, the EZ-RUN Pre-Stained Rec Protein Ladder (order number: BP3603500) from Fisher Scientific was used.

To detect primary antibodies used for immunohistochemistry, secondary antibodies linked to fluorophores were used as indicated in **Table 11**.

secondary antibody	linked to	order number	source of supply
horse anti goat	Biotin	BA-9500	Vector Laboratories, Burlingame, CA, USA
goat anti chicken	Alexa Fluor 488	A-11039	Molecular Probes, Eugene, OR, USA
rabbit anti-goat	Cy3	705-165-147	Jackson Immuno Research, West Grove, PA, USA
streptavidin	Alexa Fluor 555	SA-5001	Vector Laboratories, Burlingame, CA, USA

Table 11: Overview of secondary antibodies for histological investigations.

To avoid unspecific binding of secondary antibodies, negative controls without primary antibody were performed on additional slices. Nuclear DNA was counterstained with 4',6-diamidino-2-phenylindole (DAPI), which was part of the mounting medium (1:10) to preserve the slices.

3.1.7 Nanoparticles

NP were purchased from Nanopartz™ (Loveland, CO, USA) as accurate spherical gold NPs and manufacturer's information are listed in **Table 12**.

particle diameter	order number	polydispersity index	zeta potential
5 nm	A11-5-CIT-PBS-1-10	10%	-32 mV
50 nm	A11-50-CIT-PBS-1-25	4%	-32 mV
100 nm	A11-100-CIT-PBS-1-50	3%	-38 mV
150 nm	A11-150-CIT-PBS-1-50	3%	-38 mV

Table 12: Overview of gold nanoparticles used for ex vivo eye perfusion experiments.

Furthermore, an additional set of self-made NPs with a core size of 13 nm was investigated. NP preparation as well as HA coating were done by our cooperation partner of the Department of Pharmaceutical Technology by Silvia Babl and Tobias Sonntag.

For *ex vivo* eye perfusion experiments, the gold concentration was kept constant at 9390 ppb (parts per billion), while the particle number differed (**Table 13**).

particle diameter	particle number per ml of perfusion solution
5 nm	7.46×10^{12}
50 nm	6.78×10^{9}
100 nm	1.02×10^{9}
150 nm	2.77×10^{8}
13 nm	4.58×10^{11}

Table 13: Overview of gold nanoparticles per ml of perfusion solution for a constant gold concentration.

3.1.8 Buffers and Solutions

All buffer and solutions as well as their compositions are listed in **Table 14**.

buffer/solution	composition
detection buffer pH 9.5	12.11 g Tris 0.3 M 5.84 g NaCl 0.1 M ad 1 l dH_2O
digestion buffer for ear punches for genotyping	3.74 g KCl 0.51 g $MgCl_2 \times 6H_2O$ 0.10 g gelantine 4.5 ml Nonidet P-40 (Tergitol™) 4.5 ml Tween 20 10 ml Tris/HCl, 1 M ad 1 l dH_2O

electrode buffer, 10x for Western Blotting	30.29 g Tris/HCl 144.13 g glycine 100 ml 10% (w/v) SDS ad 1 l dH_2O
EM fixative	2.5% paraformaldehyde 2.5% glutaraldehyde in cacodylate buffer, 0.1 M
epon stem A	62 ml glycidether 100 100 ml DDSA
epon stem B	100 ml glycidether 100 89 ml NMA
glycerol, 5x for genotyping PCR	60% glycerol cresol red
Laemmli buffer, 5x pH 6.8	0.454 g Tris/HCl 3.0 ml 20% SDS 3.4 ml glycerol bromophenol blue 20% β-mercaptoethanol 10% DTT 1 M
Mowiol with DAPI as mounting medium	1.2 g Mowiol 3.0 g glycerine 3.0 ml dH_2O 6.0 ml 0.2 M Tris/HCl, pH 8.5 255 mg DABCO 1 ml DAPI
phosphate buffered saline (PBS), 10x pH 7.4	80.0 g NaCl 4.4 g Na_2HPO_4 2.4 g KH_2PO_4 2.0 g KCl ad 1 l dH_2O
paraformaldehyde (PFA), 4%	4 g PFA ad 100 ml phosphate buffer, 0.1 M
Q buffer for genotyping PCR	1.0 ml Tris, 1 M 1.0 ml $(NH_4)_2SO_4$, 1 M 75 µl $MgCl_2$, 2 M 2.0 ml KCl, 1 M ad 50 ml dH_2O
SDS solution, 10% (w/v)	10 g SDS ad 100 ml dH_2O
TBE buffer, 10x pH 7.0	108 g Tris 55 g boric acid 40 ml 0.5 M EDTA, pH 8.0 ad 1 l dH_2O
TBS buffer, 10x	30 g Tris 80 g NaCl 2 g KCl ad 1 l dH_2O
TBS-T buffer, 1x	100 ml 10x TBS 0.05% (v/v) Tween 20 ad 1 l dH_2O
transfer buffer, 10x for Western Blotting	5.8 g Tris 2.9 g glycine 200 ml methanol 3.7 ml 10% (w/v) SDS ad 1 l dH_2O

washing buffer for protein isolation	14.3 g guanidine hydrochloride in 500 ml 95% ethanol
hybridization solution for Northern Blot	112.5 ml 20x SSc 9.0 ml NaPi, 1 M, pH7.2 315.0 ml SDS, 10% 9.0 ml 50x Denhardts solution 4.5 ml dH_2O
Denhardts solution for Northern Blot	1% albumin fraction V 1% polyvinylpyrrolidone K30 1% Ficoll 400 needs heat to dissolve
SSC, 20x pH 7.0	3.0 M NaCl 0.3 M TriNa-citrate adjust pH with 1 M HCl
wash solution 1 for Northern Blot	125 ml 20x SSC 50 ml SDS, 10%
wash solution 2 for Northern Blot	25 ml SSC 50 ml SDS, 10%
cacodylate buffer, 0.1 M	10.7 g cacodylate acid ad 500 ml dH_2O
phosphate buffer, 0.1 M pH 7.4	100 ml Na_2HPO_4 x $2H_2O$ 0.2 M with NaH_2PO_4 x H_2O 0.2 M to pH 7.4 ad 200 ml dH_2O
Tris/HCl, 1.0 M pH 6.8	121.14 g Tris ad 1 l dH_2O
Tris/HCl, 1.5 M pH 8.8	181.71 g Tris ad 1 l dH_2O

Table 14: Overview of buffers and solutions including their composition.

3.1.9 Laboratory Equipment

In **Table 15**, all laboratory equipment used in this study is listed. Experiments were performed in the laboratories of the Department for Human Anatomy and Embryology of the University of Regensburg. Northern blot experiments were performed within a cooperation with the Department for Biochemistry I of the same university.

equipment	source of supply
analytical balance	Kern & Sohn GmbH, Balingen, Germany
apotome	Carl Zeiss Microscopy GmbH, Berlin, Germany
apparatus for gel electrophoresis	PeqLab, Erlangen, Germany
binoculars	Carl Zeiss Microscopy GmbH, Berlin, Germany
centrifuges, 5415D, 5415R, 5702 and 5810R	Eppendorf, Köln/Wesseling, Germany
cryostat Microm HM 500 OM	MICROM International GmbH, Walldorf, Germany
dissecting set	Fine Science Tools GmbH, Heidelberg, Germany
ELISA plate reader Sunrise	Tecan Austria GmbH, Grodig, Austria
fluorescence microscope Axio Imager Z1	Carl Zeiss Microscopy GmbH, Berlin, Germany
glass ware	Roth, Karlsruhe, Germany
Hamilton syringe	Hamilton, Bonaduz, Switzerland
heat sealer for RT-qPCR plates	4titude, Berlin, Germany
heating plate, including magnetic stirrer	IKA-Werke GmbH & Co KG, Staufen, Germany

incubator HERA cell 150	Heraeus, Hanau, Germany
incubator innova 4200 including stirrer	New Brunswick Scientific, New Jersey, USA
laminar air flow cabinet HERA safe	Heraeus, Hanau, Germany
LAS 3000	Fujifilm, Tokyo, Japan
NanoDrop™-1000	Thermo Fisher Scientific, PA, USA
Neubauer improved cell counting chamber	Paul Marienfeld GmbH & Co. KG, Lauda-Königshofen, Germany
PerfectBlue Tank Electro Blotter	PeqLab, Erlangen, Germany
pH Meter	WTW GmbH, Weilheim, Germany
pipette Pipetman Concept	Eppendorf, Köln/Wesseling, Germany
pipette Xplorer	Eppendorf, Köln/Wesseling, Germany
RT-qPCR bench Captair Bio	erlab, Val de Reuil, France
RT-qPCR cycler CFX connect	BioRad, Munich, Germany
thermomixer comfort	Eppendorf, Köln/Wesseling, Germany
tonometer TonoLab	Icare Finland Oy, Espoo, Finland
ultrapure water facilities	ELGA LabWater, Celle, Germany arium® PRO, Sartorius Lab Instruments, Göttingen, Germany
ultrasonic bath Bandelin Sonorex RK 102	Bandelin GmbH & Co. KG, Berlin, Germany
Vortex Genie 2	Scientific Industries Inc, NY, USA
water bath	Memmert GmbH & Co. KG, Schwabach, Germany

Table 15: Overview of laboratory equipment used in this study.

3.1.10 Consumables

Table 16 lists the consumables used to generate the results presented in this study.

consumables	source of supply
cell culture flasks	Sarstedt Inc., NC, USA
cell culture plates	Sarstedt Inc., NC, USA
cell scraper	Sarstedt Inc., NC, USA
cover slips	Thermo Fisher Scientific, PA, USA
falcons, 15 & 50 ml	Sarstedt Inc., NC, USA
gloves, single use	Kimberly-Clark GmbH, Koblenz/Rheinhafen, Germany
injection cannula	Henry Schein Inc, NY, USA
lab books	Kimberly-Clark GmbH, Koblenz/Rheinhafen, Germany
microtiter plate for RT-qPCR	Bio-Rad Laboratories GmbH, München, Germany
nitrile gloves, single use	VWR International GmbH, Darmstadt, Germany
object slide	Thermo Fisher Scientific, PA, USA
parafilm	Bemis, Neenah, WI, USA
Pasteur pipettes	Brand, Wertheim, Germany
pipet tips	Sarstedt Inc., NC, USA
pipette Pipetman Concept	Eppendorf, Köln/Wesseling, Germany
pipette Xplorer	Eppendorf, Köln/Wesseling, Germany
PVDF membrane, Immobilon®-P with 0.45 µm	Merck, Darmstadt, Germany
razor blades	American Safety Razor Company, Verona, VI, USA
serological pipets	Sarstedt Inc., NC, USA
syringe, single use	Henry Schein Inc, NY, USA
tubes, 0.5 ml, 1.5 ml & 2.0 ml	Eppendorf AG, Hamburg, Germany
Vivaspin 500 filtration columns	Sartorius Lab Instruments, Göttingen, Germany
Whatman paper	neoLab, Heidelberg, Germany

Table 16: Overview of consumables used in this study.

3.1.11 Animals

The βB1-CTGF transgenic (TG) mice carry a plasmid leading to the overexpression of CTGF under a lens-specific promotor. TG mice were compared to wildtype (WT) littermates and were investigated at the age of 4, 8, 12 and 15 weeks as well as after one year. The genetic background was either pure CD1, Black6/J or mixed. Timepoints were chosen to track changes in IOP depending on the genetic background. Animals of both genders were used and were kept at a 12 hours light/dark-cycle and had access to food and water *ad libitum*.

3.1.12 Cell lines

In vitro experiments were performed with primary cell lines (**Table 17**) obtained from human donors. SC (Stamer et al. 1998) and TM cells (Stamer et al. 1995) were thankfully obtained from W. Daniel Stamer's lab (Department of Ophthalmology, Duke University, Durham, NC, USA). Within the present study, the following SC cell strains from healthy donors were investigated: SC60, SC67, SC68, SC71, SC74, SC75, SC79, SC89 and SC91. From glaucomatous donors, RNA from SC57g, SC62g and SC63g was examined. Furthermore, TM cell strain TM120 was declared to be from a healthy donor.

cell line	age	gender	time from death to enucleation
SC60	58 years	na	na
SC67	44 years	male	6:16
SC68	30 years	na	4:40
SC71	44 years	male	na
SC74	8 months	male	20:40
SC75	10 years	male	8:30
SC79	33 years	male	5:45
SC89	68 years	male	4:13
SC91	74 years	female	6:00
SC57g	78 years	male	3:52
SC62g	66 years	female	2:15
SC63g	78 years	na	5:11
TM120	11 months	na	na

Table 17: Overview of SC and TM cells investigated in this study.

Beside donors age and sex, the time from death to eye enucleation (in hours) are listed if information was available (na = not available). Glaucomatous SC cell strains are indicated by a "g".

Human umbilical vein endothelial cells (HUVECs), used as model cell line for endothelial-like behavior, were obtained from GIBCO (order number: C0035C).

3.2 Cell culture

3.2.1 Passaging of cells

All *in vitro* experiments were performed under sterile conditions to avoid bacterial contamination. In addition, primary cell lines are very sensitive and difficult to handle. Extraordinary attention is demanded not to exceed a 1:3 ratio when splitting the cells.

Cells were passaged and split as soon as they reached confluency. After medium was removed, cells were washed with PBS and got trypsinized. While SC and TM cells were incubated for about 5 min in the incubator, HUVECs must be kept at room temperature (RT). Under a microscope, the detachment of the cell layer was checked. The enzymatic reaction was stopped by adding Ca^{2+}-containing medium and suspension was transferred into a 15 ml tube. To pellet the cells and get rid of the trypsin, they were centrifuged at 1,000 g for 5 min. After removing the supernatant, the cell pellet was resuspended in fresh medium and seeded into new cell culture dishes for passaging or experiments.

3.2.2 *In vitro* experiments

All *in vitro* experiments were performed under sterile conditions. While SC and TM cells were incubated at 7% CO_2, HUVECs needed 5% CO_2. Temperature was kept at 37° C and air was saturated with humidity.

For SC and TM cells, DMEM medium with low glucose (1.0 g/l) from PAN Biotech (order number: P04-01515) was used and 10% FBS and 1% antibiotics (Penicillin/Streptomycin) were added. Furthermore, it was necessary to use phenol-red free medium for Griess Assay experiments. For HUVECs, EBM-2 medium from Lonza (order number: CC-3162) was used. To receive growth medium, EGM-2 SingleQuot Kit (order number: CC-4176) was added according to manufacturer's information.

3.2.2.1 DETA-NO treatment

Cells were treated with DETA-NO (order number: D185_10MG) as soon as cells reached confluency in 6 wells (growth area: 9.6 cm^2). Since SC cells do not stand serum starvation at 0% for long, cells were not set to starvation 24 hours prior to experiments. To make experiments comparable, HUVECs were treated the same.

To dissolve solid DETA-NO, a distinct amount of DETA-NO was weighed at a special accuracy weighing machine and dissolved in appropriate amount of phosphate buffered saline (PBS) to receive a 10 mM stock solution. From this stock, 10 and 20 µl were used to obtain a 50 and 100 µM concentration in a total volume of 2 ml medium, respectively. During DETA-NO treatment, cells were exposed to 0% serum. For up to 24 hours, this was suitable for cell survival.

To be particularly precise, controls were treated with the same amount of solvent as it was used for the treatment with the highest DETA-NO concentration. Thereby, one avoids detecting any effect resulting from the solvent of a drug or chemical. Since DETA-NO was dissolved in sterile PBS, this was not expectable but necessary for good scientific research.

After incubation for 3, 5, 6, 12 or 24 hours, medium was collected and stored at -80° C until further use. To harvest cells, cell layer was washed twice with PBS and after aspiration of remaining fluid, plate was set on ice and processed as described in section 3.3.

3.2.2.2 miRNA transfection

With the help of transfection experiments, synthetic miRNA mimics and inhibitors can be brought into living cells. Thereby, their function on target genes can be investigated *in vitro*. With their sequence-specific design, they are potent tools in mimicking or inhibiting the function of the gene, resulting in a specific phenotypic effect.

According to manufacturer's information, miRIDIAN™ miRNA mimics are synthetic duplexes that represent the mature miRNAs. Like naturally occurring miRNAs, synthetic mimics are loaded into RISC (RNA-induced silencing complex) intracellularly. This complex allows for binding of target site in the 3'-UTR (untranslated region) of target mRNAs due to complementary sequences. With chemical modifications, the mature miRNA strand is said to be preferentially loaded into the RISC. With this approach, transfection with miRNA mimics allows for gain-of-function experiments.

With miRNA inhibitors, the approach is the other way around. According to manufacturer's information, inhibitors are non-hydrolyzable, single-stranded reverse constructs of the mature miRNA. Due to complementary sequences, inhibitor irreversible binds to the mature miRNA. This binding prevents interaction of miRNA with its endogenous target mRNA, resulting in the loss of miRNA function (Meister et

al. 2004). To improve the binding of the inhibitor, miRIDIAN™ miRNA hairpin inhibitors are designed with a terminal stem-look structure and chemical modifications (Vermeulen et al. 2007).

Figure 5 shows the timetable for transfection experiments of this study and the following chapter deals with the individual steps.

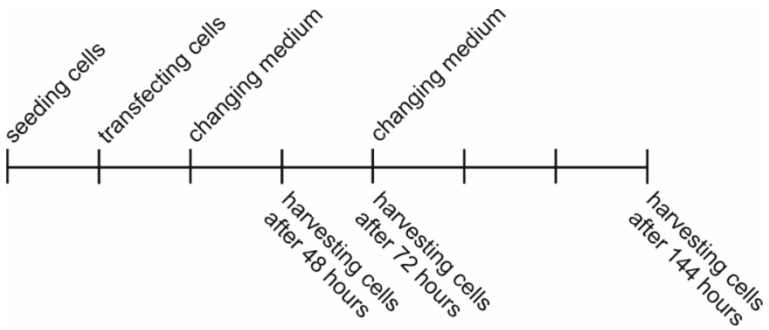

Figure 5: Timetable for transfection experiments.

3.2.2.2.1 seeding cells

Cells were seeded in 96 wells (growth area: 0.32 cm^2) the day before transfection. To receive a cell layer with 80% of confluency the following day, cells must be counted, and distinct cell numbers needed to be seeded.

To calculate cell numbers, cells were trypsinized as described above (see 3.2.1). The resuspension must be done with a defined amount of medium. The volume was chosen to dilute cells sufficiently for counting and was usually between 1 and 4 ml for cells from a confluent T75 flask.

The Neubauer improved cell counting chamber was cleaned with 70% Ethanol and the cover slip was attached in a way that excited Newton's rings. This phenomenon indicated the correct placement and thereby that the chamber depth was adjusted at 0.1 mm. Cell suspension was resuspended immediately before taking about 20 µl for counting. The fluid was brought into the counting chamber by locating the pipet tip at the edge of the chamber. Capillary force sucked fluid in the space between counting chamber and cover slip while excess amount of fluid run into the intendent channels. 0.9 µl of fluid remind in the counting area and was visible under a microscope.

The counting chamber consists of nine equal squares, divided by additional lines to facilitate counting. One of the nine big squares had an area of 1 mm^2 and with a depth of 0.1 mm a volume of 0.1 µl.

At 100x magnification, cells in four of the nine squares were counted. While additional lines helped for orientation, one must be aware not to count cells lying on top of these lines twice. Cells lying on the boundary lines of a big square had to be counted for two of the four borders. After four big squares were counted, the average was calculated.

Due to the chamber volume, the average cell number must be multiplied with 10^4 for calculating the cell concentration per ml. The total number of cells was assessable by respecting the initial dilution factor.

Initial experiments had shown that - according to different cell sizes - 7,500 SC cells, 10,000 TM cells or 12,000 HUVECs must be seeded per 96 well. Until the transfection on the following day, cells were cultured in serum-containing medium.

3.2.2.2.2 transfecting cells

Transfection of cells was performed with Dharmacon™ DharmaFECT™ 4 reagent on day 2. First, working solutions of siRNA were prepared. Since initial experiments had shown that mimics and inhibitors were most effective at different concentrations, applied amounts were different. For mimics and mimic controls, a final concentration of 100 nM requested 0.5 µl/well of the 20 µM stock solution while a final concentration of 25 nM for inhibitors and inhibitor controls demanded 0.125 µl/well. With serum-free medium, volume was set to a total volume of 10 µl/well. In another tube, DharmaFECT™ transfection reagent must be prepared to a working solution of 0.05 to 0.5 µl/well. Initial experiments revealed that 0.2 µl/well was suitable for our experiments. Diluted with serum-free medium to a total volume of 10 µl/well, the solution must be incubated for 5 min at RT before the next step. Afterwards, siRNA dilution was combined with DharmaFECT™ transfection reagent and carefully mixed by pipetting. For a control, containing transfection reagent but no siRNA, DharmaFECT™ transfection reagent was combined with 10 µl serum-free medium per well. For an additional control, containing neither transfection reagent nor siRNA, 20 µl of serum-free medium per well was used. Combined solutions were incubated 20 min at RT before the next step. Thereafter, 80 µl/well of full growth medium (containing 10% serum) was added to receive a total volume of 100 µl transfection mixture per well. To transfect cells, growth medium was replaced with the transfection mixture. **Figure 6** shows a drawn picture of the above described workflow.

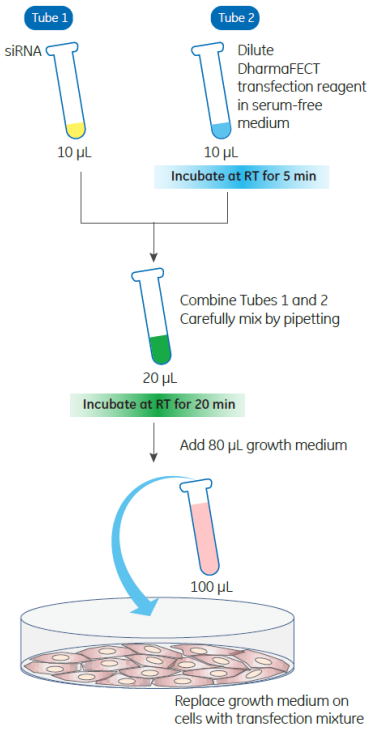

Figure 6: Workflow for transfection experiments with DharmaFECT™ transfection reagent (taken from GE Healthcare UK Limited).

To receive enough RNA from the transfected cells, three of the 96 wells were combined to one sample. Since every treatment was performed in triplets, every treatment required 9 wells.

3.2.2.2.3 changing medium and harvesting cells

24 hours after transfection, transfection mixture was replaced by 200 µl of fresh growth medium after one washing step with PBS. Cells were harvested 48, 72 or 144 hours after transfection. To supply cells adequate for long term treatment, medium was changed after 72 hours if cells were incubated for 144 hours.

3.2.2.3 flow experiments with ibidi® pump system

Flow experiments were performed following manufacturer's instructions. For static controls, 24 wells were used. Theoretically, near-static conditions of 0.1 dyn/cm² would represent the best possible control conditions (Ashpole et al. 2014). Thereby, the same number of cells can be seeded onto the same growth area and perfusion will still provide enough medium for supply. Since there was only one pump system available and one can only run experiments with the same pressure at the same time, static conditions were chosen as controls for the present study.

Perfusion under flow conditions were performed in ibidi® µ-slides (order number: 80176) with a channel height of 0.4 mm and the surface modification ibiTreat®. Cell numbers seeded on one slide and per 24 well, respectively, were calculated as mentioned at 3.2.2.2.1. For SC cells, 75,000 cells were seeded and allowed to settle for one to two hours.

For flow experiments, a ramp of 1 dyn/cm² per 30 minutes was designed to avoid cell detachment. Therefore, the final flow of 10 dyn/cm² was achieved 5 hours after experiment has started. Form that timepoint on, experiments lasted 24 hours or one week. To allow for NO concentration determination, medium was reduced to a total of 2 ml. Logically, the same amount of medium was used for static controls.

At the end of each experiments, medium was collected and stored immediately at -20° C. After cells were washed twice with PBS, cells were harvested with 300 µl peqGold TriFast™.

3.3 Biochemical techniques

3.3.1 Griess Assay

With the Griess Reagent kit (order number: G-7921) from Thermo Fisher Scientific, nitrite can be spectrophotometrically detected. According to manufacturer's instructions, the presence of nitrite allows for quantitative conversion of sulfanilic acid to a diazonium salt and, thereafter for a second coupling step, resulting in an azo dye. That dye can be detected based on its absorbance at 548 nm.

To prepare the Griess Reagent, component A and B derived with the kit must be mixed in equal volumes. Per well, 20 µl will be needed. Furthermore, every reaction mix consisted of 130 µl dH_2O and 150 µl of the nitrite-containing sample. If cell culture supernatant was investigated, phenolred-free medium must be used since the color would interfere with the method.

To allow for calibration, a standard with defined nitrite concentrations must be prepared. Therefore, component C of the kit must be diluted to concentrations between 1 to 100 µM with dH_2O. Those standard nitrite solutions are combined to the Griess Reagent and dH_2O in place of the experimental samples. Furthermore, a photometric reference sample, containing unconditioned medium instead of the nitrite containing sample, must be prepared.

Standard, sample and reference mixtures were pipetted in technical duplicates and must be incubated for 30 min at RT. Thereafter, the absorbance was measured relative to the reference and sample's nitrite concentration were calculated from relative absorbance readings of the standard. The detection limit of this method is set at 1 µM. Therefore, results below that limit were considered to be not detectable (nd).

3.3.2 Protein isolation

To investigate the effect of *in vitro* treatment on protein synthesis of cultivated cells, protein was isolated either with peqGold TriFast™ or RIPA buffer.

3.3.2.1 with peqGold TriFast™ method

PeqGold TriFast™ is a ready-to-use solution for simultaneous isolation of RNA and proteins. It contains phenol and guanidinium thiocyanate in a monophasic reagent. By adding chloroform, centrifugation leads to separation into three phases. While RNA is exclusively arranged in the upper aqueous phase, protein remains in the lower organic phase. DNA would be contained in the interphase but was not of interest for the present study.

To process cells from *in vitro* experiments, cell layers were washed with PBS and fluid was aspirated. Cell culture dishes were placed on ice and cells were overlaid with TriFast™ solution (500 µl per 6 well, 100 µl per 96 well) and incubated for 5 min on ice. Subsequent, cells were removed with a cell scraper from the bottom of the plate and the lysate was transferred into a tube. As mentioned in section 3.2.2.2, three 96 wells of the same transfection approach were pooled resulting in a total of 300 µl TriFast solution. Since processing of samples derived from 6 and 96 wells demanded different amounts of reagents, **Table 18** compiles corresponding amounts.

reagent	6 well	three 96 wells
peqGold TriFast™	500 µl	3x 100 µl
chloroform	100 µl	60 µl
100% isopropanol	750 µl	450 µl
wash buffer	1,000 µl	600 µl
95% ethanol	1,000 µl	600 µl
1% SDS incl. inhibitors	200 µl	120 µl

Table 18: Required amounts of reagents for peqGold TriFast™ protein isolation.

After adding chloroform, shaking guaranteed for dissociation. Homogenate was then centrifuged for 20 min at 12.000 g and 4° C to separate phases. After upper, aqueous phase was transferred into a fresh tube for RNA isolation (see section 3.4.1.1), protein

precipitation was performed by adding 100% isopropanol to the organic phase. Samples were stored 10 min at RT and centrifuged at 12,000 g and 4° C for 10 min.

To wash protein pellet, supernatant was removed and a wash buffer solution (containing 0.3 M guanidinium hydrochloride in 95% ethanol) was applied three times for 20 min at RT. Between washing steps, samples were centrifuged at 7,600 g and 4° C for 5 min and supernatant was removed. Next, protein pellet was vortexed once with 95% ethanol and incubated for another 20 min at RT. Samples were then centrifuged once more at 7,600 g and 4° C for 5 min.

Finally, the protein pellet was dried and dissolved in 1% SDS containing protease and phosphatase inhibitors (1:100, each). Usually, pipetting it up and down was sufficient to dissolve the pellet. Incubation overnight at RT yielded complete solubilization. Samples were then stored at -80° C for future use.

3.3.2.2 with RIPA method

The RIPA method was more suitable buffer for enzyme-linked immunosorbent assays (ELISAs) which did not interfere as SDS, but its usage did not allow for RNA isolation at the same time. Instead of with peqGold TriFast™ solution, cell layer were incubated with 300 µl RIPA buffer including protease and phosphatase inhibitors (1:100, each). After 5 min on ice, cells were removed from the cell culture dishes with a cell scraper and transferred into a fresh tube. After additional 30 min incubation on ice, samples were centrifuged for 10 min at 20,000 g and 4° C. To get rid of cell debris and insoluble components, supernatant was transferred into a fresh tube and stored at -80° C for future use.

3.3.3 Concentrating protein samples

With the help of Vivaspin™ 500 columns from Sartorius, protein samples could be concentrated two- to three-fold. Following manufacturer's instructions, columns were placed into associated collecting tubes and filled with up to 500 µl of protein sample. When placing tubes into the centrifuge, attention must be paid to the position of vertical membrane which should face outwards. By a centrifugation step of 10 min at 16,000 g, molecules smaller 5 kDa were cut off through the membrane pores. Protein of interest remained in the column and up to 20 µl of concentrated protein was used for further Western Blot analyses.

3.3.4 Protein quantification

Protein quantification was necessary to ensure balanced loading of Western Blots. Dependent on the buffer used for solubilization, quantification was performed by PCA method and/or with NanoDrop™ device.

3.3.4.1 via NanoDrop™

Protein concentration of samples dissolved in 1% SDS was assessed by NanoDrop™-1000. Therefore, the options “protein A280” and “BSA” were chosen to assess concentration and purity of protein.

Prior to measurements, device was blanked with pure 1% SDS. To avoid too high protein concentrations, 1:5 dilutions of protein samples were prepared. 2 µl of these dilutions were pipetted onto the lower measurement pedestal and measurement was started 5 times in a row. The resulting protein concentration was averaged for each sample.

3.3.4.2 via PCA assay

Protein dissolved in RIPA buffer were quantified by ROTI® Quant universal from Roth. This quantification method is based on a biuret reaction where Cu^{2+} ions were reduced to Cu^{+} ions. Whit a cooper-specific colorimetric enhancer reaction, the color change is then direct proportional to the protein concentration of the sample. Resulting cooper-protein-complexes are highly absorbing with a maximum at 503 nm.

To receive a standard curve, serial dilution of BSA from 2,000 mg/ml to 1.95 mg/ml was prepared. Therefore, BSA was weighted in to receive a 2,000 mg/ml stock solution and was dissolved in RIPA buffer. To receive a 1,000 mg/ml solution, equal amounts of the 2,000 mg/ml stock solution and RIPA buffer were combined. For solutions of 500 mg/ml to 1.95 mg/ml, procedure was similar with the next higher concentration, respectively.

1.5 µl of the samples as well as 1.5 µl of the standard curve were incubated with 10 µl of the working solution, consisting of 15/16 parts of reagent 1 and 1/16 part of reagent 2 of the ROTI® Quant solutions. To avoid pipetting errors, samples and standard were prepared in duplicates. Since the reaction is rather a continuous one then an endpoint measurement, samples were incubated for 30 min at 37° C.

Therefore, the measurement parameter of the NanoDrop™-1000 device were set to measure protein at 503 nm. Prior to measurements, device was blanked with pure RIPA buffer. Then, 2 µl of each standard-ROTI® Quant-mixture were pipetted onto the lower measurement pedestal measured and defined as the corresponding concentrations. Subsequent, samples solutions were also measured, and their concentration was calculated according to the just now created standard curve.

3.3.5 Western Blotting

Protein synthesis of *in vitro* treated cells was assessed by Western Blot technique. The first step is an SDS polyacrylamide gel electrophoresis which takes the advantage that proteins can be separated according to their molecular weight within an electric field. Thereafter, proteins were transferred onto a PVDF membrane and proteins could be detected by specific antibody-antigen-interaction.

3.3.5.1 SDS polyacrylamide electrophoresis

To pour an SDS polyacrylamide gel, two glass panels were put together, while spacer arrange an area of 10 cm² containing space for 5 ml running gel as well as 1 ml stacking gel. Glass panels were put into a frame from PeqLab and the lower aperture was covered. The running gel was poured as shown in **Table 19** while its porosity can be addressed by the percentage of the single components. After polymerization, the stacking gel was poured on top. With the help of a comb, ten pockets were built for the loading of protein samples. After another polymerization step, the frame was put into a tub and filled with electrode buffer.

solution	running gel (12%)	stacking gel
dH_2O	1.6 ml	680.0 µl
acrylamide mix, 30%	2.0 ml	170.0 µl
Tris 1.5 M, pH 8.6	1.3 ml	-
Tris 1.0 M, pH 6.8	-	130.0 µl
SDS, 10%	50.0 µl	10.0 µl
APS, 10%	50.0 µl	10.0 µl
TEMED	2.0 µl	1.0 µl

Table 19: Volume for running and stacking gels for SDS polyacrylamide electrophoresis.

The gel was loaded with 20 µg of each protein sample and Laemmli buffer was added in a 1:5 ratio. Laemmli buffer was freshly prepared with β-mercaptoethanol and DTT as mention in **Table 14**. This additional dye allows for tracking how far the separation will be progressing. Samples were cooked for 5 min to allow for protein denaturation and shortly centrifuged. Thereafter, they were placed into the gel's pockets by the use of a Hamilton® syringe. In an additional pocket, 5 µl of EZ-RUN Pre-Stained Rec

Protein Ladder from Fisher Scientific were added. Later, this will allow for the determination of the molecular weight. The gel within the buffer bath was connected to a power supply and was electroporated at 20 mA and 300 V for 1 hour.

3.3.5.2 Protein blotting on PVDF membrane

PVDF membranes with a pore size of 0.45 µm were used and a piece of 7 x 9 cm² was dunked into 100% methanol for activation.

3.3.5.2.1 via semidry blot

The semidry blotting method was used for a successful transfer of proteins up to a molecular weight of 100 kDa. Therefore, the SDS gel was released from the glass panels and placed into a blotting stack as shown in **Figure 7**. The stack was sucked with transfer buffer and air bubbles were removed. Semidry blot was performed in an apparatus from PeqLab, where the power was flatwise to the blotting stack. The blotting was performed for 45 min at 14 V and 3 mA per cm² of membrane.

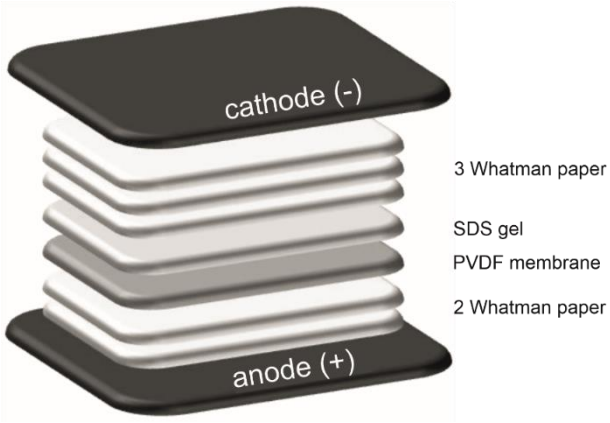

Figure 7: Composition of a semidry blotting stack for Western Blot.

3.3.5.2.2 via tank blot

To ensure that proteins bigger than 100 kDa were transferred effectively from the gel onto the membrane, tank blot transfer was performed. Therefore, the blotting stack was composed as shown in **Figure 8** and placed in another blotting apparatus from PeqLab (Erlangen, Germany), containing an excess amount of transfer buffer. Fluid was chilled and circulated to avoid an overheating of the system. Proteins were blotted overnight for 15 hours at 30 V and 60 mA.

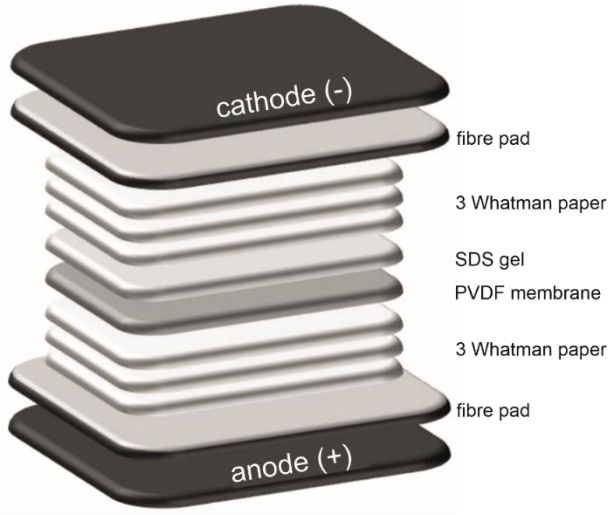

Figure 8: Composition of a tank blotting stack for Western Blot.

3.3.5.3 Detection of proteins

Before protein detection, membrane was blocked immediately after transfer in a 5% blocking solution of bovine serum albumin (BSA) or milk powder (MP) for 1 hour at RT. Thereafter, a specific primary as well as secondary antibody was used as listed in **Table 20**.

protein	blocking	primary antibody	secondary antibody
CTGF (35 kDa)	5% MP in 0.1% TBS-T 1 hour at RT	rabbit anti CTGF 1:500 in 5% MP in 0.1% TBS-T overnight at 4° C	anti rabbit HRP 1:2,000 in 5% MP in 0.1% TBS-T 1 hour at RT
eNOS (130 kDa)	5% BSA in 0.05% TBS-T 1 hour at RT	rabbit anti eNOS 1:500 in 0.5% BSA in 0.05% TBS-T 3 hours at RT, thereafter overnight at 4° C	anti rabbit HRP 1:2,000 in 0.5% BSA in 0.05% TBS-T 1 hour at RT
α-tubulin (55 kDa) loading control	n/a	rabbit anti α-tubulin 1:2,000 in 0.5% BSA or MP in 0.05% TBS-T overnight at 4° C	anti rabbit AP 1:2,000 in 0.5% BSA or MP in 0.05% TBS-T 1 hour at RT

Table 20: Blocking solutions and antibody dilutions for Western Blot.

In between incubation steps, membranes were washed three times with a TBS-T solution for 10 min each. The TBS-T solution contained 0.1% Tween-20 for CTGF Blots and 0.05% for eNOS Blots. Before developing AP signal, membranes must be incubated in detection buffer for 5 min, additionally.

Secondary antibodies were coupled to HRP or AP. When incubated 5 min with the corresponding developer in the dark (Luminata for HRP or 1:100 in detection buffer diluted CDP-Star for AP), both enzymes catalyze a chemical reaction and the thereby emitted chemiluminescence was detected with an LAS 3000 imager (Fujifilm, Tokyo, Japan).

The amount of protein of interest was calculated relative to that of α-tubulin which functioned as loading control.

3.3.6 Enzyme-linked Immunosorbent Assay (ELISA)

To detect eNOS with a more sensitive approach, ELISA was performed according to manufacturer's instructions. Plates were prepared the day before further investigations. Therefore, the capture antibody was diluted to the working concentration of 1.00 µg/ml in PBS. With 100 µl per well, plate was coated immediately thereafter, sealed, and incubated overnight at RT.

At the next day, the plate was washed three times with wash buffer. Since the provided wash buffer was a 25x concentrate, 1 ml must be diluted with 24 ml dH_2O before use. For washing, the solution was aspirated from each well while complete removal of any liquid was essential for excellent performance. Blotting the plate against a clean Kimtech towel was very helpful.

Next, the plate was blocked with 300 µl reagent diluent per well and incubated for 1 hour at RT. Since this eNOS ELISA required a concentration of 1% BSA in PBS, the provided reagent diluent concentrate was diluted 1:10 in dH_2O before use. Thereafter, the washing step was repeated.

Then, 100 µl of sample or standard - diluted in reagent diluent - were applied in duplicates. The recombinant human eNOS standard was applied from 1,250 pg/ml to 19.5 pg/ml. Sealed with an adhesive strip, plate was incubated 2 hours at RT. Thereafter, the washing step was repeated one more time.

Next, the detection antibody was diluted with reagent diluent to its working concentration of 200 ng/ml and 100 µl were added to each well. After sealing, the plate was incubated another 2 hours at RT. Furthermore, the washing step was repeated.

To detect signal, 100 µl of a 40-fold dilution of Streptavidin-HRP in reagent diluent was added to each well. Then, the plate was covered one more time and incubated for 20 min at RT in the dark. For one last time, the washing was repeated.

To develop signal, 100 µl of substrate solution - consisting of a 1:1 mixture of color reagent A and B - must be added to each well. For incubation, the plate was place further 20 min at RT into the dark. Thereafter, the fluid was not removed.

Finally, 50 µl of stop solution was added to each well. By gentle tapping, substrate and stop solutions were mixed, and color changed from pink to yellow.

The optical density was determined immediately thereafter with the Sunrise ELISA reader from Tecan (Grodig, Austria). Wavelength was set to 450 nm and wavelength correction to 540 nm. Protein concentration was calculated according to the standard curve created from the eNOS standard.

3.4 Expression analysis

3.4.1 RNA isolation

Derived from *in vitro* cell culture experiments, RNA was either isolated as total RNA, or small RNA were enriched for the analysis of miRNA. The following two chapters will outline both methods.

3.4.1.1 of total RNA with peqGold TriFast™ method

By phase separation after the addition of chloroform, the peqGold TriFast™ method allows for protein and RNA isolations in parallel. Since samples derived from 6 and 96 wells, different amounts of reagents were required, and corresponding amounts are listed in **Table 21**.

reagent	6 well	three 96 wells
peqGold TriFast™	500 µl	3x 100 µl
chloroform	100 µl	60 µl
100% isopropanol	250 µl	150 µl
75% ethanol	500 µl	300 µl
RNase-free H_2O	10 µl	10 µl

Table 21: Required amounts of reagents for peqGold TriFast™ RNA isolation.

After transferring the aqueous phase into a fresh tube (see section 3.3.2.1), ice-cold 100% isopropanol was added. RNA precipitation was forced by incubation overnight at -20° C. At the following day, samples were centrifuged for 20 min at 12.000 g and 4° C and RNA was pelleted.

To wash the RNA pellet, the supernatant was removed, and 75% ethanol was applied two times. Between washing steps, samples were vortexed and centrifuged at 12,000 g and 4° C for 10 min. Subsequently, the supernatant was removed.

Finally, the RNA pellet was dried until the rest of ethanol was volatilized. Thereafter, the pellet was dissolved in RNase-free dH_2O. Pipetting it up and down was sufficient to dissolve the pellet. Samples were then stored at -80° C for future use.

3.4.1.2 of miRNA with mirVana™ miRNA Isolation Kit

The mirVana™ miRNA Isolation Kit was designed to purify RNA suitable for miRNA investigations. According to manufacturer's instructions, cells derived from *in vitro* treatment were put on ice and lysed in 600 µl Lysis/Binding solution per 6 well. By the help of a cell scraper, cells were completely removed from the dish and transferred in a fresh tube. By vortexing, cells were further disrupted.

The organic extraction started with adding 60 µl of miRNA Homogenate Additive and vortexing. After being left on ice for 10 min, 600 µl Acid-Phenol:Chloroform was added, which must be absorbed from the lower, organic phase from the stock. By vortexing 60 sec and 5 min centrifugation at 10,000 g at RT, phases separated. If the interphase was not compact, the centrifugation step must be repeated.

To enrich small RNAs, a low concentration of ethanol will be used to immobilize large RNA on a filter. The flow-through was therefore containing mostly small RNA species. By adding more ethanol, small RNAs will be caught on filter by passing the mixture through a second filter. Thereby, the small RNA gets immobilized, can be washed, and finally eluted.

Therefore, the upper, aqueous phase was transferred into a fresh tube and the amount must be noticed. To immobilized large RNAs, ⅓ of the volume of the aqueous phase was added of 100% ethanol. After vortexing, fluid was transferred onto a filter cartridge and was passed through by centrifugation. The amount of flow-through must be noticed since it was containing the small RNA fraction. Next, it was mixed with ⅔ of 100% ethanol and vortexed. The flow-through/ethanol mixture was then brought onto a fresh filter cartridge. By centrifugation, small RNA was caught on the glass-fiber filter and flow-through was disposed.

To wash the immobilized small RNA fraction, 700 µl miRNA Wash Solution 1 was used. It was pipetted onto the filter and passed through by centrifugation. Once more, the flow-through was disposed and washing was repeated twice with 500 µl miRNA Wash Solution 2/3. Thereafter, the filter was placed into a fresh collection tube. Preheated, 95° C hot dH_2O was used to eluate the small RNA in a total volume of 100 µl by a 30 sec centrifugation step. After a second elution step was performed, small RNA can be stored at -80° C for future use.

3.4.2 RNA quantification

Large RNA was quantified by NanoDrop™ device from Thermo Fisher while small RNA was investigated via Agilent 4200 Tape Station System.

3.4.2.1 via NanoDrop™

To blank the system, 1 µl dH_2O was used. Thereafter, 1 µl of each sample was analyzed and the absorption spectrum was determined. With the absorption maximum at 260 nm for RNA, RNA concentration was determined. If the A260/A280 quotient was around 2.0, RNA was desired to be pure.

3.4.2.2 via Agilent 4200 Tape Station System

With the Agilent High Sensitivity RNA ScreenTape Assay, not only small RNA concentration but also its integrity can be determined. Sample buffer must be equilibrated at RT for 30 min. Thereafter, 1 µl of sample buffer was added to 2 µl of RNA and 2 µl of High Sensitivity RNA ScreenTape Ladder was used as well. RNA should have a maximal concentration of 10 ng/µl in total, otherwise its amount would exceed the system's capacity and RNA concentration might not be calculated exactly. Therefore, also small RNA was measured initially to Tape Station analysis with the NanoDrop™ device as described above for large RNA.

The RNA/sample buffer mixture must be centrifuged shortly before vortexing it 60 sec at 2,200 rpm. Thereafter, it was again centrifuged shortly and then kept at 72° C for 3 min to allow for denaturation. After being placed on ice for 2 min, the standard protocol for small RNA was run by the 4200 TapeStation System. It determined not only RNAs concentration but also its integrity by the RIN score which would be perfect if it reaches 10.

3.4.3 cDNA synthesis

By cDNA synthesis, RNA can be reverse transcribed to cDNA (complementary DNA) which is less susceptible for degradation than RNA. By initially determining RNAs concentration, one made sure to transcribe similar amounts of RNA.

3.4.3.1 of mRNA with qScript™ cDNA Synthesis Kit

Table 22 lists the reagents for cDNA synthesis of mRNA. While samples contained reverse transcriptase (+RT), negative controls were left without (-RT). Thereby, genomic DNA concentration can be excluded.

reagent	+RT	-RT
RNase-free H_2O	fill up to 20 µl	fill up to 20 µl
qScript™ 5x Reaction Mix	4 µl	-
qScript™ Reverse Transcriptase (RT)	1 µl	-
RNA	100 to 500 ng	100 to 500 ng

Table 22: PCR approaches for cDNA synthesis.

In **Table 23**, the cycling protocol for cDNA synthesis is listed. cDNA can be stored at -20° C.

temperature	duration
22° C	5 min
42° C	30 min
85° C	5 min

Table 23 PCR program for cDNA synthesis from mRNA.

3.4.3.2 of miRNA with TaqMan Advanced miRNA cDNA Synthesis Kit

For cDNA synthesis from small RNA, more steps were needed. All of them were performed with reagents of the TaqMan Advanced miRNA cDNA Synthesis Kit form Thermo Fisher Scientific.

In a first step, a poly(A) tail was ligated to the 3' end of miRNAs. Therefore, 2 µl RNA was added to a 3 µl master mix, consisting of 0.5 µl 10x poly(A) buffer, 0.5 µl ATP, 0.3 µl poly(A) enzyme and 1.7 µl RNase-free H_2O per sample. After short vortexing and centrifugation, poly(A) tailing was performed following the program displayed in **Table 24**.

step	temperature	duration
polyadenylation	37° C	45 min
stop reaction	65° C	10 min
hold	4° C	infinite

Table 24: PCR program for the poly(A) tailing step of cDNA synthesis from miRNA.

Next, an adaptor was ligated towards the processed miRNA. After poly(A) tailing, 10 µl of a master mix was added to the poly(A) reaction mix. The master mix consisted of 3.0 µl 5x DNA ligase buffer, 4.5 µl 50% PEG 8000, 0.6 µl 25x ligation adaptor, 1.5 µl RNA ligase and 0.4 µl RNase-free H_2O per sample. After short vortexing and centrifugation, adaptor ligation was performed as shown in **Table 25**.

step	temperature	duration
ligation	16° C	60 min
hold	4° C	infinite

Table 25: PCR program for the adaptor ligation step of cDNA synthesis from miRNA.

Thereafter, the PCR product was revere transcribed. Even though processed miRNA fragments are still short, transcription can be initialized from the previously ligated

adaptors. Therefore, the ligation mix was mixed with 15 µl master mix (consisting of 6.0 µl 5x RT buffer, 1.2 µl dNTP mix (25 mM each), 1.5 µl 20x universal RT primer, 3.0 µl 10x RT enzyme mix and 3.3 µl RNase-free H_2O per sample). After vortexing and centrifugation, reverse transcription was performed as displayed in **Table 26**.

step	temperature	duration
reverse transcription	42° C	15 min
stop reaction	85° C	5 min
hold	4° C	infinite

Table 26: PCR program for the reverse transcription step of cDNA synthesis from miRNA.

The product of this reverse transcription step can be stored at -20° C for up to 2 months. To receive material for TaqMan experiments, cDNA from miRNA must be further processed by miRNA amplification. Therefore, a 45 µl reaction mix, consisting of 25.0 µl 2x miR-Amp master mix, 2.5 µl 20x miR-Amp primer mix and 17.5 µl RNase-free H_2O per sample, was pipetted towards 5 µl of the reverse transcription product in a fresh tube. After vortexing and centrifugation, miRNA amplification was performed following the program displayed in **Table 27**.

step	temperature	duration	cycles
enzyme activation	92° C	5 min	
denaturation	95° C	3 sec	14x
annealing and extension	60° C	30 sec	
stop reaction	99° C	10 min	
hold	4° C	infinite	

Table 27: PCR program for the miRNA amplification step of cDNA synthesis from miRNA.

3.4.4 Expression analysis

The RT-qPCR bases on the principle of the PCR, whereby the distinct amount of amplificated DNA can be detected by the help of fluorescence in real-time. Another feature is that not DNA, but cDNA - reverse transcribed from RNA - is analyzed. Thereby, RT-qPCR allows for statements about expression rates of genes. To make sure that there are no inaccuracies due to pipetting, values were calculated relative to a reference gene.

The applied fluorescent dye intercalates in double-stranded DNA and thereby changes its absorption spectrum. The intensity of the emitted light was thereby directly proportional to the amount of cDNA which was amplified during the PCR. If conditions were perfect (good working enzyme, sufficient dNTPs, etc.), cDNA amount doubles with exponential progression. The cycle threshold (c(t)) describes the entrance into this phase. The less cycles were required to reach this threshold, the more cDNA was

initially present. To avoid that also genomic DNA gets amplificated, primer must be designed spanning intro-exon-borders. Thereby, only cDNA made of mRNA - which does not have introns - was amplified.

3.4.4.1 of mRNA via quantitative real-time PCR

For RT-qPCR, cDNA - processed as described at 3.4.3.1 - was used. As shown in **Table 28**, a mixture of 10 µl was pipetted onto a 96 well plate. Per well, 5 µl of a primer solution was added to a final concentration of 300 nM. This primer solution contained as well forward as revere primer and RNase-free H_2O. A negative control - containing water instead of +RT or -RT cDNA - was added to exclude contaminations.

reagent	with +RT	with -RT	with H_2O
RNase-free H_2O	1.0 µl	1.0 µl	1.3 µl
Takyon mix	7.5 µl	7.5 µlµl	7.5 µl
cDNA	0.3 µl	0.3 µl	-

Table 28: Required amounts of reagents for RT-qPCR.

To exclude inaccuracies due to pipetting, samples were analyzed in triplets. The 96 well plate was sealed with a transparent cover and by centrifugation, all components were brought together. As shown in **Table 29**, RT-qPCR was performed in a CFX cycler from Bio-Rad.

temperature	duration	cycles
95° C	3 min	
95° C	10 sec	50x
60° C	1 min	
95° C	1 min	

Table 29: PCR program for RT-qPCR.

To generate a melting curve of the RT-qPCR products, temperature was increased after RT-qPCR cycling from 55° C to 95° C, stepwise by 0.5° C. Thereby, double-stranded RT-qPCR products melted, and fluorescence decreased proportional. By differentiation with respect to the temperature, a graph can be generated. If products were pure, only one peak at the corresponding melting temperature of the RT-qPCR product was detected.

From the c(t) values of the triplets, the average and the standard error of the mean (SEM) were calculated. The average of the gene of interest was examine relative to that of a reference gene. Furthermore, values of treatment were normed to that of controls.

3.4.4.2 of mRNA and miRNA via TaqMan Assay

Since miRNA fragments are small - even after being processed to cDNA as shown at 3.4.3.2 - no RT-qPCR can be performed. Alternatively, another method named TaqMan was developed in the recent years.

Thereby, a TaqMan probe anneals specifically to its complementary sequence. At this status, the probe is intact and the proximity of reporter and quencher dye results in suppression of the reporter fluorescence. The probe site is located between those of forward (fwd) and revers (rev) primers. By the enzymatic activity of DNA polymerase, hybridized probes get cleaved and thereby, the reporter dye separates from the quencher dye. This separation results in increased fluorescence by the reporter.

As shown for RT-qPCR, every cycle of PCR amplification increases cDNA amount and thereby fluorescence. The earlier the specific fluorescent signal emerges from background, the more of this specific cDNA was initially present. Furthermore, values were calculated relatively to that of a reference miRNA.

cDNA was used in a 1:10 dilution with dH_2O and 5 µl were used per well. As a negative control, an approach without cDNA but dH_2O was performed. Furthermore, 15 µl of a master mix as shown in **Table 30**, containing miRNA probe, was added to each well.

reagent	amount
2x TaqMan Fast Advanced Master Mix	10.0 µl
RNase-free H_2O	4.0 µl
miRNA Sonde	1.0 µl

Table 30: Required amounts of reagents for TaqMan.

As by RT-qPCR, plates were sealed and shortly centrifuged. Thereafter, TaqMan were performed as shown in **Table 31**. To avoid inaccuracies due to pipetting, approaches were performed in triplets.

temperature	duration	cycles
95° C	3 min	
95° C	10 sec	50x
60° C	1 min	

Table 31: PCR program for TaqMan.

Since fluorescence of TaqMan products does not come from the integration of a dye into double stranded cDNA, no melting curve can be performed. The purity of the products must be created by a probe design that is specifically complementary to the target sequence.

3.4.4.3 of miRNA via Northern blot

Northern Blot experiments were performed according to an established protocol of the Department for Biochemistry I. According to this, a 12% denaturing polyacrylamide gel must be prepared. For a 60 ml gel, 28.8 ml of the concentrate, 25.2 ml of the diluent and 6.0 ml of 10x TBE buffer are required. After gentle mixing, 300 ml 10% APS and 30 µl TEMED were added. Gel was poured into an apparatus and a comb was inserted to generate 12 chambers. Thereafter, the gel could settle for at least 30 min.

MiRNA samples should contain 15 µg of RNA and was combined with the same amount of RNA loading dye. Initially, the gel should pre-run in 1x TBE at 350-400 V with a metal plate attached behind for approximately 20 min. This step was important to warm up the glass plates which was important to keep the RNA in a linear form. After the pre-run was finished, miRNA samples must be heated for up to 5 min at 95° C. Furthermore, the gel chambers must be extensively washed to get rid of the urea by a 1x TBE filled syringe. This cleaning step should be repeated immediately prior to loading the sample.

After samples and standard were loaded on the gel, the gel was run at constant 400 V. The gel should run until the lower dye was migrated for 6 to 7 cm which took approximately 1 hour. To control the loading, an ethidium bromide staining was performed. After disassembling the gel, it was put into a 1:20,000 ethidium bromide solution in 1x TBE. After 10 min on the shaker, a picture can be taken, and degraded miRNA would be recognized.

For Northern Blotting, a blotting stack as shown in **Figure 9**, was prepared. Northern Blot was performed at 20 V for 30 min.

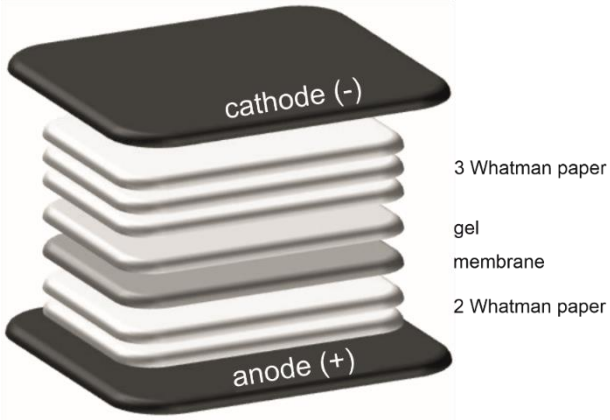

Figure 9: Composition of a blotting stack for Northern Blot.

The crosslinking solution was prepared by 61.25 µl 1-methylimidazol, 2.25 ml dH_2O and solution was adjusted to pH 7.5 using approximately 75 µl 1 M HCl. Immediately before use, 188 mg EDC was added and filled up to 6 ml with dH_2O. Fresh Whatman paper were sucked with crosslinking solution and distributed equally. Excess solution was removed with a towel. Thereafter, membrane was put onto those Whatman paper with the RNA side facing up. Membrane was put into the hybridization oven for 1 hour at 50° C.

By rinsing the membrane three times for 20 sec with dH_2O, the crosslinking solution was removed. While all so far mentioned steps were performed in the laboratory, the following steps must be performed in an isotope laboratory.

To label the miRNA probes, a solution as mentioned in **Table 32** was prepared for every probe, equal if miRNA of interest or reference miRNA.

reagent	amount
oligodeoxynucleotide, 20 µM	1.0 µl
10x PNK buffer A	2.0 µl
PNK	1.0 µl
dH_2O	14.0 µl
g-32P-ATP, 20 µCi	2.0 µl

Table 32: Required amounts of reagents for labeling miRNA probes from Northern Blot.

The solution was incubated at 37° C for 1 hour. By adding 30 µl EDTA (30 mM), the reaction was stopped. Furthermore, the solution was purified by gel filtration columns to get rid of free g-32P-ATP.

Thereafter, the hybridization was performed. Therefore, all solutions must be pre-heated to 50° C to avoid precipitation of SDS. The membrane was transferred into a flask (with the RNA site facing towards the inside) and hybridization solution was added. Furthermore, the labeled probe was added. Thereby, it must have been taken care not to pipet directly onto the membrane but into the solution. For hybridization, membrane was incubated over night at 50° C under rotation.

At the next day, membrane was washed after hybridization solution was completely removed. It was washed two times with 30 ml wash solution 1 and one time with 30 ml wash solution 2. Thereafter, exposure was performed.

If further investigations should be performed, the membrane must be stripped. Therefore, the membrane was put back into a flask and washed twice with boiling

0.1% SDS solution in dH_2O for 10 min each. Thereafter, it was washed once more with boiling dH_2O.

3.5 Biomolecular methods

3.5.1 Isolation of genomic DNA

To genotype animals, tissue punches were taken from the ear under an isoflurane® anesthesia by the age of 3 weeks. The position of the punch was also used to identify individual animals within one cage. **Figure 10** shows the scheme used in our laboratory following Dickies suggestions.

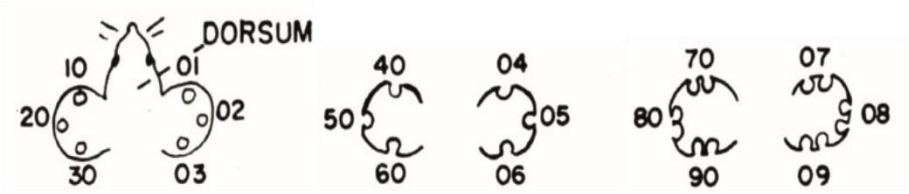

Figure 10: Punching code for identification of animals (Dickie 1975).

Punches were lysed overnight at 55° C in 100 µl digestion buffer and 2.5 µl proteinase K in a shaking thermal cycler. The following day, proteinase K was inactivated at 95° C for 10 min and the lysate was centrifuged for another 10 min at full speed to pellet the non-lysed debris. Deoxyribonucleic acid (DNA) was present in the supernatant and was stored at 4° C.

3.5.2 Genotyping of animals

To discriminate transgenic mice from WT littermates, DNA from ear punches was assessed by genotyping PCR. PCR is a method to manifold a specific DNA fragment wherefore Kary B. Millis received the Nobel prize for chemistry in 1993. Two single-stranded, about 20 nucleotide-long fwd and rev primer are used with a complementary base sequence to the flanks of the fragment of interest. When the initial DNA double-strand gets denatured by heat, primer anneal sequence-specifically to that sequence. Beginning on that double-stranded primer-DNA-hybrid and with the help of a heat-stable DNA polymerase, double-stranded DNA can be synthesized with deoxynucleotide triphosphates (dNTPs) according to the DNA matrix. Those steps must be cyclically repeated to achieve exponential multiplication of the initial material.

To genotype animals of the βB1-CTGF strain, two PCRs with primers detecting the chicken βB1 promotor in front of the CTGF construct (Reinehr et al. 2019) as well as

one with a primer pair that spans from the SV40 small T-intron to the polyA-sequence at the end of the transgenic construct (Junglas et al. 2012). In **Table 33**, approaches for both PCRs are shown. To allow for an internal control, both PCRs were combined with primers detecting a 161 bp fragment of WT decorin (DCN) (Danielson et al. 1997). Thereby, one was sure to have loaded sufficient amount and quality of DNA. Otherwise, a failed detection of the βB1 or SV40 construct would erroneously be classified as WT.

reagent	βB1 PCR	SV40 PCR
H_2O	5.55 µl	5.55 µl
10x Q buffer	1.50 µl	1.50 µl
1:10 diluted fwd βB1 primer	0.30 µl	-
1:10 diluted rev βB1 primer	0.30 µl	-
1:10 diluted fwd SV40 primer	-	0.30 µl
1:10 diluted rev SV40 primer	-	0.30 µl
1:10 diluted fwd DCN primer	0.15 µl	0.15 µl
1:10 diluted rev DCN primer	0.15 µl	0.15 µl
10 µM dNTPs	0.30 µl	0.30 µl
25 mM $MgCl_2$	0.15 µl	0.15 µl
5x glycerol	3.00 µl	3.00 µl
A taq	0.60 µl	0.60 µl

Table 33: Required amounts of reagents for PCR approaches for genotyping βB1-CTGF mice.

12 µl of the PCR approach were combined with 3 µl of genomic DNA. A transgenic animal functioned as positive control while an approach lacking DNA (containing 3 µl of H_2O instead) served as negative control.

Table 34 shows the cycling program that was performed with all samples. Since the PCR products of βB1 and SV40 PCR were approximately of the same size and the same DNA taq was used, the cycling program was the same for both PCRs.

temperature	duration	cycles
94° C	2 min	
94° C	30 sec	35x
55° C	30 sec	
72° C	45 sec	
72° C	5 min	
10° C	∞	

Table 34: PCR program for genotyping βB1-CTGF mice.

3.5.3 Agarose gel electrophoresis

Electrophoresis is a technique to separate negatively charged, linear DNA according to its size, following an electric field in a porous agarose gel. The smaller a DNA fragment, the faster it moves through the porous gel and the other way around. Hence, a bigger fragment gets less far in the same time span. By adding ethidium bromide to

the gel, it intercalated into double-stranded DNA and thereby changes its absorption spectrum. Thereby, DNA becomes visible under UV light.

For a 2% gel, 2 mg agarose were solubilized in 100 ml TBE buffer by microwave heating. After chilling the liquid to avoid cancerogenic vapor, 3 µl ethidium bromide were added to a final concentration of 50 ng/ml. The liquid was poured into a frame and a comb was inserted to provide pockets for sample loading. After the gel was hardened, the comb was removed, and the gel was placed in an electrophoresis chamber filled with TBE buffer.

The first pocket was filled with 2 µl of the 100 bp Gene Ruler as DNA marker. Since with reddish 5x glycerol, the samples already contained stain and weight, following pockets were filled with 15 µl of PCR product without further additions. To fragment the DNA, electrophoresis was performed for 30 min at 120 V. Thereafter, the agarose gel was put onto an UV shield and PCR products were detected and documented by taking a photo of the PCR result.

All sufficiently lysed biopsies should provide the 161 bp fragment. If that internal positive control signal was missing, genotyping must be repeated. Animals showing a 360 bp fragment after the βB1 PCR as well as a 300 bp fragment after the SV40 were considered transgenic while animals missing those bands were declared WT.

3.6 Preparation of animal tissue

3.6.1 Measurement of intraocular pressure

From earlier studies of our working group, it is known that transgenic mice of the βB1-CTGF strain develop POAG-like changes due to their CTGF overexpression (Junglas et al. 2012). To investigate if the CTGF effect is consistent within different genetic backgrounds, IOP was measured with the help of rebound tonometry. Different genetic backgrounds were investigated at different ages while the focus was set on 4, 8, 12 and 15 weeks as well as the age of 1 year.

Therefore, mice were anesthetized with the help of an isoflurane® evaporator and the duration and depth of torpidity were kept the same for all animals of an experiment. The tonometer pin was placed upright towards the center of the cornea and measurement was started. By rebound tonometry, one measures the force, the eye subtends towards the pin when it hits the cornea. The higher the IOP, the bigger the

counteracting force the pin detects. The TonoLab tonometer from Icare Finland calculated the mean of a series of measurements, thereby indicating how much the single measurements diverged. Only values with little divergence were included into analysis. Finally, the mean value of several measurements per eye was calculated and IOP of transgenic animals was compared to WT IOP.

3.6.2 Preparation of murine eyes

All procedures including animal tissue were conformed to the tenets of the National Institutes of Health Guidelines on the Care and Use of Animals in Research.

Eyes from βB1-CTGF mice with a pure CD1 background were taken at the age of 15 weeks to investigate changes in the retina. To fixate the tissue, PFA was used, which cross-links the tissue's proteins. Since its penetration depth is restricted, incubation in a PFA bath alone is not sufficient. The fixative was brought via the blood system directly into the tissue.

3.6.2.1 PFA-fixation

To isolate tissue, mice were anesthetized with a mixture of Ketamine (75 mg/ml) and Xylazine (5 mg/ml). The thorax was opened, and the heart was punctured into the left ventricle. A solution of 0.89% $NaCl_2$, containing heparin (1:1000), was perfused into the circulatory system. An incision into the right atrial auricle allowed for tension relief. Thereby, the blood with its auto-fluorescent erythrocytes, was removed. Thereafter, a 4% PFA solution in 0.1 M phosphate buffer (Php) was used to fixate the tissue.

Eyes were enucleated and incubated in 4% PFA overnight at 4° C. For better penetration, a hole was cut into the cornea after the first hour of fixation.

3.6.2.2 Embedding

To produce cryo sections, eyes must be dehydrated by a series of increasing sucrose concentrations. After three initial washing steps with 0.1 M Php for 20 min each, eyes were incubated in 10%, 20% as well as 30% sucrose (in 0.1 M Php) for at least 4 hours each.

As embedding medium for perfused and dehydrated eyes, Tissue-Tek from Sakura was used. By the help of a binocular, eyes were brought into a horizonal position. Surrounded by Tissue-Tek, eyes were held in fluid nitrogen which freezes and hardens the Tissue-Tek. Blocks were stored at -20° C until cutting.

3.6.2.3 Cryo sectioning

Of the embedded eyes, 12 µm thin sagittal sections were produced. To avoid defrosting, sectioning was done in a cryostat at -20° C. Sections were put onto object slides and used for histological staining (see 3.7.1).

3.6.3 *Ex vivo* perfusion of porcine eyes

Porcine eyes derived from a local abattoir. Carried on ice, experiments were performed soon after slaughtering. Eyes with defects as those of cornea epithelium were excluded. Palpebra, extraocular muscles and other remaining tissue was removed while the integrity of the bulbus was kept intact.

3.6.3.1 Perfusion with gold nanoparticles

Eyes were placed onto gaze facing upwards at 35° C in a water bath and were surrounded by 0.89% $NaCl_2$. One needle, connected to the perfusion chamber, was inserted into the anterior chamber, and placed behind the iris. A second needle was placed into the anterior chamber to allow for the exchange of the AH. Therefore, it was connected to a collection reservoir and only open during exchange steps.

Initially, both parts of the system were filled with a 5 mM glucose solution in PBS, providing sufficient nutrients to keep the tissue alive. To avoid air bubbles, glucose solution was outgased in an ultrasonic bath. First, the AH was replaced be an excess amount of glucose, then, the glucose was replaced by the AuNP solution.

Ex vivo perfusion experiments were performed at 10 mmHg, which was adjusted by a height difference of the eye's limbus and the solution column in the perfusion reservoir. During the 3 hours of perfusion, eyes were perfused via the natural AH outflow pathway. Thereafter, AuNP solution was replaced by an excess amount of glucose and perfusion was performed another 2 hours to flush the outflow pathway.

3.6.3.2 Preparation of tissues of the anterior chamber

To investigate the gold content of distinct tissues of the anterior chamber, eyes were dissected after perfusion. The bulbus was opened along the equator and vitreous was removed. The lens was the first tissue to be collected and could be easily captured by forceps. Next, the anterior chamber was cut into two pieces. By an incisura, the iris was cut off and collected, too. Furthermore, the ciliary body was removed by a micro-scissor and collected as well.

At that point, tiny slices of the remaining cornea-scleral tissue - containing the TM and the aqueous plexus (AP) - was isolated and fixed for transmission electron microscopy (TEM) experiments (see 3.6.3.3). A piece of each quarter was taken to cover the different outflow areas at its best.

Thereafter, the TM was isolated from the four remaining pieces. By tiny cuts, it was restricted and could be extracted by forceps. Finally, the cornea was removed and collected as well. Tissue was frozen at -80° C until further processed by ICP-MS, performed by our cooperation partners.

3.6.3.3 Epon embedding for semi thin sections

Cornea-scleral slices were fixed in EM fixans for 24 hours at 4° C and washed three times with 0.1 M cacodylate buffer for 20 min thereafter. Eye were further fixed in 1% osmiumtetraoxid and washed again with 0.1 M cacodylate buffer for 20 min.

By an ascending alcohol series of 70%, 80%, 90% and 100%, eyes were dehydrated and embedded thereafter. The standard protocol was a series of the following solutions: ethanol and acetone in a 1:1 ratio, 100% acetone, Epon and acetone in a 1:2 ratio, thereafter in a 2:1 ratio. Finally, 100% Epon was used. For hardening, eyes were incubated for 24 hours at 60° C and 48 hours at 90° C. For embedding, Epon stem A and stem B were used in a 1:1 ratio. Finally, 1 µm sections were performed by Angelika Pach and analyzed by TEM.

3.7 Histological techniques

3.7.1 Immunohistochemical staining of tissue sections with fluorescent dyes

To allow for the determination of the presence and the abundance of proteins, immunohistochemical staining of the murine retinae were performed.

Semithin sagittal sections were prepared as described at 3.6.2.3. After thawing, the object slides were washed in 0.1 M Php to remove the Tissue-Tek. To avoid unspecific antibody binding, slices were blocked 1 hour at RT with blocking solutions listed in **Table 35**. There, the corresponding antibody dilutions and their incubation times are listed as well. The object slides were kept in a wet chamber to avoid drying as well as in the dark to avoid fading.

To safe animal material, GS and GFAP as well as VIM and GFAP staining were performed as double staining. To avoid unwanted interaction of the secondary antibodies, GS or VIM staining must be performed before the GFAP staining.

protein	blocking	primary antibody	secondary antibody
GS	3% BSA, 0.1% Triton in 0.1 M Php 1 hour at RT	goat anti GS 1:250 in 1:10 diluted blocking solution overnight at 4° C	rabbit anti goat Cy3 1:2,000 in 1:10 diluted blocking solution 1 hour at RT
VIM	3% BSA, 0.1% Triton in 0.1 M Php 1 hour at RT	goat anti VIM 1:100 in 1:10 diluted blocking solution overnight at 4° C	biotinylated anti goat IIG 1:500 in 1:10 diluted blocking solution 1 hour at RT
			Streptavidin Alexa 555 1:1,000 in 1:10 diluted blocking solution 1 hour at RT
GFAP	2% BSA, 0.2% CWFG, 0.1% Triton in 0.1 M Php 1 hour at RT	chicken anti GFAP 1:2,000 in 1:10 diluted blocking solution overnight at 4° C	goat anti chicken Alexa 488 1:1,000 in 1:10 diluted blocking solution 1 hour at RT

Table 35: Blocking and antibody dilutions for immunohistochemical staining.

After the blocking as well as in between incubation steps with antibodies, slices were washed three times for 5 min with 0.1 Php, each. The last washing step consisted of a 5 min incubation in dH_2O. Thereafter, the slices were covered with fluorescent mounting medium (Mowiol) containing DAPI to stain nuclear DNA.

To exclude unspecific binding of the secondary antibodies, slices were stained without primary antibodies. Slices were incubated with 1:10 diluted blocking solution instead. Those slices were declared as negative controls. Additional to those negative controls without primary antibodies, controls must be performed to exclude interactions of the two secondary antibodies with the other primary antibody.

3.7.2 Labeling of cells with Phalloidin

SC cells and HUVECs were seeded onto glass coverslips and cultivated until they were 80% confluent. After DETA-NO treatment (see 3.2.2.1), medium was removed and cells were washed twice with PBS. Thereafter, cells on coverslips were fixed with chilled 4% PFA for 5 min and washed twice with 0.1 M Php.

Phalloidin (order number: P1951-.1MG) was dissolved 1:1,000 in 0.1 M Php and incubated on the slides for 1 hour in the dark. Afterwards, coverslips were washed three times with 0.1 M Php and mounted with Mowiol (containing DAPI for nuclear

staining) onto a microscope slide. After slides were dried overnight, fluorescence was assessed by a fluorescent microscope.

3.7.3 Calcein-AM stain

With the Calcein AM kit (order number:4892-010-K) from Trevigen, cell viability and cytotoxity can be determined. According to manufacturer's information, Calcein AM is a non-fluorescent compound that easily permeates cell membranes of living cells. Intracellularly, Calcein AM gets hydrolyzed to calcein which is strongly fluorescent. Since the permeation into cells is an active transport, only viable cells were fluorescent within their cytoplasm.

Calcein AM is resuspended in DMSO to provide a 2 mM stock solution. Therefrom, a 2x Calcein AM working solution must be prepared by dilution with 1x Calcein AM Dilution/Wash Buffer. Per well, 50 µl will be required. The best fitting Calcein AM concentration ranges from 1 to 10 µM and must be determined for each cell type in preliminary experiments.

Adherent cells – ideally grown on black-welled plates - were cultured to appropriate confluence. Thereafter, medium was removed and 100 µl of 1x Dilution/Wash Buffer added. The Wash Buffer was removed and replaced by 50 µl of fresh 1x Calcein AM Dilution/Wash Buffer. Thereafter, 50 µl of freshly prepared 2x Calcein AM working solution was added to each well.

After an incubation step of 30 min under standard cell culture conditions, fluorescence was detected using a 490 nm excitation filter and a 520 nm emission filter. The fluorescence intensity was direct proportional to the number of viable cells.

3.7.4 Microscopy

Fluorescent microscopy was performed with *in vitro* treated cells as well as sagittal sections from murine eyes. Therefore, the Axio Imager Z1 microscope from Carl Zeiss (Göttingen, Germany) was used.

For investigations of the retina, images were made at a 40x magnification. Four pictures were taken from each slice while two were taken peripheral and two almost central, next to the papilla. Since 6 slices were investigated, a total of 24 images per animal were analyzed.

EM sample processing, cutting and evaluation of EM images were thankfully done by Angelika Pach.

3.8 Software and statistical analysis

For qPCR data analysis, the Bio-Rad CFX Manager 3.1 software was used and ΔΔc(t)-method was applied for normalization. Western Blot analysis was done with the Image Lab software from Bio-Rad (version 6.0.1, Feldkirchen Germany). ELISA and Griess Assay data were assessed by www.myassays.com.

Student's t-test was used for statistical analysis and significant outliers were identified by Grubbs' test. Data were presented a mean ± SEM. Level of significance was set to $p \leq 0.05$ and was indicated by *. Differences with $p \leq 0.01$ were indicated by ** and with $p \leq 0.001$ by ***.

4 Results

4.1 Analysis of a glaucoma mouse model overexpressing CTGF under a lens-specific promotor

Our working group established a transgenic mouse model, overexpression CTGF under a lens-specific promotor (βB1-CTGF). These mice have been shown to develop elevated IOP and a reduced number of optic nerve axons by age while showing no structural abnormalities in the iridocorneal angle. (Junglas et al. 2012)

While Junglas et al. investigated the βB1-CTGF mouse in a mixed FVB/N and CD1 background, this study addressed the question whether the glaucoma-causing effect of CTGF is ubiquitous but not specific for this mouse strain. Therefore, βB1-CTGF transgenic mice were bred into additional mouse strains.

4.1.1 Genotyping of transgenic βB1-CTGF mice and WT littermates

Independent of the genetic background, transgenic mice must be discriminated from WT littermates. Therefore, DNA from ear punches was assessed by genotyping PCR. After amplification and gel electrophoresis, mice carrying the transgenic construct had a 360 bp DNA fragment after βB1 PCR as well as a band at 300 bp after a SV40 PCR while WT littermates had no fragment at that height (**Figure 11**).

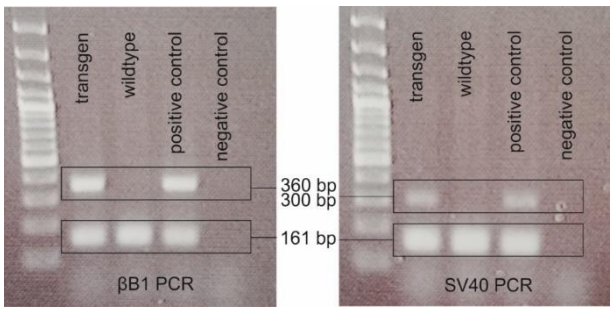

Figure 11: Detection of PCR products after agarose gel electrophoresis.

Transgenic animals show a 360 bp band after βB1 PCR as well as a band at 300 bp after SV40 PCR, while wildtype animals miss that signal. All DNA-containing samples must have the 161 bp fragment, functioning as internal control, while negative control, containing water instead of DNA, must lack any signal. As positive control, DNA of a securely transgenic animal was used. As standard, the 100 bp Gene Ruler was used.

To allow for an internal control, both PCRs were combined with primers detecting a 161 bp fragment of WT decorin (Danielson et al. 1997). By detecting any WT fragment, both genotypes should provide, one was sure to have loaded sufficient amount and quality of DNA. Otherwise, a failed detection of the βB1 or SV40 construct due to

insufficient DNA would erroneously be classified as WT. Results from both PCRs were expected to exhibit similar results and only animals with corresponding results were used for experiments.

As negative control, a sample containing water instead of DNA was treated the same as the others. The lack of any signal there assures, that the signal in the other samples was specific. As positive control, DNA of a securely transgenic animal was used.

4.1.2 Overexpression of CTGF leads to activation of retinal macroglia and glaucomatous changes

The present study contributed to the publication Reinehr et al. in 2019 by investigating macroglia activation in the retina. Therefore, astrocytes were stained with glial fibrillary acidic protein (GFAP), and vimentin (VIM) and glutamine synthetase (GS) were stained to label Müller cells (compare 3.7.1).

While the GFAP as well as the VIM staining showed a slightly increased stain-positive area in βB1-CTGF^{CD1} transgenic mice, GS signal was significantly increased in comparison to WT^{CD1} littermates (**Figure 12**). These findings indicate macroglia activation under the high IOP conditions of the transgenic animals.

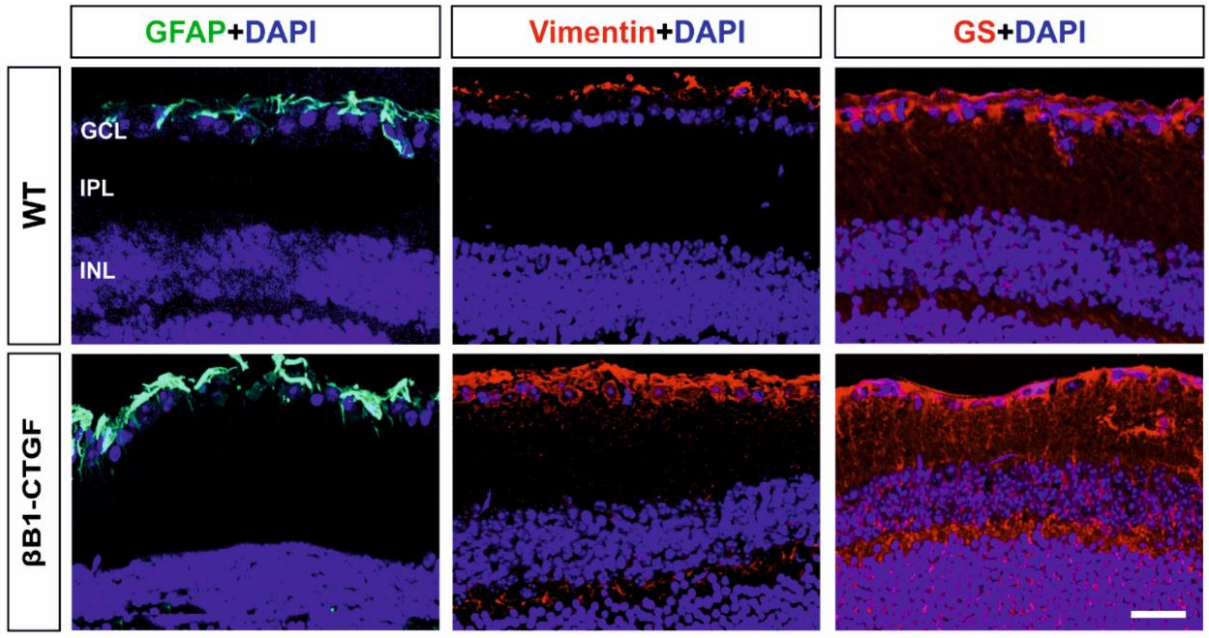

Figure 12: Macroglia activation in βB1-CTGF (CD1) transgenic mice.

Macroglia were stained with specific antibodies against green fluorescent acidic protein (GFAP, green), vimentin (red) and glutamine synthetase (GS, red). Cell nuclei were labeled with DAPI (blue). While GFAP and vimentin showed slightly increased stain^{+} areas, GS^{+} area was significantly increased in βB1-CTGF^{CD1} retinae compared to wildtype^{CD1} (WT) retinae (Reinehr et al. 2019). Scale bar represents 20 µm with n = 5 eyes per group (GCL = ganglion cell layer, IPL = inner plexiform layer, INL = inner nuclear layer).

4.1.3 Pure-breeding of βB1-CTGF transgenic mice in additional genetic backgrounds

While transgenic βB1-CTGF mice, purebred in the CD1 background, were already available in our working group, purebred Black6/J (BL6) mice were generated within this study. Therefore, a βB1-CTGF transgenic mouse with CD1 background was bred with a WT Black6/J mate. After a total of eight generations, the βB1-CTGF transgene construct was brought into the pure Black6/J background and mice were considered to be purebred. Both, transgenic as well as WT littermates were viable and fertile (data not shown).

4.1.4 CTGF overexpression leads to increase of IOP, independent of genetic background

While Junglas et al. found significantly increased IOP in the βB1-CTGF mice with a mixed FVB/N and CD1 background (first generation) at the age of 4, 8 as well as 12 weeks, Reinehr et al. reported an influence of the genetic background since there, the βB1-CTGF mice within a pure CD1 background showed no increase of IOP until the age of 15 weeks.

However, the present study showed that the increase in IOP is conserved at the age of 1 year in mice with the pure CD1 background (**Figure 13**). While WT^{CD1} animals had an IOP of 12.67 ± 0.79 mmHg, $\beta B1\text{-}CTGF^{CD1}$ mice had a significantly increased IOP of 15.76 ± 1.00 mmHg ($p \leq 0.05$).

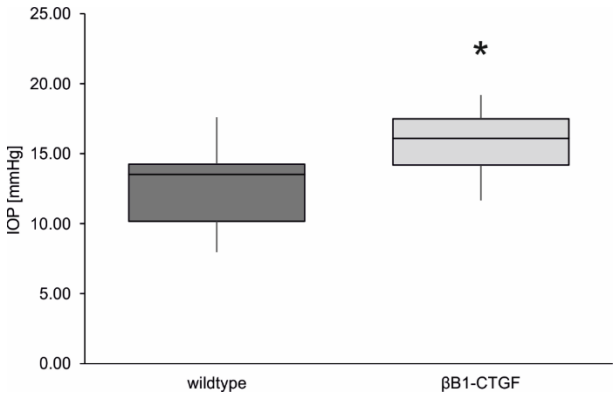

Figure 13: IOP was significantly increased in 1-year old βB1-CTGF (CD1) mice compared to wildtype littermates.

IOP was measured from both eyes with rebound tonometry in mice, anesthetized with isoflurane®. At the age of 1 year, transgenic βB1-CTGF mice (n = 7) with a pure CD1 background had significantly increased IOP compared to wildtype littermates (n = 14, p ≤ 0.05).

Within this study, βB1-CTGF mice were bred into the Black6/J background. Exemplarily, the 7th generation of the breeding into the Black6/J background was investigated (**Figure 14**). Therefore, the same animals from one litter (n = 3 for both groups) were investigated subsequently at the age of 4, 8 and 12 weeks. IOP was measured from both eyes of each animal with rebound tonometry in anesthetized mice. While IOP was almost identical at the age of 4 weeks (WT^{BL6}: 12.50 ± 1.02 mmHg, $βB1\text{-}CTGF^{BL6}$: 13.07 ± 0.57 mmHg), transgenic mice had significantly increased IOP at the age of 8 weeks (WT^{BL6}: 12.44 ± 1.00 mmHg, $βB1\text{-}CTGF^{BL6}$: 16.54 ± 0.99 mmHg with $p \leq 0.05$). and high significantly increased IOP at the age of 12 weeks (WT^{BL6}: 12.87 ± 0.37 mmHg, $βB1\text{-}CTGF^{BL6}$: 16.27 ± 0.90 mmHg with $p \leq 0.01$).

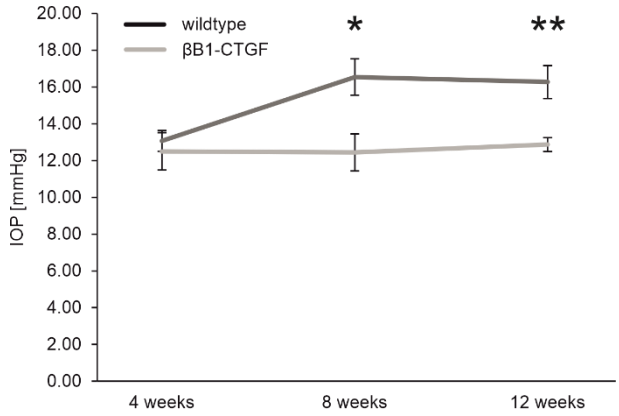

Figure 14: IOP was significantly increased in 8 and 12-week old βB1-CTGF (CD1 and Black6/J, 7th generation) mice compared to wildtype littermates.

IOP was measured from both eyes with rebound tonometry in mice, anesthetized with isoflurane®. The same animals from one litter (n = 3 for both groups) were investigated subsequently at the age of 4, 8 and 12 weeks.

While IOP was almost identical at the age of 4 weeks, $βB1\text{-}CTGF^{BL6}$ transgenic mice had significantly increased IOP at the age of 8 ($p \leq 0.05$) and high significantly increased IOP at the age of 12 weeks ($p \leq 0.01$).

Further genetic backgrounds were investigated within the doctoral thesis of Felix Hutmacher, a medical student who was supervised throughout this study.

Even if there are slight differences concerning the timepoint and the extent, the increase of IOP emerges in transgenic mice, the CTGF-induced increase in IOP is sustained over all investigated genetic backgrounds. These findings underline the power of the established mouse model and make it an even stronger and very valid mouse model for glaucoma. Furthermore, the likelihood of CTGF to play a key role during the pathology of POAG is supported by those findings.

4.2 Effect of Nitric Oxide on biomechanical behavior and expression profile of outflow tissue cells

In recent years, the relaxing effect of NO signaling gained attention as potential approach to treat glaucoma. Therefore, the mean topic of this thesis was the analysis whether NO has an influence of the biomechanical behavior and on the expression profile of endothelial cells. The focus was on the *in vitro* treatment of SC cells (and HUVECs) with an exogenous NO donor, DETA-NO. This study was supported by a cooperation with Prof. Dr. Johnson's lab as well as Ramona Pawlak who did her master thesis on this topic.

4.2.1 DETA-NO as exogenous NO donor *in vitro*

To investigate the NO effects, endothelial cells were treated with DETA-NO in different concentrations (50 and 100 µM) *in vitro*. Prior to experiments, Calcein-AM staining was performed to eliminate the risk that the chosen concentrations do negatively affect cell viability. SC cells were treated with 100 µM DETA-NO for 3 or 5 hours before staining (**Figure 15**). Since there were no significant changes in cell viability to PBS-treated controls, 50 and 100 µM DETA-NO were eligible for further *in vitro* experiments.

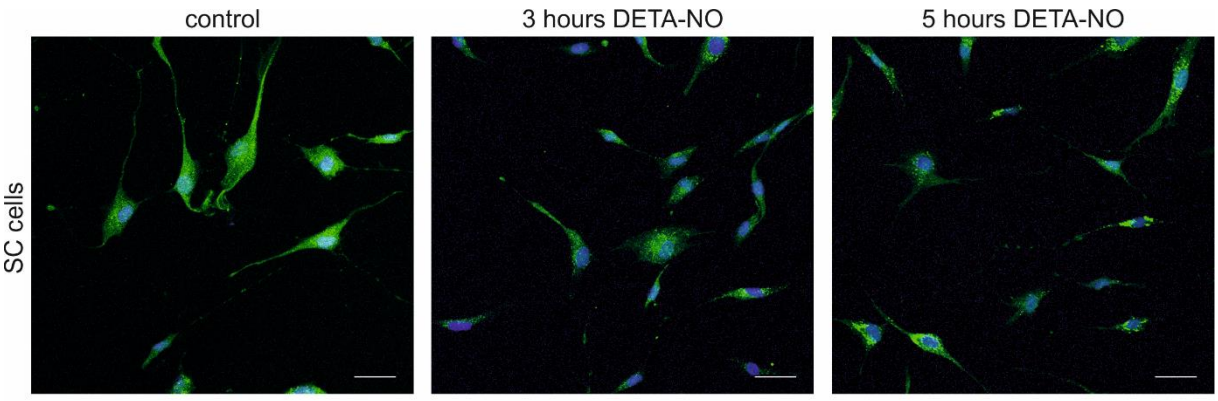

Figure 15: DETA-NO did not impair cell viability.

Calcein-AM staining of SC cells. Green fluorescence indicates viable cells, blue nuclear staining. If compared to PBS-treated controls, neither 3 nor 5 hours of DETA-NO treatment (100 µM) did cause a significant change in cell viability. Scale bars: 50 µm.

In a next step, the ability of DETA-NO to release NO into cells supernatant under the given *in vitro* conditions was investigated (SC71 and SC79, n = 4 each). Great interest was put on the temporal course over up to 24 hours. The NO concentration was indirectly determined by measuring the nitrite concentration by Griess reagent analysis. While PBS-treated controls revealed a concentration below the detection limit

of 1.0 µM nitrite for this assay (3 hours: 0.34 ± 0.06 µM; 6 hours: 0.22 ± 0.05 µM; 24 hours: 0.43 ± 0.07 µM), DETA-NO did highly significantly increase NO in the supernatant of SC cells over a period of up to 24 hours (**Figure 16**). The increase of nitrite concentration with increasing DETA-NO concentration was consistent ($p \leq 0.001$) while there was no significant difference between the investigated timepoints of 3, 6 and 24 hours (3 hours: 50 µM DETA-NO: 20.85 ± 0.85 µM, 100 µM DETA-NO: 36.49 ± 1.15 µM; 6 hours: 50 µM DETA-NO: 21.17 ± 1.08 µM, 100 µM DETA-NO: 33.54 ± 1.86 µM;. 24 hours: 50 µM DETA-NO: 20.14 ± 1.01 µM, 100 µM DETA-NO: 36.00 ± 2.01 µM). This finding has shown that a treatment for up to 24 hours generates consistent NO concentrations after DETA-NO supplementation.

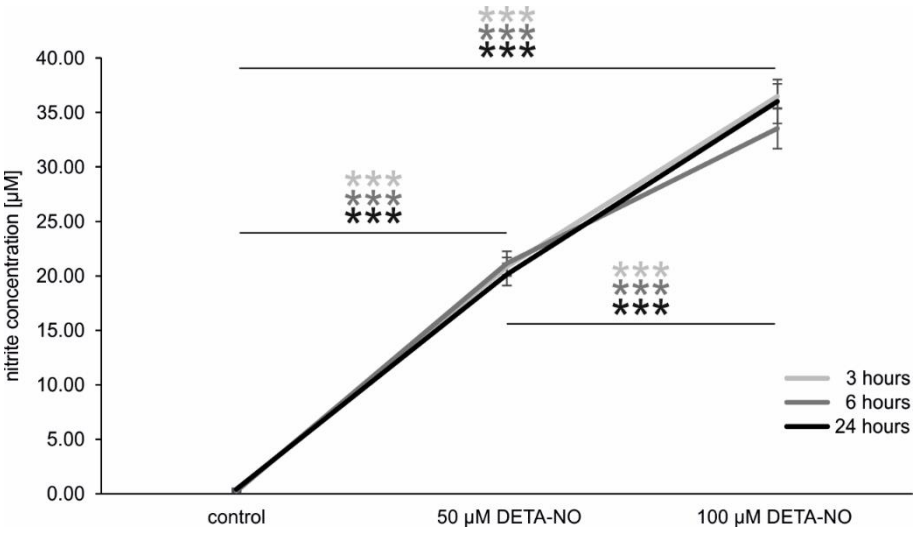

Figure 16: DETA-NO did increase NO concentration in cells supernatant.

NO concentration was indirectly determined by measuring the nitrite concentration by Griess reagent analysis in the supernatant of PBS-treated, 50 µM and 100 µM DETA-NO treated SC cells (SC71 and SC79, n = 4 each). PBS-treated controls showed a concentration below the detection limit of 1.0 µM nitrite for this assay. DETA-NO treatment did significantly increase the nitrite concentration after 3 (light gray), 6 (dark gray) as well as 24 hours (black) of treatment ($p \leq 0.001$).

In this study, the focus of gene expression studies was set on 6, 12 and 24 hours of DETA-NO treatment. The relative mRNA expression was investigated in PBS-treated, 50 µM and 100 µM DETA-NO treated SC cells via RT-qPCR. To analyze whether DETA-NO can induce NO response genes, the expression of heme oxygenase 1 (HO-1), a ubiquitous and inducible heme-containing member of the heat shock proteins, was investigated. HO-1 is induced in fibroblasts after a 2 to 4 hour treatment with a NO donor (SNAP) and its response depends directly on NO since it was strongly reduced after the addition of L-NAME, a NOS inhibitor (Hemish et al. 2003).

In SC cells, the increase of HO-1 mRNA was significant after 6 hours of treatment not only when comparing 50 µM (2.18 ± 0.32, $p \leq 0.01$) and 100 µM DETA-NO treatment (3.98 ± 0.69, $p \leq 0.01$) to the PBS-treated control but also when comparing the DETA-NO treatments among each other ($p \leq 0.05$). After 12 hours of treatment, the induction was reduced and longer significant (50 µM DETA-NO: 1.48 ± 0.36, 100 µM DETA-NO: 2.29 ± 0.63 with $p = 0.057$). No change in mRNA expression was found after 24 hours of DETA-NO treatment (50 µM DETA-NO: 0.90 ± 0.20, 100 µM DETA-NO: 1.00 ± 0.18). This finding has shown that the treatment with DETA-NO at the given concentrations are sufficient to cause expression changes in SC cells (**Figure 17**).

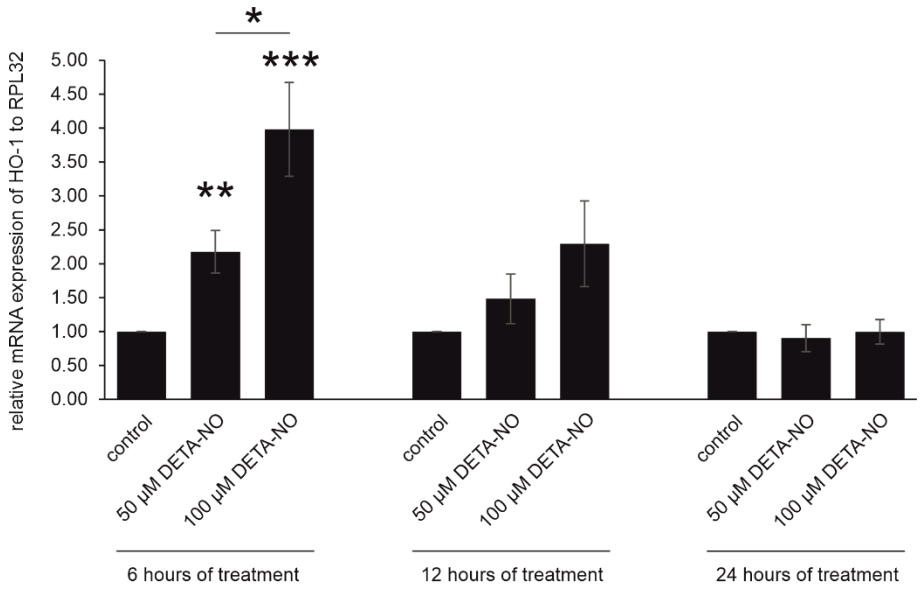

Figure 17: DETA-NO did induce the expression of the NO response gene HO-1.

Relative mRNA expression of HO-1 was investigated in PBS-treated, 50 µM and 100 µM DETA-NO treated SC cells (SC68, SC74 and SC79, n = 3 each).DETA-NO treatment did significantly increase HO-1 mRNA expression after 6 hours of treatment ($p \leq 0.05$, $p \leq 0.01$, $p \leq 0.001$). After 12 hours of treatment, the induction was reduced and no longer significant ($p = 0.057$ for 100 µM DETA-NO treatment). No change in mRNA expression was found after 24 hours of DETA-NO treatment. RPL32 was used as reference gene.

4.2.2 HUVECs as suitable endothelial model cell line for SC cells

Since human SC cells are difficult to isolate (Stamer et al. 1998) and our access to supply is limited, having a suitable model cell line is essential to establish experimental setups. HUVECs have been proven to be a suitable endothelial cell model for SC cells (Perkumas and Stamer 2012; Ashpole et al. 2014).

Using a cell strain as model for another strain, one must be aware that there are some limitations. Differences in expression profile of distinct genes may occur in different cell strains. Within this study, we investigated the expression profile of decorin (DCN), a gene that has been shown to be associated to POAG (Grisanti et al. 2005; Hill et al.

2015; Hill et al. 2016; NikhalaShree et al. 2019). While we have shown that SC cells do express DCN (Overby et al. 2014), HUVECs have been proven to have no endogenous DCN expression (Buraschi et al. 2013). These findings have been reproduced in this study, even if DETA-NO did not have influence on DCN gene expression in three investigated SC cell strains (**Figure 18**, 6 hours: 50 µM DETA-NO: 0.70 ± 0.11, 100 µM DETA-NO: 0.89 ± 0.15; 12 hours: 50 µM DETA-NO: 0.85 ± 0.09, 100 µM DETA-NO: 0.62 ± 0.14; 24 hours: 50 µM DETA-NO: 1.26 ± 0.27, 100 µM DETA-NO: 0.78 ± 0.19).

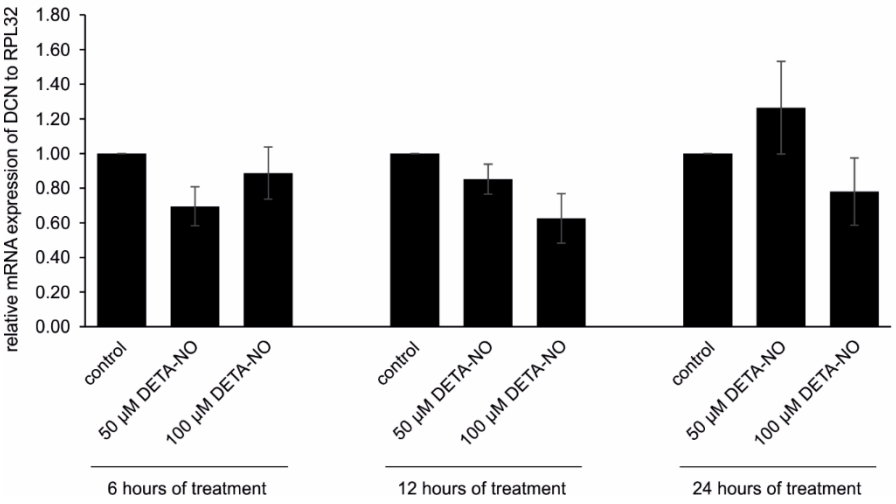

Figure 18: DETA-NO did not affect the expression of DCN but investigations revealed that DCN is expressed in SC cells but not in HUVECs.

Relative mRNA expression of DCN was investigated in PBS-treated, 50 µM and 100 µM DETA-NO treated SC cells (SC68, SC74 and SC79, n = 3 each). DETA-NO treatment did have no effect on DCN mRNA expression after 6, 12 or 24 hours of treatment (p > 0.05). RPL32 was used as reference gene.

4.2.3 Induction of NO signaling in endothelial cells

Within initial experiments, we tried to detect major components of the NO signaling pathway under cell culture conditions. Therefore, two approaches were used to analyze eNOS and NO in SC cells. One attempt was to use DETA-NO as exogenous NO donor to induce intracellular NO signaling (compare 4.2.3.1) while the other was to mimic *in vivo* conditions by flow-induced shear stress (compare 4.2.3.2).

4.2.3.1 DETA-NO treatment

To investigate the effect of exogenous NO on NO signaling, the expression of eNOS in DETA-NO treated HUVECs and SC cells was investigated.

In SC cells, eNOS was not detectable at mRNA level, neither by RT-qPCR nor TaqMan (data not shown). Furthermore, the two other isoforms of NOS, iNOS and nNOS were also not detectable in SC cells (data not shown).

On the other hand, HUVECs expressed detectable eNOS mRNA amount (**Figure 19**). There, DETA-NO treatment did have not significant effect on eNOS expression but revealed tendencies towards a dose-dependent affection (n = 4; 50 µM DETA-NO: 1.40 ± 0.20 with p = 0.057, 100 µM DETA-NO: 1.59 ± 0.37).

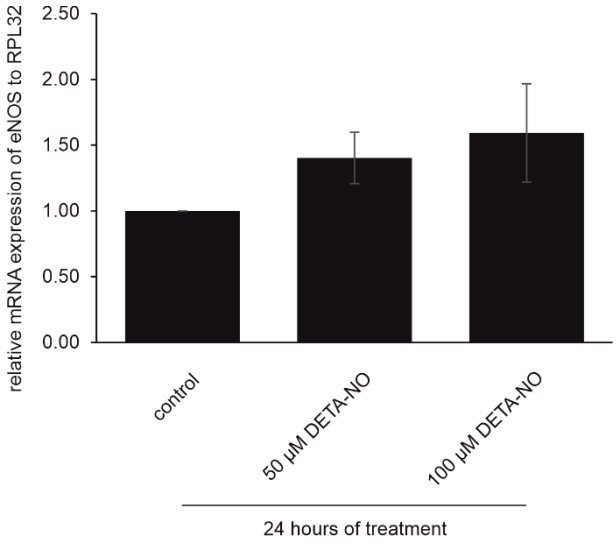

Figure 19: DETA-NO did not affect the expression of eNOS in HUVECs.

Relative mRNA expression of eNOS was investigated in PBS-treated, 50 µM and 100 µM DETA-NO treated HUVECs (n = 4). DETA-NO treatment had no significant effect on eNOS mRNA expression after 24 hours of treatment, even if a tendency towards a dose-dependent increase was revealed with p = 0.057 for the 50 µM treatment.

To further investigate if the DETA-NO treatment had impact on eNOS protein synthesis, HUVECs were investigated after treatment with 50 and 100 µM DETA-NO for 6, 12 or 24 hours. By Western Blot analysis, no changes of eNOS synthesis was observed (**Figure 20**, 6 hours (n = 5): 50 µM DETA-NO: 1.20 ± 0.18, 100 µM DETA-NO: 1.30 ± 0.55; 12 hours (n = 4): 50 µM DETA-NO: 1.10 ± 0.19, 100 µM DETA-NO: 1.37 ± 0.74; 24 hours (n = 4): 50 µM DETA-NO: 2.31 ± 0.58, 100 µM DETA-NO: 1.54 ± 0.34).

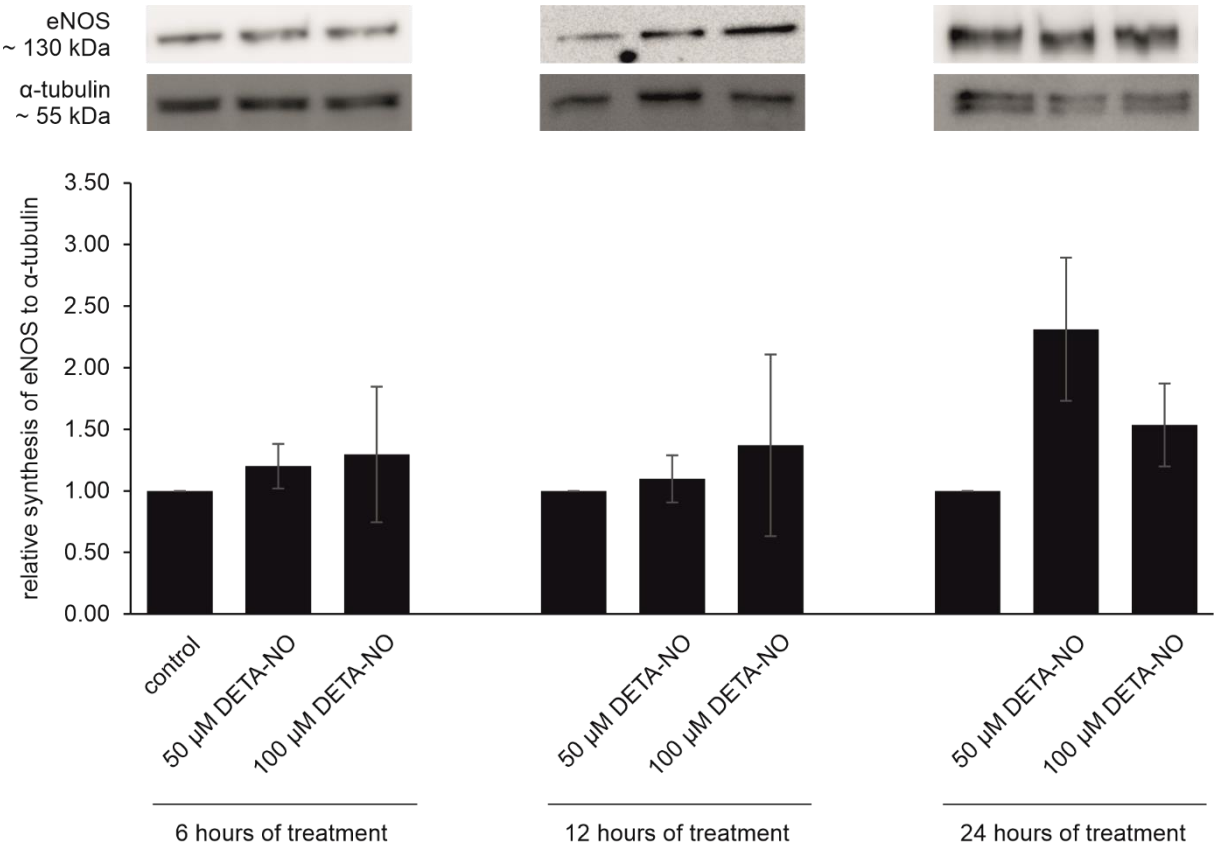

Figure 20: DETA-NO did not affect the synthesis of eNOS in HUVECs after 6,12 and 24 hours of treatment.

Relative protein synthesis of eNOS was investigated in PBS-treated, 50 µM and 100 µM DETA-NO treated HUVECs (6 hours: n = 5, 12 hours: n = 4, 24 hours: n = 4). DETA-NO treatment did not have significant effect on eNOS protein synthesis at any of the investigated timepoints ($p > 0.05$). Representative images of eNOS (~ 130 kDa) and α-tubulin (~ 55 kDa) Western Blots are shown.

The next attempt was to investigate eNOS synthesis in SC cells by Western Blot technique. Neither samples dissolved in 1% SDS (n = 3) nor in RIPA buffer (n = 3) had detectable eNOS protein (**Figure 21**). Even if cells were kept one week confluent to undergo differentiation, no eNOS protein could be detected by this method. Untreated HUVECs functioned as positive control and provided chemiluminescent signal at ~ 130 kDa. As loading control, α-tubulin was used to ensure adequate loading and sufficient signal for all seven samples was detected.

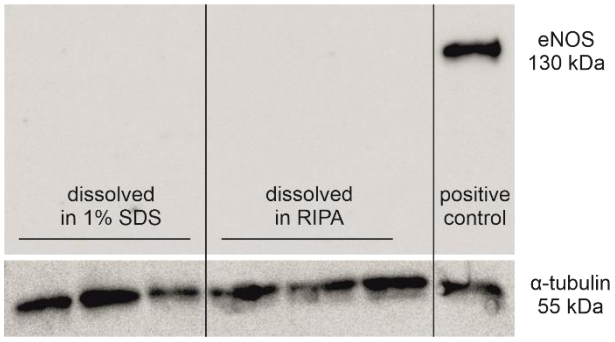

Figure 21: eNOS protein was not detectable in SC cells by Western Blot.

The protein synthesis of eNOS was investigated in SC cells (SC91) via Western Blot analysis after cells were kept one week confluent to undergo differentiation. Proteins from untreated cells, either dissolved in 1% SDS (n = 3) or in RIPA buffer (n = 3), were separated by electrophoresis and transferred to a PVDF membrane. When incubated with rabbit-anti-eNOS antibody, only positive control (untreated HUVECs) provided chemiluminescent signal at ~ 130 kDa. As loading control, rabbit-anti-α-tubulin antibody was used to ensure adequate loading and sufficient signal for all seven samples was detected.

As a more sensitive method, eNOS ELISA was performed. This method requires a standard with defined amounts of eNOS (compare 3.3.6). Thereby, initial investigations revealed, that SDS buffer interfered with ELISA reagents (data not shown).

Dissolved in RIPA buffer, sample sets from three different SC cell strains (SC68, SC74 and SC89, n = 14 in total) were investigated (**Figure 22**). After 24 hours, DETA-NO treatment did not have any effect on eNOS protein synthesis after 24 hours (control: 133.29 ± 12.95 pg/ml, 50 µM DETA-NO: 126.43 ± 15.11 pg/ml, 100 µM DETA-NO: 130.82 ± 15.47 pg/ml).

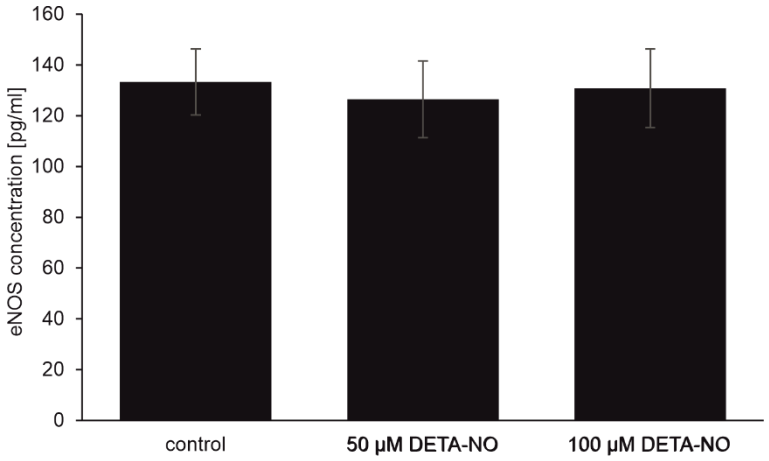

Figure 22: eNOS protein was detectable in SC cells by ELISA, but synthesis was not affected by DETA-NO treatment.

The protein synthesis of eNOS was investigated via ELISA. Other than with Western Blot technique, eNOS was detectable in SC cell samples dissolved in RIPA buffer. In this overall survey of three investigated SC cell strains (SC68, SC74 and SC89, n = 14 in total), DETA-NO treatment had no effect on eNOS protein synthesis.

As shown by Western Blot analysis for HUVECs, neither 50 µM nor 100 µM DETA-NO did significantly affect eNOS protein synthesis in SC cells. Since eNOS was undetectable at mRNA level and only detectable at protein level when dissolved in RIPA buffer and investigated by the sensitive ELISA method, standard cell culture conditions seem to lead to very low eNOS in SC cells.

4.2.3.2 flow conditions

To mimic the *in vivo* situation *in vitro*, allowing for a more suitable setup, flow experiments were performed. Thereby, a continuous flow of medium was induced by

an ibidi® pump system (see also 3.2.2.3). This shear stress mimicked the *in vivo* conditions, where SC cells are also exposed to flow of AH.

Next, it was investigated if the high flow conditions can induce NO production in SC cells (**Figure 23**). By Griess reagent analysis, the supernatant of SC cells was assessed (SC68, SC74 and SC89, n = 17 for 0 dyn/cm² and n = 10 for 10 dyn/cm² after one day and n = 21 for 0 dyn/cm² and n = 9 for 10 dyn/cm² after one week in total) which were kept one day or one week under flow conditions (10 dyn/cm²). Results were compared to controls kept under static conditions (0 dyn/cm²).

Thereby, results for SC cells kept under static conditions were below the detection limit of 1.0 µM for this assay (compare with results from controls of DETA-NO treated SC cells in **Figure 16**). If kept under flow conditions, nitrite was increased in the supernatant from SC cells already after one day of incubation (0 dyn/cm²: 0.26 ± 0.06 µM, 10 dyn/cm²: 1.53 ± 0.19 µM). This increase was even more pronounced and high significantly higher after one week of incubation (0 dyn/cm²: 0.61 ± 0.06 µM, 10 dyn/cm²: 3.99 ± 0.81 µM, with p ≤ 0.01).

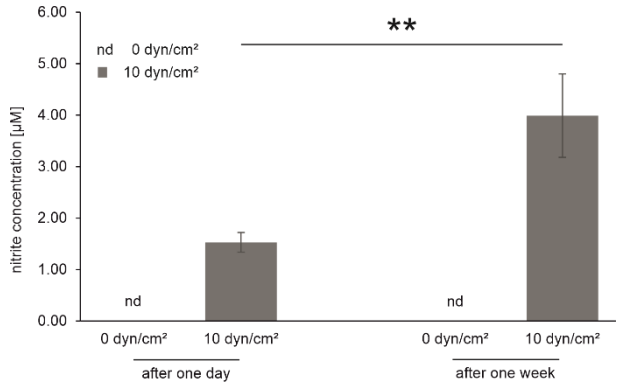

Figure 23: NO was induced in SC cells under flow conditions in vitro already after one day of incubation.

NO concentration was indirectly determined by measuring the nitrite concentration by Griess reagent analysis in the supernatant of SC cells (SC68, SC74 and SC89, n = 17 for 0 dyn/cm² and n = 10 for 10 dyn/cm² after one day and n = 21 for 0 dyn/cm² and n = 9 for 10 dyn/cm² after one week in total) which were kept one day or one week under flow conditions (10 dyn/cm²). Results were compared to controls kept under static conditions (0 dyn/cm²).

*SC cells incubated under static conditions produced nitrite concentrations below the detection limit of 1.0 µM for this assay. Already after one day of incubation, SC cells under flow conditions produced detectable amounts of nitrite. This increase was even more pronounced and significantly higher after one week of incubation (** ≤ 0.01).*

These findings indicate that flow conditions mimic the *in vivo* situation and lead to a stimulation of NO production in SC cells. Based on the increased NO production, we investigated eNOS expression. Therefore, cells were harvested after one week under

flow conditions and cells cultured in parallel for one week under static conditions served as control.

The expression of eNOS mRNA in SC cells (SC68, SC74 and SC89) was investigated after one week of incubation (**Figure 24**). Flow conditions slightly induced eNOS mRNA expression compared to static control (0 dyn/cm² (n = 11): 1.00 ± 0.12, 10 dyn/cm² (n = 9): 2.11 ± 1.04) but the increase was not significant.

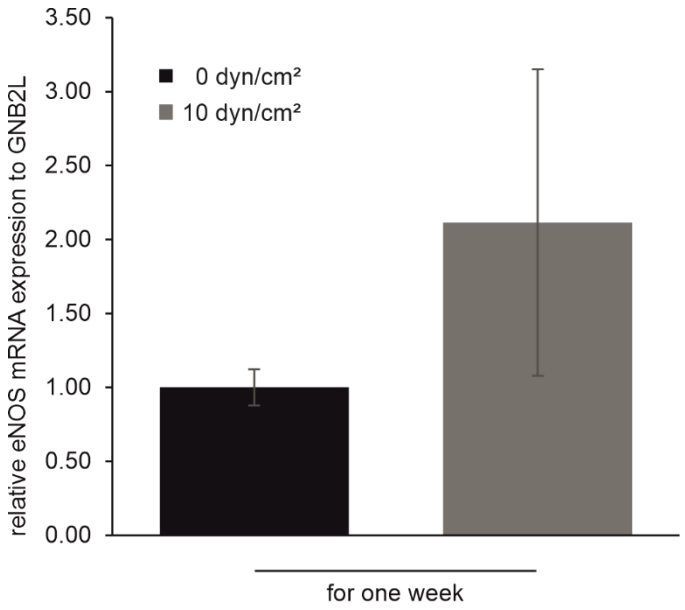

Figure 24: eNOS mRNA expression in SC cells was slightly induced by flow conditions in vitro.

eNOS mRNA expression was investigated by RT-qPCR in SC cells (SC68, SC74 and SC89) after one week under flow conditions. The incubation under flow (10 dyn/cm², n = 9) slightly induced the expression of eNOS mRNA compared to static controls (0 dyn/cm², n = 11), but the increase was not statistically significant.

4.2.4 Effect of flow conditions on the expression of glaucoma relevant genes

Since high flow resistance and thereby high pressure within the TM and SC are symptoms of POAG, glaucoma-associated factors were investigated under flow conditions.

TGF-β2 mRNA expression was investigated in SC cells (SC68, SC74 and SC89) under flow conditions (**Figure 25**). Neither one day, nor one week of incubation had any effect on TGF-β2 mRNA expression (one day: 0 dyn/cm² (n = 10): 1.00 ± 0.10, 10 dyn/cm² (n = 9): 0.80 ± 0.12; one week: 0 dyn/cm² (n = 11): 1.00 ± 0.04, 10 dyn/cm² (n = 10): 0.75 ± 0.26).

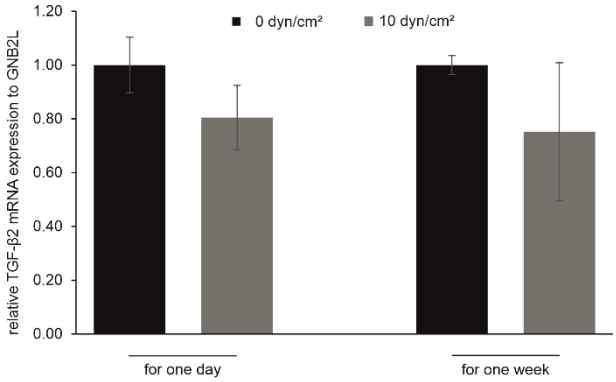

Figure 25: TGF-β2 mRNA expression in SC cells was unaffected by in vitro flow conditions.

TGF-β2 mRNA expression was investigated by qPCR in SC cells (SC68, SC74 and SC89) after one day (n = 10 for 0 dyn/cm² respective n = 9 for 10 dyn/cm² in total) as well as after one week (n = 11 for 0 dyn/cm² respective n = 10 for 10 dyn/cm² in total) under flow conditions. Neither one day nor one week of incubation had any effect on TGF-β2 mRNA expression compared to static controls.

Furthermore, CTGF as a downstream mediator of TGF-β signaling (Ihn 2002; Leask and Abraham 2004) was investigated in SC cells (SC68, SC74 and SC89, **Figure 26**). As TGF-β2, CTGF mRNA expression was not affected by flow conditions. Neither after one day of incubation, nor after one week under flow conditions, CTGF mRNA was affected compared to static controls (one day: 0 dyn/cm² (n = 11): 1.00 ± 0.19, 10 dyn/cm² (n = 11): 1.50 ± 0.38; one week: 0 dyn/cm² (n = 12): 1.00 ± 0.05, 10 dyn/cm² (n = 11): 1.59 ± 0.63).

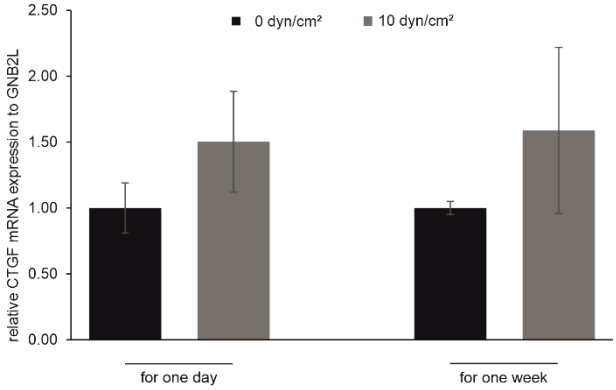

Figure 26: CTGF mRNA expression in SC cells was unaffected by in vitro flow conditions.

CTGF mRNA expression was investigated by qPCR in SC cells (SC68, SC74 and SC89) after one day (n = 11 for 0 dyn/cm² respective n = 11 for 10 dyn/cm² in total) as well as after one week (n = 12 for 0 dyn/cm² respective n = 11 for 10 dyn/cm² in total) under flow conditions. At both time points, flow conditions had no significant impact on CTGF mRNA expression compared to static control.

4.2.5 Effect of exogenous NO on actin cytoskeleton and cell stiffness

The effect of exogenous NO on actin cytoskeleton and cell stiffness was investigated. By phalloidin labeling (compare 3.7.2), actin cytoskeleton was displayed.

Thereby, PBS-treated HUVECs had saturated signal derived from actin stress fibers (**Figure 27**). After DETA-NO treatment (100 µM), cells revealed less stress fibers. These changes were already observed after 3 hours of treatment and sustained until 5 hours.

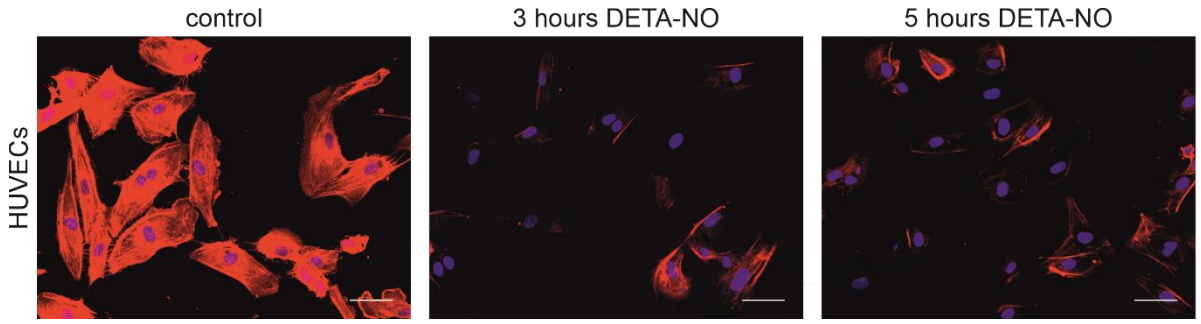

Figure 27: DETA-NO causes changes of the actin cytoskeleton of HUVECs.

Phalloidin labeling of HUVECs. Red fluorescence indicates actin cytoskeleton, blue nuclear staining. Untreated controls show filamentous actin cytoskeleton, while DETA-NO treated cells (100 µM) show less actin stress fibers. Changes were already observed 3 hours after treatment and sustained until 5 hours. Scale bars: 50 µm.

In SC cells, plenty of longitudinally arranged actin stress fibers were found (**Figure 28**). As shown in HUVECs, SC cells had less stress fibers after DETA-NO treatment (100 µM). Furthermore, these changes were observed after 3 hours of treatment and more pronounced after 5 hours.

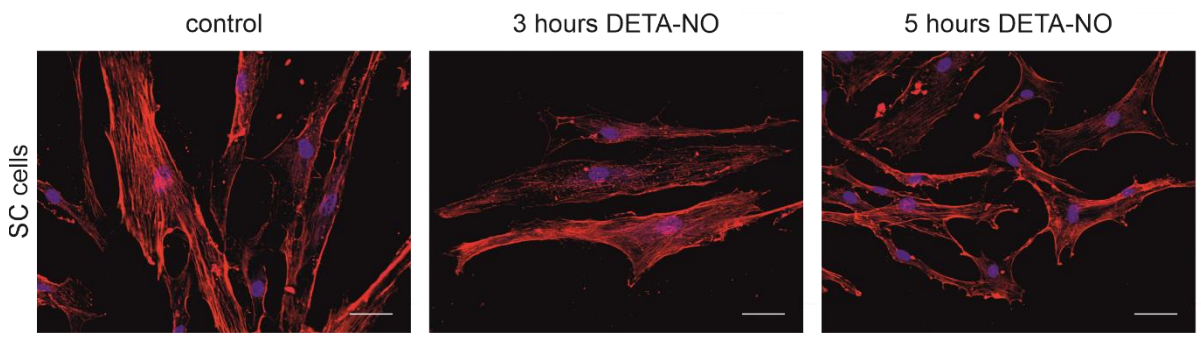

Figure 28: DETA-NO causes changes of the actin cytoskeleton of SC cells.

Phalloidin labeling of SC cells (SC71). Red fluorescence indicates actin cytoskeleton, blue nuclear staining. Untreated controls show filamentous actin cytoskeleton, while DETA-NO treated cells (100 µM) show less actin stress fibers. Changes were already observed 3 hours after treatment and even more pronounced after 5 hours. Scale bars: 50 µm.

Next, the expression of α-SMA - as major component of actin cytoskeleton - was investigated.

In HUVECs, results were not explicit. While the 100 µM DETA-NO treatment for 6 hours significantly increased the α-SMA expression, the 50 µM DETA-NO treatment high significantly reduced the expression after 12 hours of treatment (**Figure 29**;

6 hours: 50 µM DETA-NO: 1.06 ± 0.15, 100 µM DETA-NO: 1.89 ± 0.35 with p ≤ 0.05; 12 hours: 50 µM DETA-NO: 0.46 ± 0.13 with p ≤ 0.01, 100 µM DETA-NO: 0.72 ± 0.21; 24 hours: 50 µM DETA-NO: 1.05 ± 0.36, 100 µM DETA-NO: 1.46 ± 0.34).

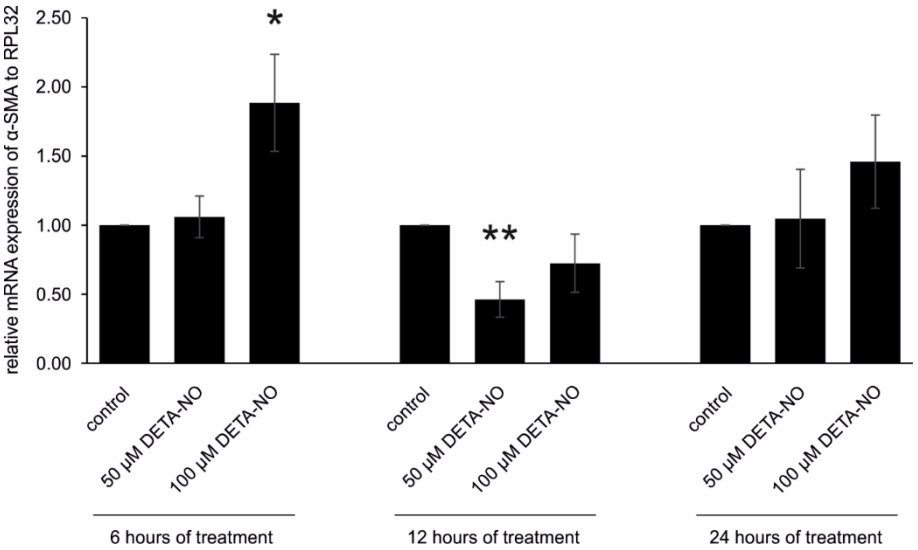

Figure 29: DETA-NO did affect the expression of α-SMA in HUVECs.

Relative mRNA expression of α-SMA was investigated in PBS-treated, 50 µM and 100 µM DETA-NO treated HUVECs (n = 4 each). While 6 hours of treatment with 100 µM DETA-NO did significantly increase α-SMA mRNA expression (p ≤ 0.05), 12 hours of 50 µM DETA-NO treatment did high significantly reduce the α-SMA mRNA expression (p ≤ 0.01).

In SC cells, DETA-NO treatment for 6 and 12 hours did not affect the expression of α-SMA. However, 100 µM DETA-NO treatment did highly significantly reduce the expression of α-SMA after 24 hours (**Figure 30**; 6 hours: 50 µM DETA-NO: 0.90 ± 0.10, 100 µM DETA-NO: 0.87 ± 0.10; 12 hours: 50 µM DETA-NO: 0.92 ± 0.05, 100 µM DETA-NO: 1.00 ± 0.20; 24 hours: 50 µM DETA-NO: 0.89 ± 0.10, 100 µM DETA-NO: 0.84 ± 0.00 with p ≤ 0.001).

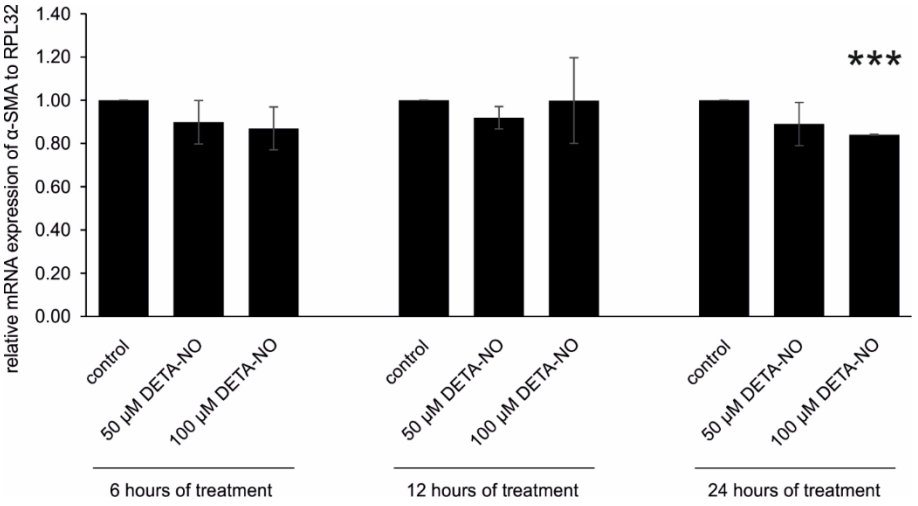

Figure 30: DETA-NO did reduce the expression of α-SMA in SC cells.

Relative mRNA expression of α-SMA was investigated in PBS-treated, 50 µM and 100 µM DETA-NO treated SC cells (SC68, SC74 and SC79, n = 3 each). DETA-NO treatment did have highly significant effect on α-SMA mRNA expression after 24 hours of treatment with 100 µM DETA-NO (p ≤ 0.001).

Whether DETA-NO treatment has an effect on cell stiffness, cell stiffness was analyzed with atomic force microscopy (AFM, **Figure 31**). By investigating HUVECs and SC cells, the very low indentation depth of sharp tips allows for analysis of the cell cortex. With a spherical tip, the subcortical cell stiffness was analyzed.

Investigating cell stiffnesses of PBS- and 50 µM DETA-NO treated HUVECs (middle panel) and SC cells (lower panel) by sharp AFM tips (left column), a highly significant reduction (p ≤ 0.001) of cortical cell stiffness was observed after DETA-NO treatment. For AFM measurements with spherical tips (right column), HUVECs as well as SC cells also revealed a highly significant reduction (p ≤ 0.001) of cell stiffness, thereby in the subcortical region.

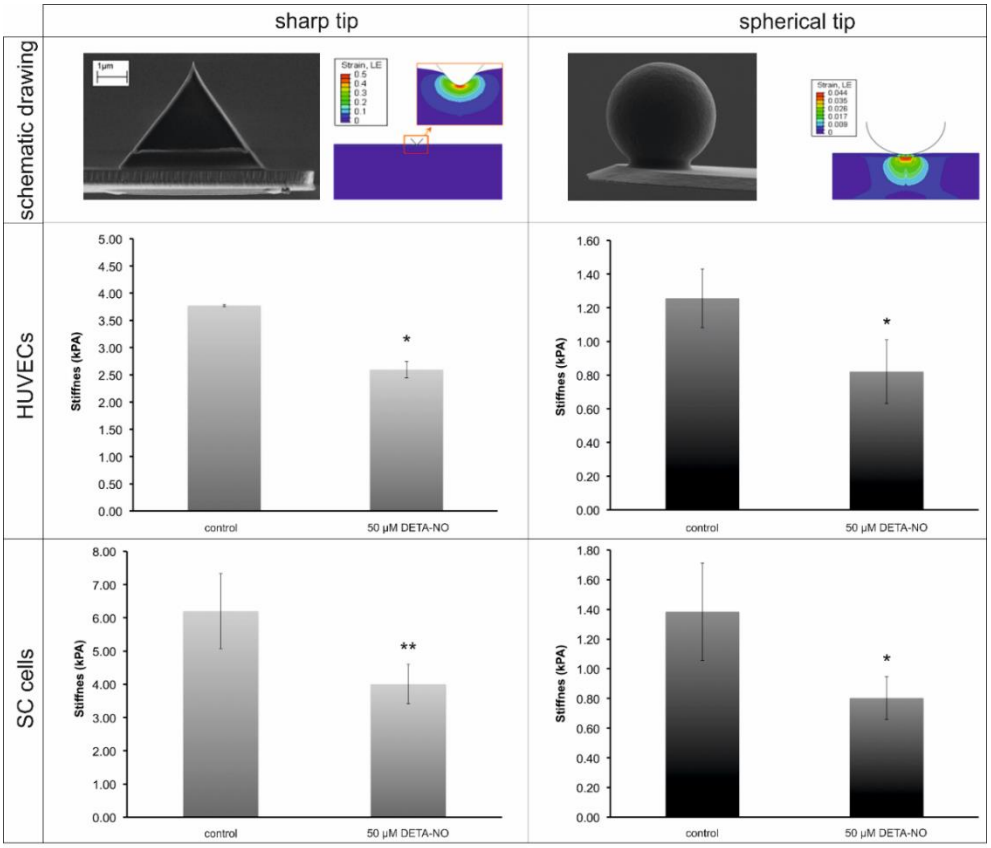

Figure 31: DETA-NO treatment reduced cell stiffness in HUVECs and SC cells.

Cell stiffness [in kPA] was analyzed by atomic force microscopy (AFM). Upper panel shows images of the AFM tips and schematic drawing visualizes the indentation depth (Vargas-Pinto et al. 2013). Experiments were performed with a 20 nm sharp tip (left column) and a 10 µm spherical tip (right column). HUVECs (middle panel) and SC cells (lower panel) were assessed either when PBS-treated as control or after 50 µM DETA-NO treatment. DETA-NO treatment lead to significant reduced cell stiffness in the cortical as well as subcortical region of HUVECs and SC cells. Mean values ± SD of three independent experiments are given. Asterisks mark statistically significant differences.

4.2.6 Effect of exogenous NO on the expression of genes affecting the NO pathway

First, caveolin-1 (CAV-1), the coat protein of caveolae and an inhibitor of eNOS activity, was investigated.

In HUVECs, CAV-1 mRNA was highly significantly reduced after 50 µM DETA-NO treatment already after 6 hours of DETA-NO treatment. After 12 hours of treatment, both DETA-NO concentrations significantly or even high significantly reduced CAV-1 expression. After 24 hours, mRNA expression was no longer significantly affected (**Figure 32**; 6 hours: 50 µM DETA-NO: 0.53 ± 0.06 with $p \leq 0.001$, 100 µM DETA-NO: 1.02 ± 0.35; 12 hours: 50 µM DETA-NO: 0.49 ± 0.19 with $p \leq 0.05$, 100 µM DETA-NO: 0.40 ± 0.15 with $p \leq 0.01$, 24 hours: 50 µM DETA-NO: 0.81 ± 0.20, 100 µM DETA-NO: 0.91 ± 0.13).

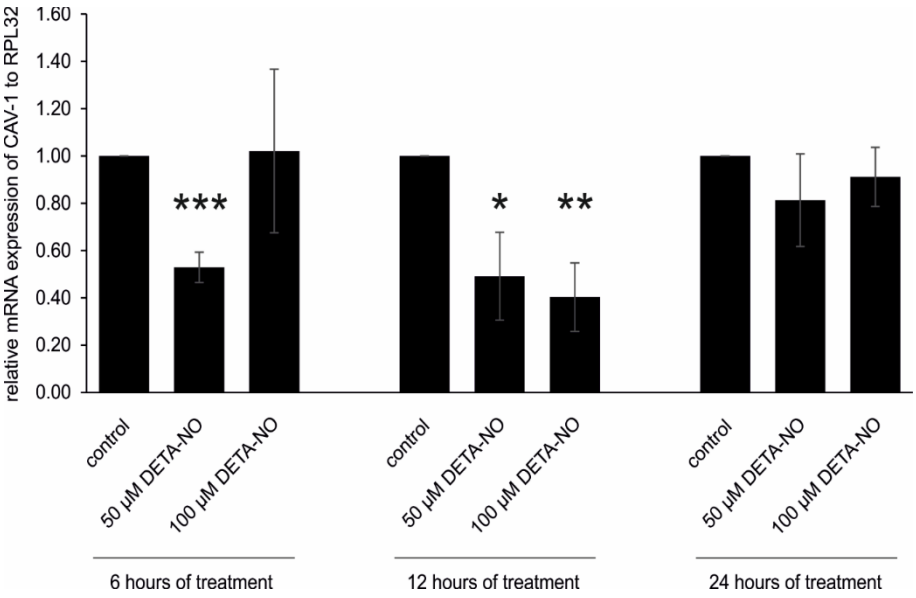

Figure 32: DETA-NO did reduce the expression of CAV-1 in HUVECs.

Relative mRNA expression of CAV-1 was investigated in PBS-treated, 50 µM and 100 µM DETA-NO treated HUVECs (n = 4 each). DETA-NO treatment did significantly reduce CAV-1 mRNA expression after 6 and 12 hours of treatment ($p \leq 0.05$, $p \leq 0.01$, $p \leq 0.001$).

In SC cells, CAV-1 expression was not affected by 6 and 12 hours of DETA-NO treatment. However, CAV-1 mRNA was significantly reduced after the 50 µM DETA-NO treatment and high significantly reduced by the 100 µM treatment after 24 hours (**Figure 33**; 6 hours: 50 µM DETA-NO: 0.77 ± 0.15, 100 µM DETA-NO: 0.83 ± 0.16; 12 hours: 50 µM DETA-NO: 0.90 ± 0.12, 100 µM DETA-NO: 0.75 ± 0.21; 24 hours: 50 µM DETA-NO: 0.67 ± 0.10 with $p \leq 0.05$, 100 µM DETA-NO: 0.56 ± 0.07 with $p \leq 0.01$).

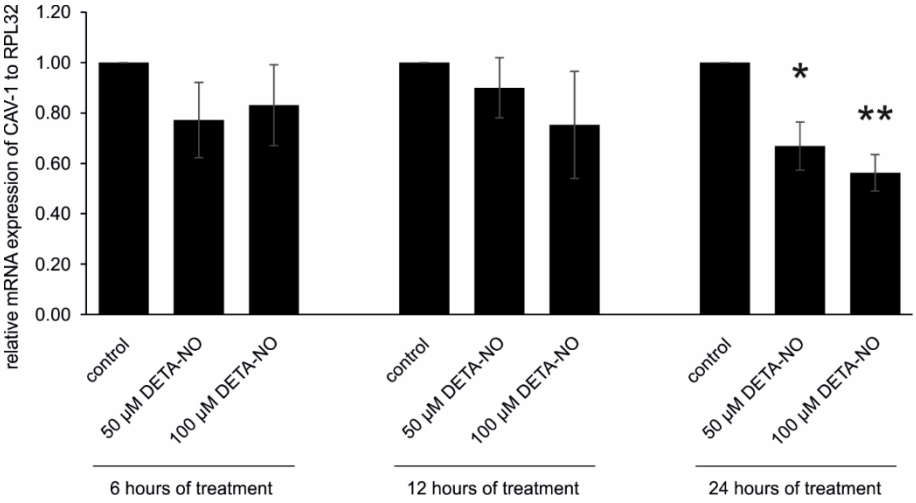

Figure 33: DETA-NO did reduce the expression of CAV-1 in SC cells.

Relative mRNA expression of CAV-1 was investigated in PBS-treated, 50 µM and 100 µM DETA-NO treated SC cells (SC68, SC74 and SC79, n = 3 each). DETA-NO treatment did have significant effect on CAV-1 mRNA expression after 24 hours of treatment with 50 µM ($p \leq 0.05$) and high significant effect when treated with 100 µM DETA-NO ($p \leq 0.01$).

Next, calmodulin-1 (CALM-1) was investigated at mRNA level. Induced by Ca^{2+}, CALM-1 builds a complex with eNOS which is then freed from CAV-1, thereby becoming active and NO producing (Sriram et al. 2016).

In HUVECs, already 6 hours of 50 µM DETA-NO treatment did highly significantly reduce CALM-1 mRNA expression. After 12 hours of DETA-NO treatment, a dose-dependent reduction of CALM-1 mRNA expression was found. 24 hours of DETA-NO treatment did no longer have significant impact on CALM-1 mRNA expression (**Figure 34**; 6 hours: 50 µM DETA-NO: 0.40 ± 0.08 with $p \leq 0.001$, 100 µM DETA-NO: 1.04 ± 0.29 with $p > 0.05$; 12 hours: 50 µM DETA-NO: 0.42 ± 0.12 with $p \leq 0.01$, 100 µM DETA-NO: 0.32 ± 0.07 with $p \leq 0.001$; 24 hours: 50 µM DETA-NO: 0.89 ± 0.16, 100 µM DETA-NO: 1.04 ± 0.15).

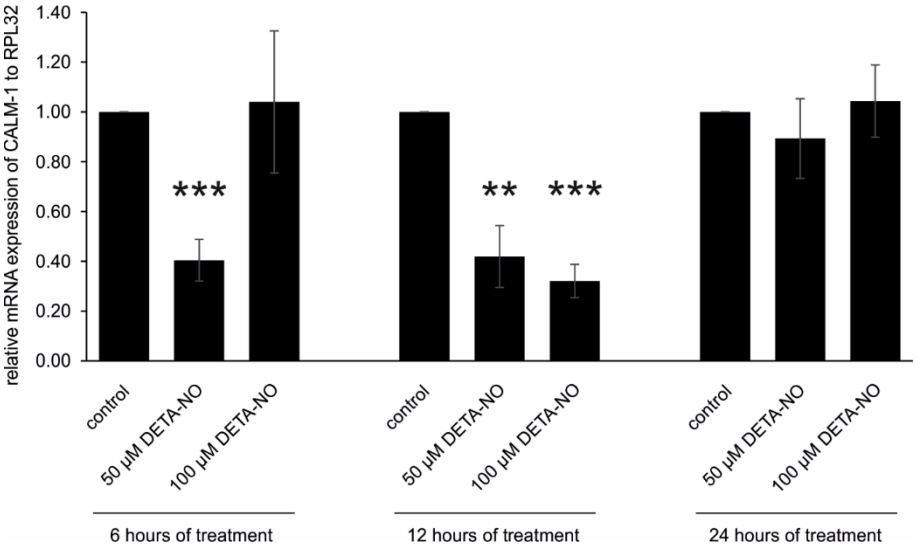

Figure 34: DETA-NO did reduce the expression of CALM-1 in HUVECs.

Relative mRNA expression of CALM-1 was investigated in PBS-treated, 50 µM and 100 µM DETA-NO treated HUVECs (n = 4 each). DETA-NO treatment did have significant effect on CALM-1 mRNA expression after 6 and 12 hours of treatment with DETA-NO (p ≤ 0.01 and p ≤ 0.001, respectively).

CALM-1 mRNA expression was also affected in SC cells. While 6 and 12 hours of DETA-NO treatment did not affect CALM-1 expression, 24 hours of treatment significantly reduced CALM-1 mRNA expression by the 100 µM DETA-NO treatment (**Figure 35**; 6 hours: 50 µM DETA-NO: 0.85 ± 0.13, 100 µM DETA-NO: 0.89 ± 0.13; 12 hours: 50 µM DETA-NO: 0.93 ± 0.04, 100 µM DETA-NO: 0.82 ± 0.10; 24 hours: 50 µM DETA-NO: 0.86 ± 0.09, 100 µM DETA-NO: 0.72 ± 0.08 with p ≤ 0.05).

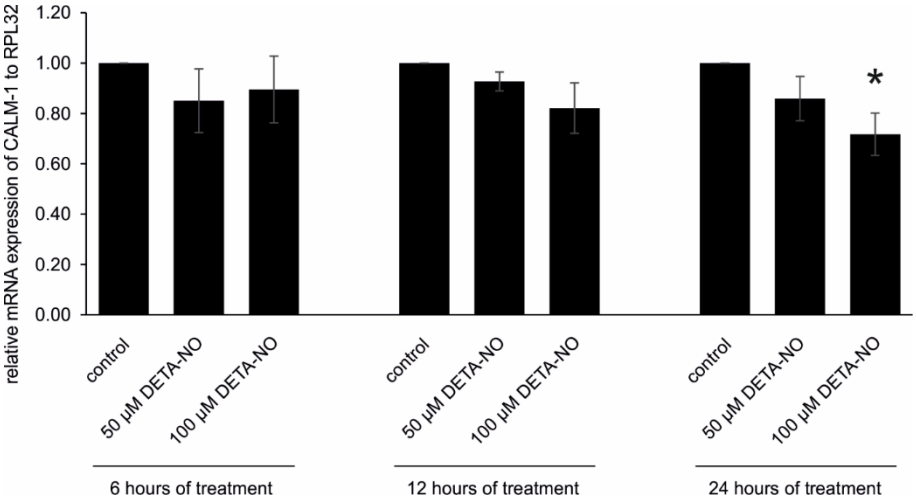

Figure 35: DETA-NO did reduce the expression of CALM-1 in SC cells.

Relative mRNA expression of CALM-1 was investigated in PBS-treated, 50 µM and 100 µM DETA-NO treated SC cells (SC68, SC74 and SC79, n = 3 each). DETA-NO treatment did have significant effect on CALM-1 mRNA expression after 24 hours of treatment with 100 µM DETA-NO (p ≤ 0.05).

Heat shock protein-90 (HSP-90) which was shown to mediate balance between NO and superoxide anion production from eNOS (Pritchard et al. 2001) was also investigated.

In HUVECs, 6 hours of DETA-NO treatment did high significantly reduced HSP-90 expression after 50 µM DETA-NO treatment. After 12 hours of treatment, both DETA-NO concentrations had high significant or even highly significant impact on HSP-90 expression. After 24 hours, mRNA expression was no longer significantly affected (**Figure 36**; 6 hours: 50 µM DETA-NO: 0.47 ± 0.14 with $p \leq 0.01$, 100 µM DETA-NO: 0.94 ± 0.29; 12 hours: 50 µM DETA-NO: 0.31 ± 0.12 with $p \leq 0.01$, 100 µM DETA-NO: 0.30 ± 0.07 with $p \leq 0.001$; 24 hours: 50 µM DETA-NO: 0.81 ± 0.32, 100 µM DETA-NO: 1.42 ± 0.70).

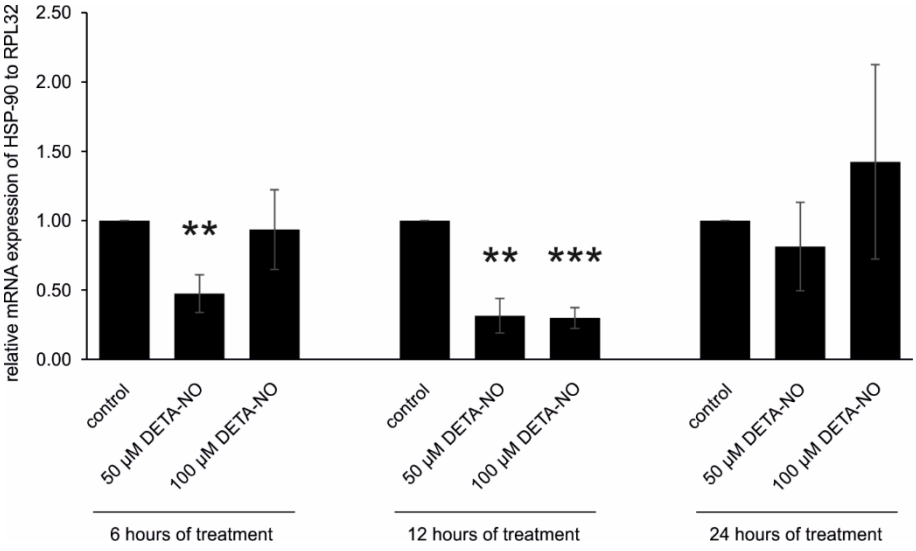

Figure 36: DETA-NO did reduce the expression of HSP-90 in HUVECs.

Relative mRNA expression of HSP-90 was investigated in PBS-treated, 50 µM and 100 µM DETA-NO treated HUVECs (n = 4 each). DETA-NO treatment did have significant effect on HSP-90 mRNA expression after 6 and 12 hours of treatment with DETA-NO ($p \leq 0.01$ and $p \leq 0.001$, respectively).

In SC cells, the DETA-NO treatment for 6 and 12 hours did not affect HSP-90 mRNA expression, RT-qPCR analysis detected that HSP-90 mRNA was significantly reduced by 100 µM DETA-NO treatment after 24 hours (**Figure 37**; 6 hours: 50 µM DETA-NO: 0.95 ± 0.06, 100 µM DETA-NO: 0.83 ± 0.11; 12 hours: 50 µM DETA-NO: 1.25 ± 0.32, 100 µM DETA-NO: 0.91 ± 0.23; 24 hours: 50 µM DETA-NO: 1.16 ± 0.42, 100 µM DETA-NO: 0.63 ± 0.13 with $p \leq 0.05$).

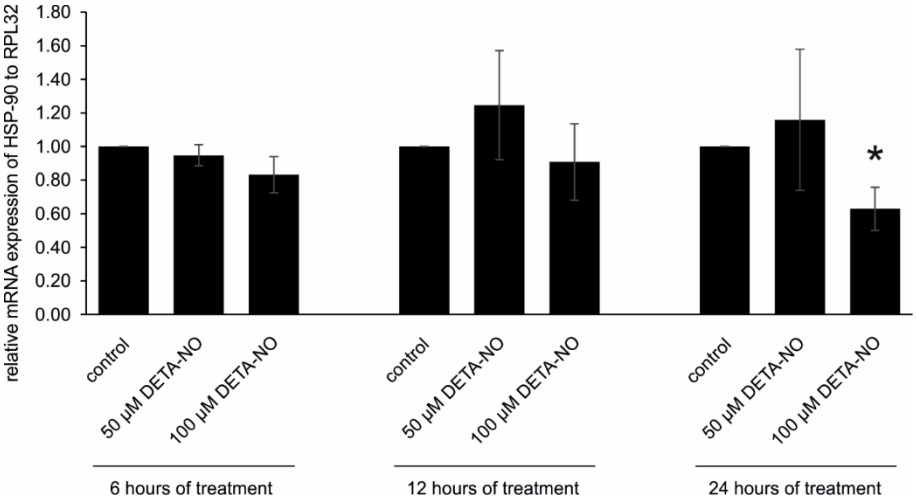

Figure 37: DETA-NO did reduce the expression of HSP-90 in SC cells.

Relative mRNA expression of HSP-90 was investigated in PBS-treated, 50 µM and 100 µM DETA-NO treated SC cells (SC68, SC74 and SC79, n = 3 each). DETA-NO treatment did have significant effect on HSP-90 mRNA expression after 24 hours of treatment with 100 µM DETA-NO ($p \leq 0.05$).

4.2.7 Effect of exogenous NO on the expression of glaucoma relevant genes

So far, it is not known whether NO influences the expression of growth factors. Therefore, the effect of exogenous NO on the expression of glaucoma relevant genes was investigated. TGF-β2 as global player was investigated first.

A significant impact of DETA-NO treatment was revealed on TGF-β2 mRNA expression in HUVECs. Already after 6 hours of DETA-NO treatment, TGF-β2 mRNA expression was high significantly reduced by the 50 µM DETA-NO treatment. Furthermore, 24 hours of the same treatment also reduced TGF-β2 expression significantly. 100 µM DETA-NO as well as the treatment for 12 hours had no significant impact on TGF-β2 mRNA expression (**Figure 38**; 6 hours: 50 µM DETA-NO: 0.58 ± 0.11 with $p \leq 0.01$, 100 µM DETA-NO: 1.04 ± 0.14; 12 hours: 50 µM DETA-NO: 1.03 ± 0.32, 100 µM DETA-NO: 2.29 ± 0.61; 24 hours: 50 µM DETA-NO: 0.63 ± 0.10 with $p \leq 0.05$, 100 µM DETA-NO: 1.32 ± 0.38).

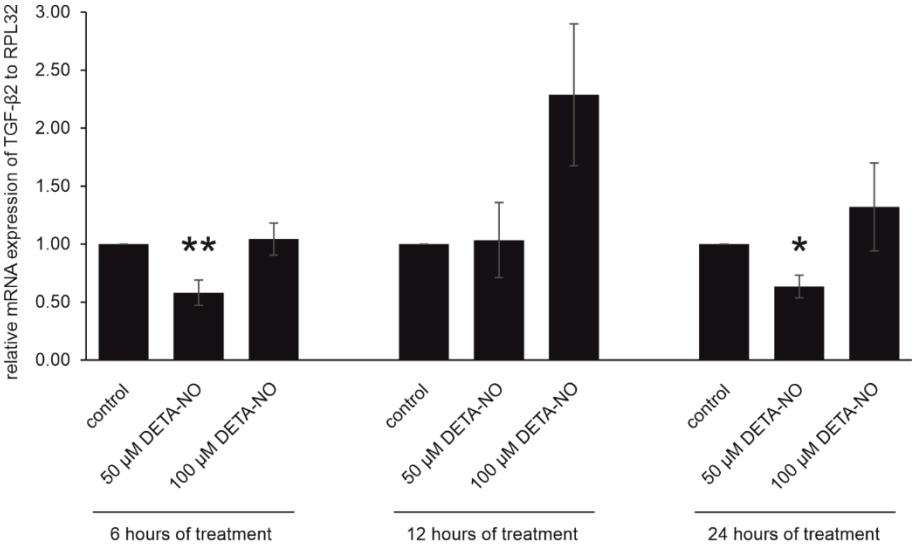

Figure 38: DETA-NO did reduce the expression of TGF-β2 in HUVECs.

Relative mRNA expression of TGF-β2 was investigated in PBS-treated, 50 µM and 100 µM DETA-NO treated HUVECs (n = 4 each). 50 µM DETA-NO treatment did have significant impact and reduced TGF-β2 mRNA expression high significantly after 6 hours of treatment and significantly after 24 hours of treatment ($p \leq 0.05$ and $p \leq 0.01$, respectively).

In SC cells, TGF-β2 expression was not affected by the DETA-NO treatment. For neither of the investigated timepoints, TGF-β2 mRNA was significantly altered (**Figure 39**; 6 hours: 50 µM DETA-NO: 0.89 ± 0.10, 100 µM DETA-NO: 0.85 ± 0.15; 12 hours: 50 µM DETA-NO: 1.44 ± 0.53, 100 µM DETA-NO: 0.97 ± 0.24; 24 hours: 50 µM DETA-NO: 0.84 ± 0.13, 100 µM DETA-NO: 0.70 ± 0.12).

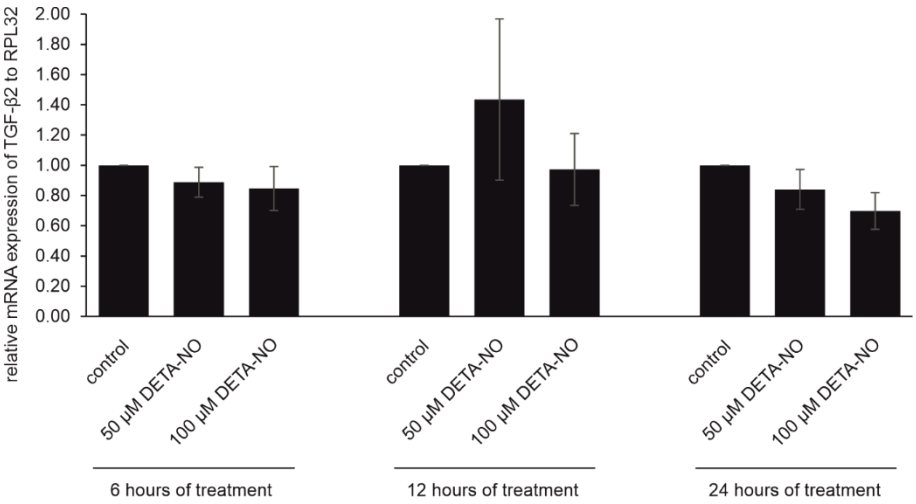

Figure 39: DETA-NO did not significantly influence the expression of TGF-β2 in SC cells.

Relative mRNA expression of TGF-β2 was investigated in PBS-treated, 50 µM and 100 µM DETA-NO treated SC cells (SC68, SC74 and SC79, n = 3 each). DETA-NO treatment did have no effect on TGF-β2 mRNA expression after 6, 12 or 24 hours of treatment ($p > 0.05$).

Next, the expression of TGF-β response genes as PAI-1 were investigated.

For expression analysis in HUVECs, PAI-1 was found to be significantly reduced at mRNA expression by the DETA-NO treatment. There, 6 hours of 50 µM DETA-NO treatment significantly reduced the PAI-1 mRNA expression. Furthermore, 12 hours of DETA-NO treatment did also have high significant impact on PAI-1 mRNA expression with both DETA-NO concentrations. On the other hand, 24 hours of DETA-NO treatment had**Figure 40**; 6 hours: 50 µM DETA-NO: 0.75 ± 0.07 with p ≤ 0.05, 100 µM DETA-NO: 1.11 ± 0.48; 12 hours: 50 µM DETA-NO: 0.42 ± 0.10, 100 µM DETA-NO: 0.55 ± 0.06 with p ≤ 0.01; 24 hours: 50 µM DETA-NO: 1.33 ± 0.34, 100 µM DETA-NO: 1.53 ± 0.15).

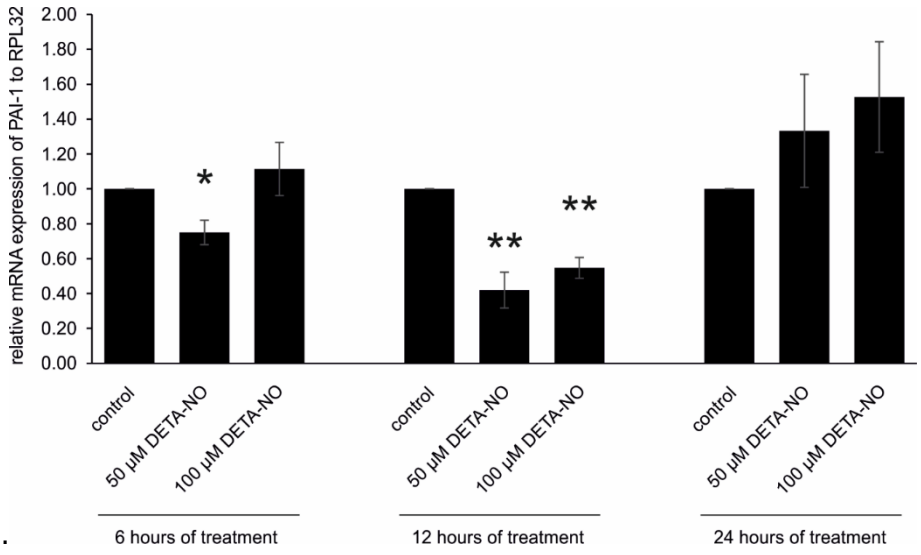

Figure 40: DETA-NO did reduce the expression of PAI-1 in HUVECs.

Relative mRNA expression of PAI-1 was investigated in PBS-treated, 50 µM and 100 µM DETA-NO treated HUVECs (n = 4 for 6 and 24 hours, n = 3 for 12 hours of treatment). DETA-NO treatment did significantly reduce PAI-1 mRNA expression after 6 hours of treatment with 50 µM DETA-NO (p ≤ 0.05). After 12 hours of DETA-NO treatment, both DETA-NO concentrations high significantly reduced PAI-1 mRNA expression (p ≤ 0.01).

Even if TGF-β2 itself was not significantly affected by DETA-NO treatment in SC cells, PAI-1 as a TGF-β2 response gene, was. While 6 and 12 hours of DETA-NO treatment had no effect, the 24-hour DETA-NO treatment did significantly reduce PAI-1 mRNA expression. Both DETA-NO concentrations highly significantly reduced the expression (**Figure 41**; 6 hours: 50 µM DETA-NO: 0.88 ± 0.16, 100 µM DETA-NO: 0.85 ± 0.09; 12 hours: 50 µM DETA-NO: 1.03 ± 0.12, 100 µM DETA-NO: 1.41 ± 0.41; 50 µM DETA-NO: 0.65 ± 0.02 with p ≤ 0.001, 100 µM DETA-NO: 0.80 ± 0.02 with p ≤ 0.001).

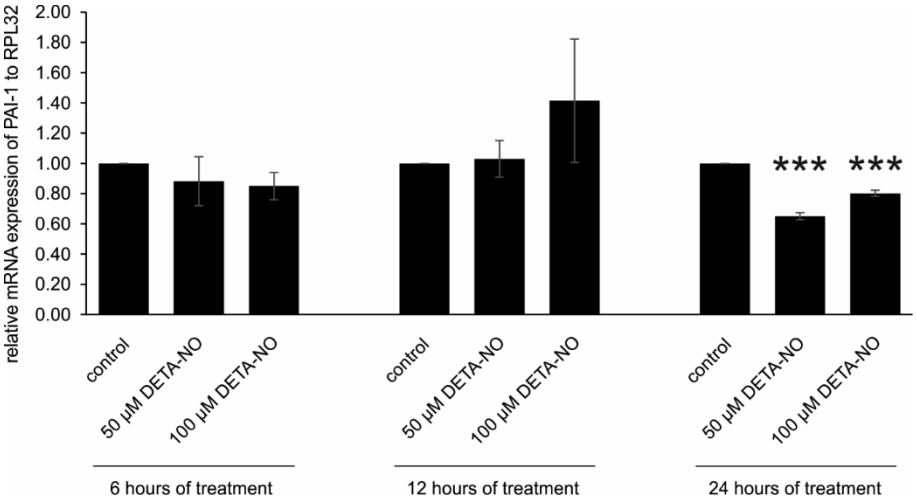

Figure 41: DETA-NO did reduce the expression of PAI-1 in SC cells.

Relative mRNA expression of PAI-1 was investigated in PBS-treated, 50 µM and 100 µM DETA-NO treated SC cells (SC68, SC74 and SC79, n = 3 each). DETA-NO treatment did have highly significant effect on PAI-1 mRNA expression after 24 hours of treatment with 50 and 100 µM DETA-NO (p ≤ 0.001).

CTGF as another downstream mediator of TGFβ-2 signaling was further investigated.

In HUVECs, a high significant reduction of CTGF mRNA expression was found after 6 hours of treatment with 50 µM DETA-NO as well as after 12 hours of treatment with both DETA-NO concentrations. After 24 hours of DETA-NO treatment, no significant impact was found (**Figure 42**; 6 hours: 50 µM DETA-NO: 0.63 ± 0.10 with p ≤ 0.01, 100 µM DETA-NO: 1.35 ± 0.35; 12 hours: 50 µM DETA-NO: 0.55 ± 0.15 with p ≤ 0.01, 100 µM DETA-NO: 0.60 ± 0.13 with p ≤ 0.01; 24 hours: 50 µM DETA-NO: 0.86 ± 0.18, 100 µM DETA-NO: 1.16 ± 0.24).

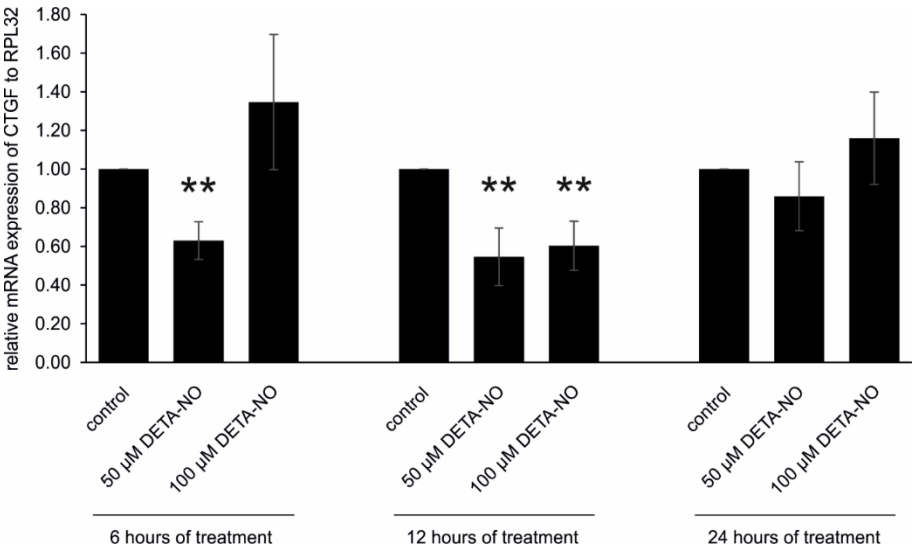

Figure 42: DETA-NO did reduce the expression of CTGF in HUVECs.

Relative mRNA expression of CTGF was investigated in PBS-treated, 50 µM and 100 µM DETA-NO treated HUVECs (n = 4 each). 6 hours of treatment with 50 µM DETA-NO did as well as both DETA-NO concentrations did high significantly reduce CTGF mRNA expression (p ≤ 0.01).

In SC cells, CTGF mRNA expression was highly significantly reduced by the 100 µM DETA-NO treatment already after 6. After 12 hours of treatment, 50 µM DETA-NO significantly reduced the CTGF mRNA expression. Furthermore, 24 hours of treatment had also impact on CTGF expression. While 50 µM DETA-NO did high significantly reduce the CTGF mRNA expression, 100 µM DETA-NO did significantly reduce the expression. Therefore, DETA-NO treatment did have significant impact on CTGF expression at all three investigated timepoints (**Figure 43**; 6 hours: 50 µM DETA-NO: 0.84 ± 0.09; 100 µM DETA-NO: 0.69 ± 0.02 with p ≤ 0.001; 12 hours: 50 µM DETA-NO: 0.82 ± 0.06 with p ≤ 0.05, 100 µM DETA-NO: 0.77 ± 0.13; 24 hours: 50 µM DETA-NO: 0.68 ± 0.04 with p ≤ 0.01, 100 µM DETA-NO: 0.63 ± 0.10 with p ≤ 0.05).

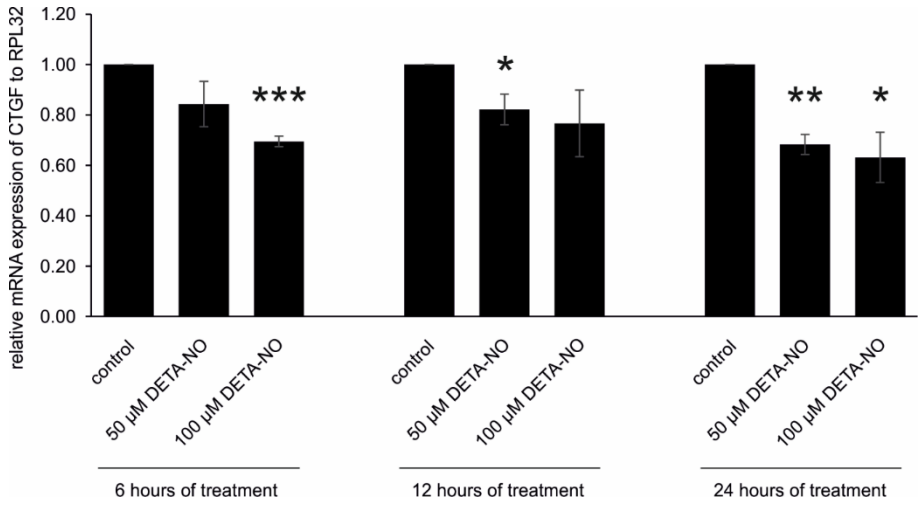

Figure 43: DETA-NO did reduce the expression of CTGF in SC cells.

Relative mRNA expression of CTGF was investigated in PBS-treated, 50 µM and 100 µM DETA-NO treated SC cells (SC68, SC74 and SC79, n = 3 each). DETA-NO treatment already did have highly significant effect on CTGF mRNA expression after 6 hours of treatment with 100 µM DETA-NO (p ≤ 0.001). After 12 hours of treatment, 50 µM of DETA-NO treatment significantly reduced the CTGF expression (p ≤ 0.05). After 24 hours, 50 as well as 100 µM DETA-NO treatment did have significant effect. While 50 µM DETA-NO high significantly reduced the expression of CTGF (p ≤ 0.01), 100 µM DETA-NO treatment reduced CTGF expression significantly (p ≤ 0.05).

Further it was investigated if a reduced CTGF mRNA expression leads to a reduced protein synthesis in SC cells as well (**Figure 44**). While 50 µM DETA-NO treatment had no effect on CTGF protein synthesis (0.90 ± 0.08, p > 0.05), 100 µM DETA-NO treatment reduced CTGF synthesis highly significantly (0.37 ± 0.04 with p ≤ 0.001).

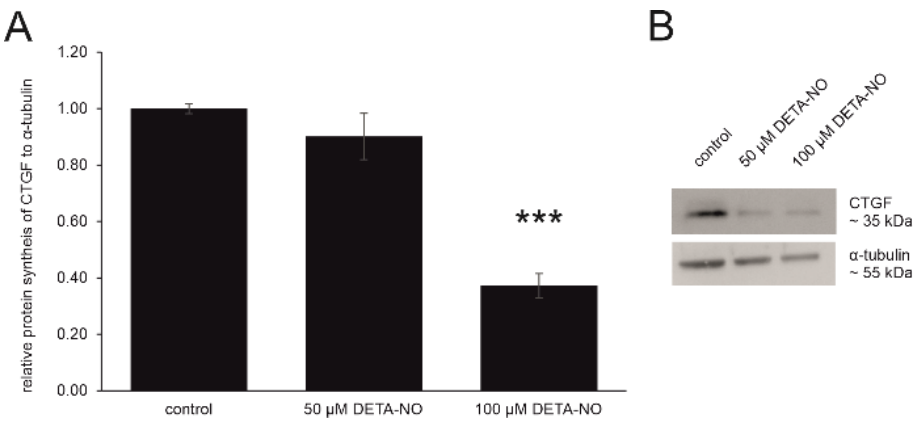

Figure 44: DETA-NO did reduce the synthesis of CTGF in SC cells.

Relative protein synthesis of CTGF was investigated by Western Blot in three SC cell strains (SC71 n = 3, SC74 n = 4 and SC79 n = 5) after 24 hours of DETA-NO treatment. α-tubulin was used as reference protein.

A) CTGF protein synthesis was highly significantly reduced by the 100 µM DETA-NO treatment ($p \leq 0.001$) while 50 µM treatment did have no effect. This finding underlines the finding at mRNA expression.

B) Representative Western Blot of CTGF (~ 35 kDa) and the reference protein α-tubulin (~ 55 kDa).

4.2.8 Effect of exogenous NO on the expression of ECM components

Since changes in the composition of the ECM play a major role in the pathogenesis of POAG, its components were investigated in the present study. One of them, nidogen-1 (NID-1), is a component of the basement membrane and binds collagen type IV as well as laminin, thereby connecting them and leading to stabilization.

DETA-NO treatment of SC cells had no effect on the relative mRNA expression of NID-1 after 6 and 12 hours of treatment. However, the expression of NID-1 was significant reduced after 24 hours by both DETA-NO concentrations (**Figure 45**; 6 hours: 50 µM DETA-NO: 1.06 ± 0.11, 100 µM DETA-NO: 0.91 ± 0.10; 12 hours: 50 µM DETA-NO: 0.91 ± 0.07, 100 µM DETA-NO: 0.96 ± 0.14; 24 hours: 50 µM DETA-NO: 0.77 ± 0.09 with $p \leq 0.05$, 100 µM DETA-NO: 0.88 ± 0.05 with $p \leq 0.05$).

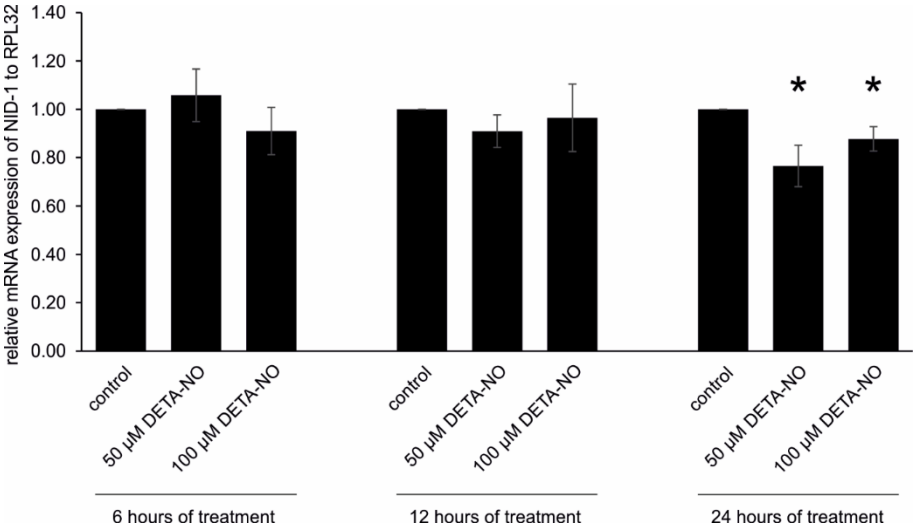

Figure 45: DETA-NO did reduce the expression of NID-1, a component of the basement membrane.

Relative mRNA expression of NID-1 was investigated in PBS-treated, 50 µM and 100 µM DETA-NO treated SC cells (SC68, SC74 and SC79, n = 3 each). DETA-NO treatment did significantly reduce NID-1 mRNA expression after 24 hours of treatment (p ≤ 0.05).

Furthermore, other ECM components of interest were investigated. After 24 hours of DETA-NO treatment, COL4A2 and FN gene expression was investigated in SC cells. There, COL4A2 expression was highly significantly decreased after the treatment with 100 µM DETA-NO compared to the PBS-treated control (**Figure 46** A; 50 µM DETA-NO: 0.79 ± 0.17, 100 µM DETA-NO: 0.39 ± 0.16 with p ≤ 0.001). The reduction of FN mRNA expression was also highly significantly after the treatment with 100 µM DETA-NO (**Figure 46** B; 50 µM DETA-NO: 1.08 ± 0.08, 100 µM DETA-NO: 0.78 ± 0.03 with p ≤ 0.001).

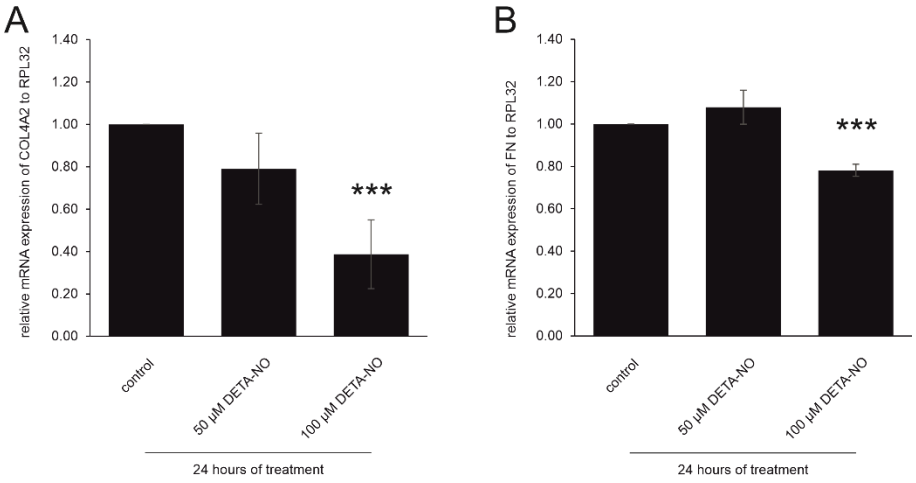

Figure 46: DETA-NO did reduce the expression of the ECN components COL4A2 and FN.

Relative mRNA expression of (A) COL4A2 and (B) FN was investigated in PBS-treated, 50 µM and 100 µM DETA-NO treated SC cells (SC68, SC74 and SC79, n = 3 each). COL4A2 and FN mRNA expression was high significantly reduced after 24 hours of 100 µM DETA-NO treatment (p ≤ 0.001). Role of miRNA in glaucomatous outflow resistance dysregulation.

4.2.9 Small RNA sequencing revealed altered miRNA profile of glaucomatous SC cells

Research of recent years had shown that miRNA seem to have regulatory function in many processes as neurodegenerative disorders (Eacker et al. 2009; Ferrarelli 2015), their influence on POAG development came into focus. Therefore, this study investigated the altered miRNA profile of glaucomatous SC cells and focused further on the influence of miRNA alteration on glaucoma relevant genes.

In preliminary investigations, small RNA sequencing was performed by this working group to identify differentially expressed miRNAs in glaucomatous and normal SC cell strains. Therefore, full transcriptome sequencing of four normal and three glaucomatous SC cell strains was performed, collecting reads per million (RPM) for each miRNA in each sample set.

In total, 1317 miRNAs were identified with altered expression patterns in the glaucomatous SC strains compared to normal SC strains. 138 among them were differentially regulated with an expression ratio differences of either greater than $\log_2(0.8)$ or less than $\log_2(-0.8)$.

The calculation of $\log_2$-fold changes does level the disadvantages of only calculating quantity changes which might miss differently expressed miRNAs with large differences but small ratio. To avoid these incorrect weighting, the following equation was used: $\log_2$ fold = $\log_2$(mean RPM(glaucoma)) - $\log_2$(mean RPM(normal)).

Out of the strongly altered 138 miRNAs, 39 were predicted to the NO system. In **Figure 47**, the 26 up-regulated miRNAs are presented while the 13 down-regulated miRNAs are shown in **Figure 48**.

SC cells	Glaucoma	Normal	
miRNA	mean $RPM_{annot.}$	mean $RPM_{annot.}$	log2fold
hsa-miR-376a-3p	159.5	0.5	8.2
hsa-miR-29b-3p	126.6	1.3	6.7
hsa-miR-495-3p	63.0	1.3	5.6
hsa-miR-19b-3p	156.4	5.1	4.9
hsa-miR-193a-3p	49.4	3.0	4.0
hsa-miR-136-3p	694.5	70.4	3.3
hsa-miR-20a-5p	42.0	5.2	3.0
hsa-miR-106b-5p	46.6	8.0	2.5
hsa-miR-17-5p	37.1	7.1	2.4
hsa-miR-30c-5p	242.1	46.2	2.4
hsa-miR-221-5p	159.4	35.5	2.2
hsa-miR-299-5p	161.9	41.1	2.0
hsa-miR-138-5p	123.5	32.3	1.9
hsa-miR-185-5p	273.4	74.1	1.9
hsa-miR-23a-3p	980.9	296.8	1.7
hsa-miR-181c-5p	439.2	143.7	1.6
hsa-miR-130a-3p	196.1	66.2	1.6
hsa-miR-16-5p	232.6	82.4	1.5
hsa-miR-28-5p	130.8	49.9	1.4
hsa-miR-222-3p	56,572.1	22,580.9	1.3
hsa-miR-493-3p	302.9	146.3	1.1
hsa-miR-29a-3p	3,330.6	1,614.2	1.0
hsa-miR-181c-3p	70.9	35.4	1.0
hsa-miR-455-3p	128.0	66.3	0.9
hsa-miR-31-5p	9,115.9	4,819.5	0.9
hsa-miR-598-3p	62.1	35.2	0.8

Figure 47: Up-regulated miRNAs related to the NO pathways.

By small RNA sequencing, 1317 miRNAs were found to be differentially expressed in glaucomatous SC cells compared to normal SC cells. Out of the 138 moist regulated miRNAs, 26 up-regulated miRNAs were related to the NO pathway. RPM = reads per million, hsa = homo sapiens.

SC cells	Glaucoma	Normal	
miRNA	mean $RPM_{annot.}$	mean $RPM_{annot.}$	log2fold
hsa-miR-184	14.5	762.2	-5.7
hsa-miR-935	6.8	37.6	-2.5
hsa-miR-199a-5p	401.6	1,466.1	-1.9
hsa-miR-625-5p	14.4	36.9	-1.4
hsa-miR-214-5p	12.9	30.0	-1.2
hsa-miR-1270	30.2	65.6	-1.1
hsa-miR-320c	31.6	64.4	-1.0
hsa-let-7a-5p	58.4	113.9	-1.0
hsa-miR-106b-3p	224.7	430.4	-0.9
hsa-let-7d-5p	567.1	1,077.7	-0.9
hsa-let-7b-5p	93,404.4	174,824.9	-0.9
hsa-miR-27b-5p	66.7	114.6	-0.8
hsa-miR-204-5p	142.2	248.9	-0.8

Figure 48: Down-regulated miRNAs related to the NO pathways.

By small RNA sequencing, 1317 miRNAs were found to be differentially expressed in glaucomatous SC cells compared to normal SC cells. Out of the 138 moist regulated miRNAs, 13 down-regulated miRNAs were related to the NO pathway. RPM = reads per million, hsa = homo sapiens.

4.2.10 Correlation analysis between miRNA expression and cell stiffness in SC cells

For all 39 miRNAs, associated to the NO system, correlation analysis was performed. Thereby, the miRNA abundance - given by small RNA sequencing as mean RPM for glaucomatous as well as normal SC cells - was set in correlation of stiffness data by AFM.

As indicated by the sequencing results, miRNAs were either more abundant in glaucomatous SC or in normal SC cells, dependent on its up- or down-regulation (compare **Figure 47** and **Figure 48**). Furthermore, glaucomatous SC cell strains were in general stiffer compared to normal SC cell strains (Overby et al. 2014).

For four miRNAs, a statistically significant correlation of miRNA abundance and cell stiffness was found. For miR-30c-5p, miR-138-5p, miR-222-3p and miR-455-3p, which all were found to be up-regulated in the sequencing study (compare **Figure 47**), the miRNA abundance was the higher, the stiffer the cells. For miR-30c-5p, a correlation of r = 0.94 with p = 0.0050 was found. miR-138-5p had a correlation of r = 0.98 with p = 0.0006 and miR-222-3p a correlation of r = 0.91 with p = 0.0090. Moreover, the correlation of miR-455-3p was r = 0.93 with p = 0.0070 (**Figure 49**).

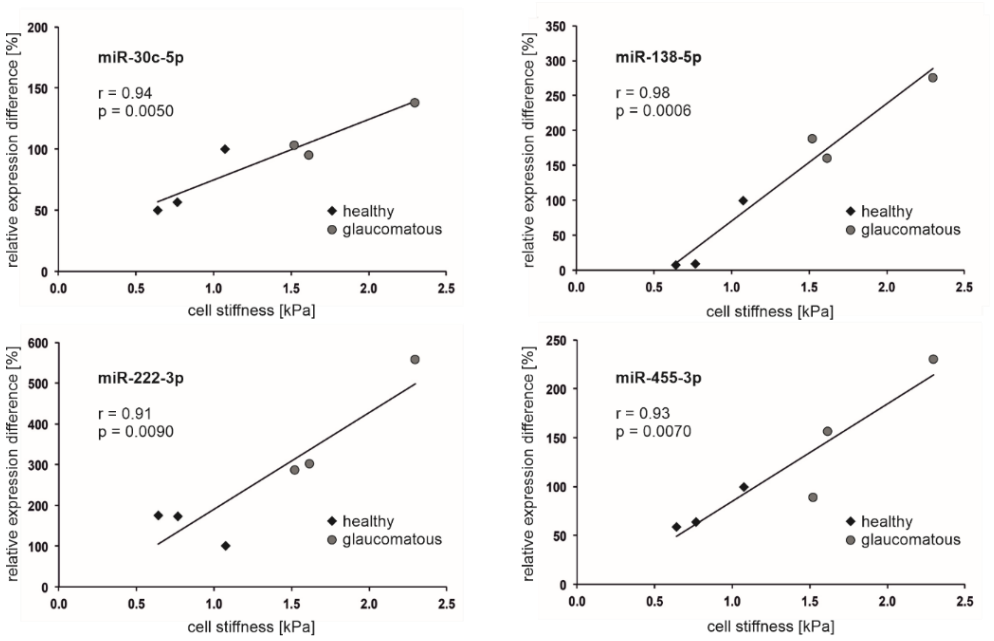

Figure 49: Correlation analysis between miRNA expression and cell stiffness.

For four miRNAs, a positive correlation of miRNA abundance and cell stiffness was found ($p \leq 0.001$, $r \sim 1$ with exact values mentioned within the graph). The more miRNA was detected by small RNA sequencing, concerning miR-30c-5p, miR-138-5p, miR-222-3p and miR-455-3p, the stiffer the cell strain was found by atomic force microscopy (Overby et al. 2014).

Furthermore, all mentioned miRNAs were more abundant in glaucomatous SC cells strains compared to healthy cell strains. Additionally, glaucomatous SC cell strains were stiffer in general. Black diamond: healthy SC cell strain, dark gray circle: glaucomatous SC cell strain.

4.2.11 Verification of small RNA sequencing data by TaqMan technique

With the positive correlation of miRNA abundance and cell stiffness, the focus was set on miR-30c-5p, miR-138-5p, miR-222-3p and miR-455-3p for further investigations. Initially, the small RNA sequencing results were verified by TaqMan technique.

RNA from four healthy SC cell strains (SC60, SC67, SC71 and SC75) and three glaucomatous SC cell strains (gSC57, gSC62 and gSC63) was investigated while miR-26a-5p was used as reference miRNA (**Figure 50**). For miR-30c-5p and miR-138-5p a significant increase of miRNA in glaucomatous SC cell strains could not be confirmed since only slight increases were detected (miR-30c-5p: healthy: 1.00 ± 0.32, glaucomatous: 1.28 ± 0.36; miR-138-5p: healthy: 1.00 ± 0.23, glaucomatous: 1.90 ± 0.40). MiR222-3p as well as miR455-3p revealed a significant increase of both miRNAs (miR-222-3p: healthy: 1.00 ± 0.13, glaucomatous: 3.06 ± 0.59 with $p \leq 0.01$; miR-455-3p: healthy: 1.00 ± 0.40, glaucomatous: 2.26 ± 0.24 with $p \leq 0.05$). Thereby, initial miRNA sequencing data were verified for miR-222-3p and miR-455-3p.

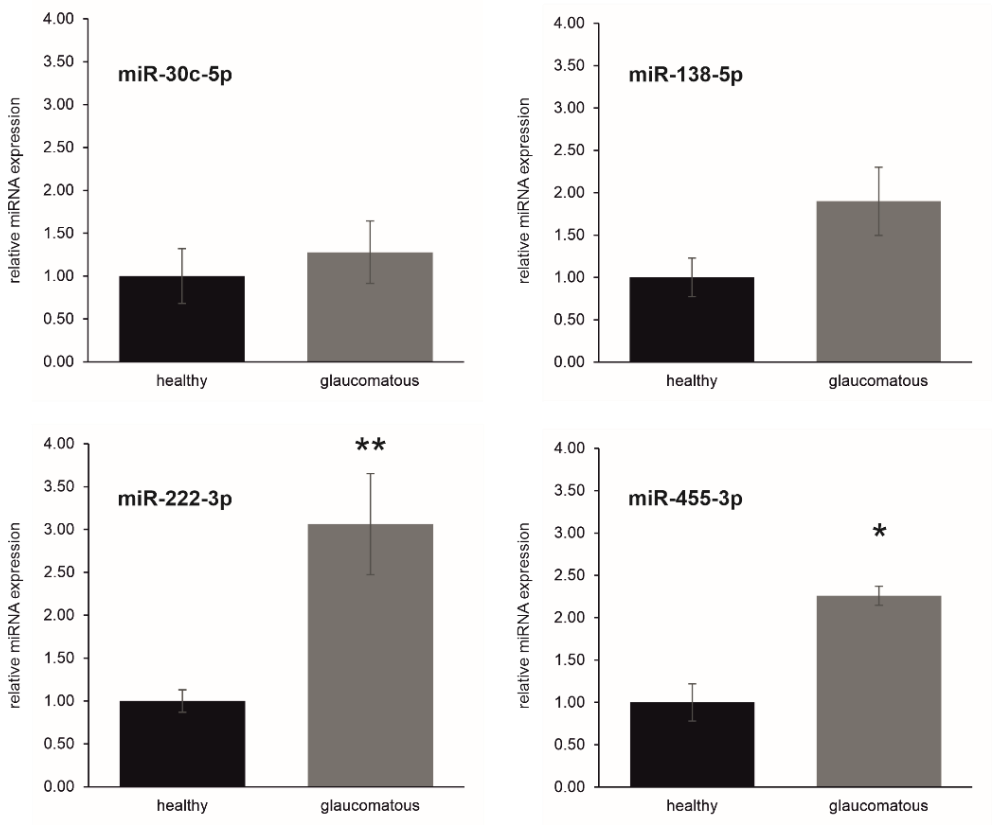

Figure 50: Verification of initial small RNA sequencing data.

Relative miRNA expression of those four miRNAs with positive correlation between miRNA abundance and cell stiffness was investigated in RNA from four healthy SC cell strains (SC60, SC67, SC71 and SC75) and three glaucomatous SC cell strains (SC57g, SC62g and SC63g) by TaqMan technique, while miR-26a-5p was used as reference miRNA.

For miR-30c-5p and miR-138-5p, a significant increase of miRNA in glaucomatous SC cell strains could not be confirmed since only slight increases were detected. However, miR222-3p as well as miR455-3p were proven to be significantly increased in glaucomatous SC cells compared to healthy controls ($p \leq 0.05$, $p \leq 0.01$).

Furthermore, all four miRNAs revealed expression differences between healthy and glaucomatous SC cell strains when presenting TaqMan data as changes of the $\log_2$ fold. Thereby, the $\log_2$ fold of the mean difference between miRNA expression in healthy and glaucomatous SC cell strains was greater than $\log_2(0.8)$ for three of the four miRNAs (**Table 36**). For miR-30c-5p, the $\log_2$ fold of expression difference was only 0.36, but for miR-138-5p with 0.93, for miR-222-3p with 1.61 and for miR-455-3p with 1.18 greater than the cut-off set for this study.

	array data	verification by TaqMan		
miRNA	$\log_2$ fold of expression difference	mean expression in healthy SC cells	mean expression in glaucomatous SC cells	$\log_2$ fold of expression difference
miR-30c-5p	2.4	1.00	1.28	0.36
miR-138-5p	1.9	1.00	1.90	0.93
miR-222-3p	1.3	1.00	3.06	1.61
miR-455-3p	0.9	1.00	2.26	1.18

Table 36: MiRNA expression differences of healthy and glaucomatous SC cells, presented as $\log_2$ fold.

Three of four investigated miRNAs revealed $\log_2$ fold of expression differences greater than $\log_2(0.8)$, indicating great expression differences between healthy and glaucomatous SC cells.

Likewise, these results support the assumption that miR-138-5p, miR-222-3p as well as miR-455-3p are strongly up-regulated in SC cells under glaucomatous conditions while the upregulation was less pronounce for miR-30c-5p.

4.2.12 Exogenous NO effectively reduced miRNA abundance in DETA-NO treated SC cells

This study has already presented a significantly reduced cortical and subcortical cell stiffness of DETA-NO treated SC cells (compare 4.2.5). To reveal if NO affects the expression of miRNAs, SC cells were investigated via TaqMan after DETA-NO treatment for 6, 12 or 24 hours (**Figure 51**).

For miR-30c-5p (n = 5) and miR-138-5p (n = 4), no significant changes of miRNA were found in DETA-NO treated SC cells compared to PBS-treated controls (miR-30c-5p: control: 1.00 ± 0.00, 50 µM DETA-NO: 0.89 ± 0.22, 100 µM DETA-NO: 0.91 ± 0.20; miR-138-5p: control: 1.00 ± 0.00, 50 µM DETA-NO: 0.66 ± 0.20, 100 µM DETA-NO:

0.74 ± 0.20). For miR-222-3p (n = 4), a significant decreased expression was found in 100 µM DETA-NO treated SC cells after 6 hours of treatment (control: 1.00 ± 0.00, 50 µM DETA-NO: 1.11 ± 0.31, 100 µM DETA-NO: 0.67 ± 0.21 with $p \leq 0.05$). After 24 hours of treatment, miR-455-3p (n = 4) was high significantly reduced in 50 µM DETA-NO treated SC cells (control: 1.00 ± 0.00, 50 µM DETA-NO: 0.48 ± 0.10 with $p \leq 0.01$, 100 µM DETA-NO: 0.94 ± 0.28). Thereby, DETA-NO treatment reduces the expression of miRNAs that were found to be elevated under glaucomatous conditions.

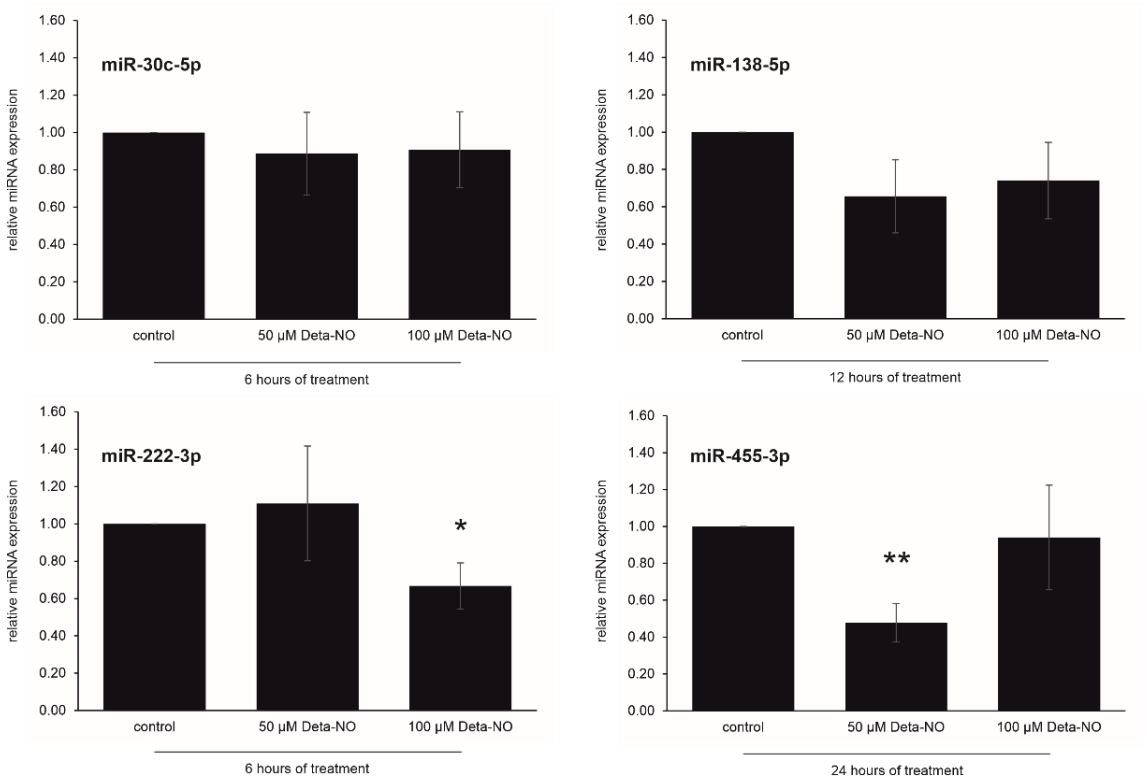

Figure 51: DETA-NO treatment reduced miRNA expression that were found to be elevated under glaucomatous conditions.

Relative miRNA expression of miRNAs was investigated via TaqMan technique in SC cells (SC68) after DETA-NO treatment for 6, 12 or 24 hours. miR-191-5p was used as reference miRNA.

For miR-30c-5p (n = 5) and miR-138-5p (n = 4) no significant changes of miRNA was found in DETA-NO treated SC cells compared to PBS-treated controls. For miR-222-3p, a significant decreased expression was found in 100 µM DETA-NO treated SC cells after 6 hours of treatment (n = 4, $p \leq 0.05$). After 24 hours of treatment, miR-455-3p was high significantly reduced in 50 µM DETA-NO treated SC cells (n = 4, $p \leq 0.01$).

To assure that the TaqMan technique is viable and its results are resilient, Northern Blots were performed to validate TaqMan results (**Figure 52**). Relative miRNA expression of miR-222-3p was investigated by Northern Blot (SC68, n=1) and U6 was used as loading control. MiR-222-3p as with 22,580.9 RPM the most abundant one of the investigated miRNAs was detectable by a radioactive probe and seems to be

affected in a dose-dependent manner by DETA-NO treatment (control: 1.00, 50 µM DETA-NO: 0.66, 100 µM DETA-NO: 0.53).

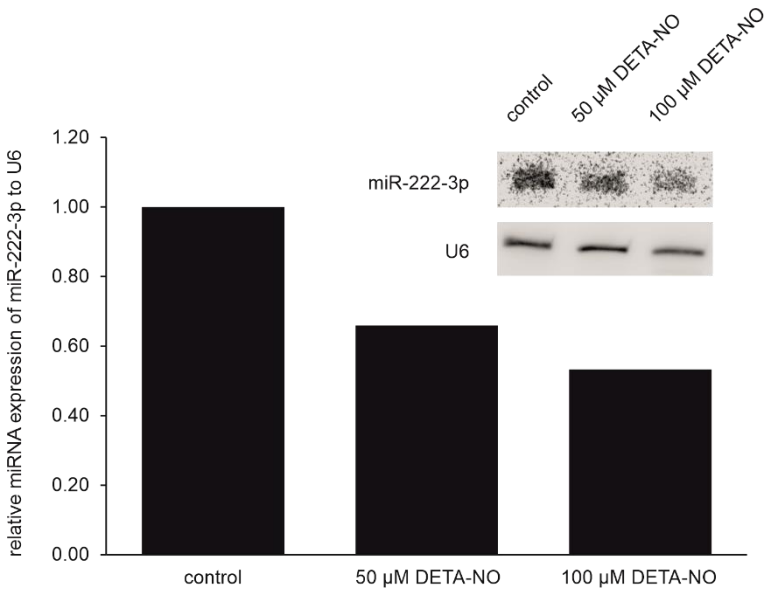

Figure 52: Verification of TaqMan results by Northern Blot.

Relative miRNA expression of miR-222-3p was investigated by Northern Blot (SC68, n = 1) to verify TaqMan data. U6 was used as loading control. MiR-222-3p as with 22,580.9 RPM the most abundant one of the investigated miRNAs was easily detectable by a radioactive probe.

MiR-455-3p on the other hand was not detectable due to its low abundance of only 66.3 RPM (data not shown).

4.2.13 MiRNA-transfected cells reveal alterations in the expression profile of glaucoma relevant genes

Thereafter, the effect of the miRNA abundance on the expression profile of glaucoma relevant genes was investigated. Therefore, four SC cell strains (SC68, SC71, SC74 and SC79), one TM cell strain (TM120) as well as HUVECs were transfected with miRNA mimics or inhibitors and its appropriate controls (see 3.2.2.2).

Within initial experiments, a concentration of 100 nM of miRNA mimics and 25 nM of miRNA inhibitors have been found to be a suitable concentration for transfection experiments (data not shown). Consequently, the corresponding controls were used at the same concentrations. Furthermore, controls not only differed within the applied concentrations but also concerning their design. Due to those facts, different controls for miRNA mimic and inhibitor experiments were chosen.

Next, the effectiveness of miRNA inhibition was proven (SC68, SC71 and SC79). MiRNA level were investigated after transfection with miR-222-3p inhibitors for 144 hours (**Figure 53**).

By comparing the miR-222-3p amounts after treatment with transfection reagent alone (dharmacon-co) and transfection with non-targeting controls (inhibitor-co), no significant changes were observed (0.73 ± 0.14 and 1.00 ± 0.23, respectively). Thereby, the non-targeting inhibitor controls were proven to have no influence on miR-222-3p expression. When transfected with miR-222-3p inhibitors, miR-222-3p was highly significantly reduced in comparison to both controls (0.17 ± 0.03 with $p \leq 0.001$ in comparison to both controls). These findings underlined the efficiency of the miRNA inhibitors used for transfection experiments.

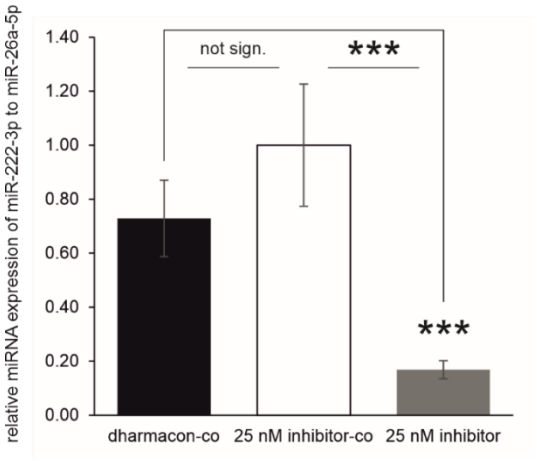

Figure 53: Proof of effective inhibition of miR-222-3p expression by transfection with miR-222-3p inhibitors.

Relative miRNA expression of miR-222-3p was investigated via TaqMan technique in three SC cell strains (SC68, SC71 and SC79, n = 3 each) after transfection with miR-222-3p inhibitor for 144 hours. miR-26a-5p was used as reference miRNA.

When transfected with miR-222-3p inhibitors, miR-222-3p was highly significantly reduced ($p \leq 0.001$). On the other side, treatment with transfection reagent alone (dharmacon-co) and transfection with non-targeting controls (inhibitor-co) did not lead to significant differences concerning miR-222-3p abundance (not sign.).

Additionally, the specificity of miRNA inhibition was proven. Relative miRNA expression of miR-222-3p was investigated in SC cells after transfection with miR-455-3p inhibitor for 144 hours (**Figure 54**).

When miR-455-3p was inhibited by transfection with miR-455-3p inhibitors, miR-222-3p was not affected (dharmacon-co: 0.90 ± 0.12, 25 nM inhibitor-co: 1.00 ± 0.07, 25 nM inhibitor (for miR-455-3p): 1.02 ± 0.06). This finding underlined the specificity of inhibitors used for transfection experiments.

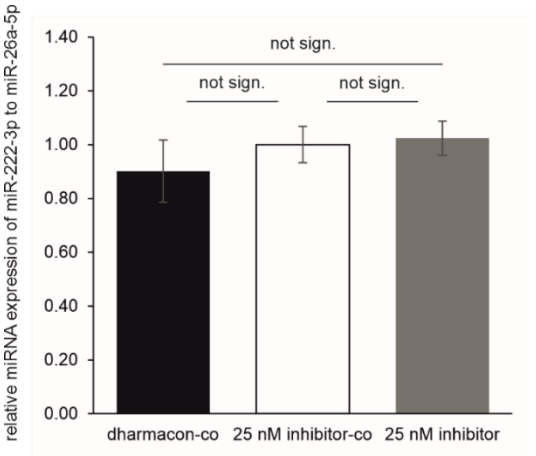

Figure 54: Proof of specific inhibition with miR-455-3p that did not affect the expression of miR-222-3p.

Relative miRNA expression of miR-222-3p was investigated via TaqMan technique in SC cells (SC71, n = 3) after transfection with miR-455-3p inhibitor for 144 hours. miR-26a-5p was used as reference miRNA.

When miR-455-3p was inhibited by transfection with miR-455-3p inhibitors, miR-222-3p was not affected (not sign.). This finding underlined the specificity of inhibitors used for transfection experiments.

All following transfection results are calculated relative to the specific, non-targeting mimic or inhibitor control experiments which will be indicated by dashed lines. Thereby, the influence of miRNA alterations was investigated on the expression profile of glaucoma relevant genes.

4.2.13.1 transfection effects of miR-222-3p mimic and inhibitors

TGF-β2

After the transfection with miR-222-3p mimics and inhibitors, the expression of TGF-β2 was investigated (**Figure 55**). **Table 37** summarizes the findings.

In HUVECs (n = 4 for 48 hours, n = 3 for 72 hours and n = 5 for 144 hours), TGF-β2 expression was slightly reduced after 48 hours and high significantly after 72 hours. At that timepoint, miR-222-3p inhibition significantly increased the expression of TGF-β2. After 144 hours of treatment, no effect on TGF-β2 expression was investigated.

In SC cells (SC68, SC71, SC74 and SC79, n = 3 each) TGF-β2 expression was unaffected at all three investigated timepoints.

When TM cells (TM120, n = 3 for 48 hours, n = 6 for 72 hours, n = 3 for 144 hours) were transfected with miR-222-3p mimics, TGF-β2 expression was high significantly reduced. On the other hand, the transfection with miR-222-3p inhibitors did not significantly affect TGF-β2 expression.

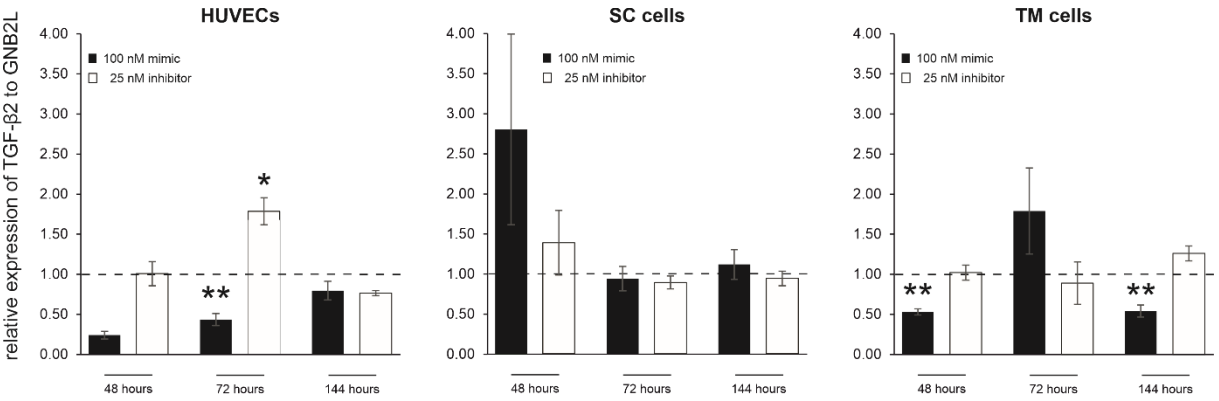

Figure 55: TGF-β2 expression was affected by transfection with miR-222-3p mimics and inhibitors in HUVECs and TM cells, but not in SC cells.

Relative mRNA expression of TGF-β2 was investigated in HUVECs (n = 4 for 48 hours, n = 3 for 72 hours and n = 5 for 144 hours), four SC cell strains (SC68, SC71, SC74 and SC79, n = 3 each) and TM cells (TM120, n = 3 for 48 hours, n = 6 for 72 hours, n = 3 for 144 hours) after transfection with miR-222-3p mimics and inhibitors as well as appropriate controls (set to 1, indicated by the dashed lines) for 48, 72 and 144 hours. GNB2L was used as reference gene.

TGF-β2	48 hours		72 hours		144 hours	
	miR-222-3p mimics	miR-222-3p inhibitors	miR-222-3p mimics	miR-222-3p inhibitors	miR-222-3p mimics	miR-222-3p inhibitors
HUVECs	0.24 ± 0.05 p = 0.07	1.00 ± 0.15	0.43 ± 0.07 p ≤ 0.01	1.78 ± 0.17 p ≤ 0.05	0.79 ± 0.12	0.77 ± 0.03
SC cells	2.67 ± 1.13	1.32 ± 0.38	0.89 ± 0.14	0.85 ± 0.08	1.06 ± 0.17	0.89 ± 0.09
TM cells	0.53 ± 0.04 p ≤ 0.01	1.02 ± 0.09	1.79 ± 0.54	0.89 ± 0.27	0.54 ± 0.08 p ≤ 0.01	1.26 ± 0.09 p = 0.06

Table 37: Summary of transfection effects on the expression of TGF-β2 after miR-222-3p transfection.

TGF-β2 expression after miR-222-3p transfection calculated in relation to appropriate controls. Given are expression changes ± SEM and relevant p-values. Significant changes are highlighted in red.

PAI-1

Since TGF-β2 expression was affected by miR-222-3p transfection, the expression of its response gene PAI-1 was investigated, too (**Figure 56**). **Table 38** summarizes the results.

In HUVECs (n = 4 for 48 hours, n = 6 for 72 hours and n = 5 for 144 hours), the expression of PAI-1 was not affected at any investigated timepoint.

When SC cells (SC68, SC71, SC74 and SC79, n = 3 each) were transfected with miR-222-3p mimics, PAI-1 expression was high significantly reduced after 144 hours of transfection. On the other hand, miR-222-3p inhibitors did not have any effect on PAI-1 expression.

When TM cells (TM120, n = 3 for 48 hours, n = 6 for 72 hours, n = 3 for 144 hours) were transfected with miR-222-3p mimics, PAI-1 expression was high significantly

reduced after 144 hours of transfection which was equally to the findings in SC cells. The transfection with miR-222-3p inhibitors did not significantly affect PAI-1 expression at any of the investigated timepoints.

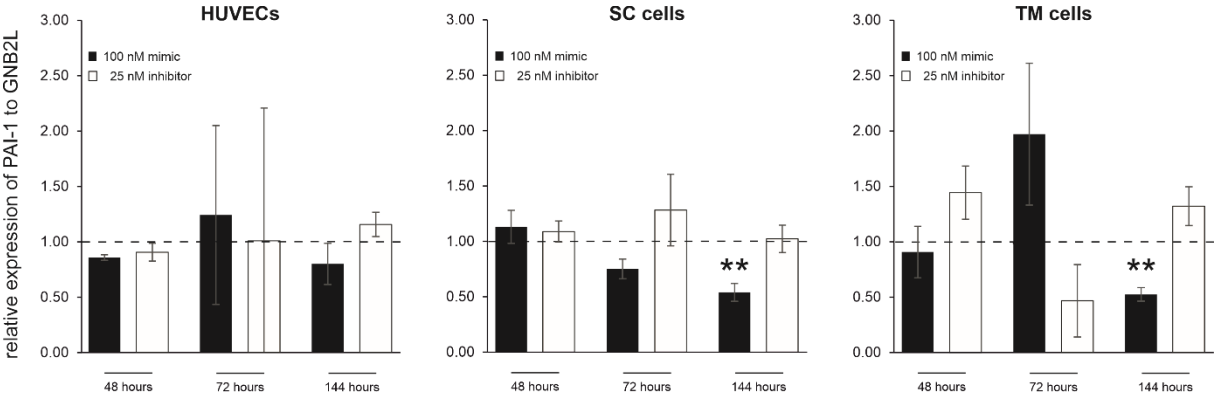

Figure 56: PAI-1 expression was affected by transfection with miR-222-3p mimics in SC and TM cells, but not at all in HUVECs.

Relative mRNA expression of PAI-1 was investigated in HUVECs (n = 4 for 48 hours, n = 6 for 72 hours and n = 5 for 144 hours), four SC cell strains (SC68, SC71, SC74 and SC79, n = 3 each) and TM cells (TM120, n = 3 for 48 hours, n = 6 for 72 hours, n = 3 for 144 hours) after transfection with miR-222-3p mimics and inhibitors as well as appropriate controls (set to 1, indicated by the dashed lines) for 48, 72 and 144 hours. GNB2L was used as reference gene.

PAI-1	48 hours		72 hours		144 hours	
	miR-222-3p mimics	miR-222-3p inhibitors	miR-222-3p mimics	miR-222-3p inhibitors	miR-222-3p mimics	miR-222-3p inhibitors
HUVECs	0.85 ± 0.03	0.90 ± 0.08	1.24 ± 0.81	1.00 ± 1.19	0.80 ± 0.19	1.16 ± 0.11
SC cells	1.19 ± 0.16	1.15 ± 0.10	0.78 ± 0.09 p = 0.09	1.35 ± 0.34	0.56 ± 0.08 p ≤ 0.01	1.08 ± 0.13
TM cells	0.90 ± 0.23	1.44 ± 0.24	1.97 ± 0.64	0.47 ± 0.33	0.52 ± 0.06 p ≤ 0.01	1.32 ± 0.17

Table 38: Summary of transfection effects on the expression of PAI-1 after miR-222-3p transfection.

PAI-1 expression after miR-222-3p transfection calculated in relation to appropriate controls. Given are expression changes ± SEM and relevant p-values. Significant changes are highlighted in red.

CTGF

As indicated by alterations in PAI-1 expression, TGF-β signaling seems to be affected by miRNA alterations. As CTGF is another down-stream effector of active TGF-β signaling and associated to the pathogenesis of POAG, its expression also was investigated after miR-222-3p transfection (**Figure 57**). In **Table 39**, results are summarized.

When HUVECs (n = 4 for 48 hours, n = 6 for 72 hours and n = 5 for 144 hours) were transfected with miR-222-3p mimics, CTGF expression was highly significantly

reduced after 48 hours of treatment. On the other hand, miR-222-3p inhibition did not significantly affect the CTGF expression at any of the investigated timepoints.

In SC cells (SC68, SC71, SC74 and SC79, n = 3 each), transfection with miR-222-3p mimics highly significantly reduced CTGF expression at all three investigated timepoints. Transfection with miR-222-3p inhibitors led to the opposite result. While 48 and 72 hours of miR-222-3p inhibition slightly increased CTGF expression, the 144 hour treatment did highly significantly increase it.

Also, when TM cells (TM120, n = 3 for 48 hours, n = 6 for 72 hours, n = 3 for 144 hours) were transfected with miR-222-3p mimics, CTGF expression was highly significantly reduced after 144 hours of transfection. On the other hand, transfection with miR-222-3p inhibitors led to the opposite result and significantly increased the CTGF expression after 144 hours.

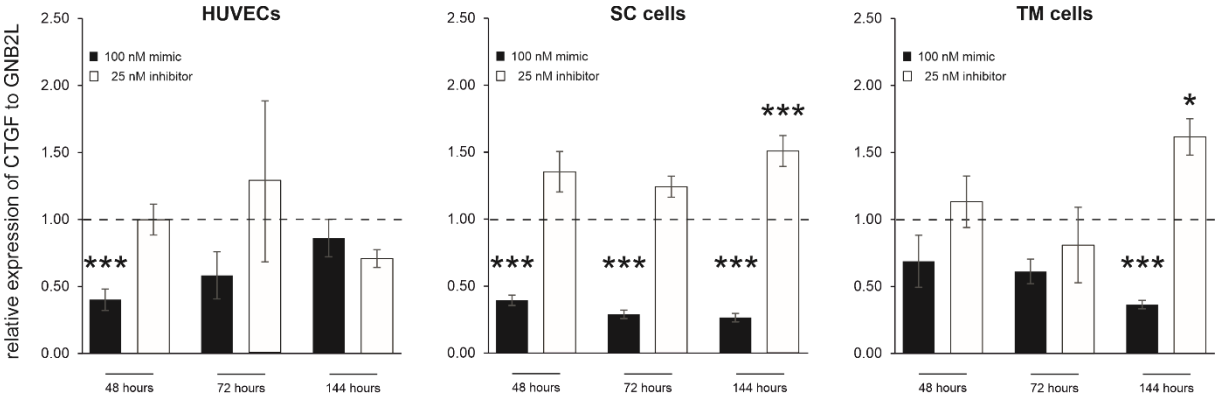

Figure 57: CTGF expression was affected by transfection with miR-222-3p mimics and inhibitors in HUVECs, SC and TM cells.

Relative mRNA expression of CTGF was investigated in HUVECs (n = 4 for 48 hours, n = 6 for 72 hours and n = 5 for 144 hours), four SC cell strains (SC68, SC71, SC74 and SC79, n = 3 each) and TM cells (TM120, n = 3 for 48 hours, n = 6 for 72 hours, n = 3 for 144 hours) after transfection with miR-222-3p mimics and inhibitors as well as appropriate controls (set to 1, indicated by the dashed lines) for 48, 72 and 144 hours. GNB2L was used as reference gene.

CTGF	48 hours		72 hours		144 hours	
	miR-222-3p mimics	miR-222-3p inhibitors	miR-222-3p mimics	miR-222-3p inhibitors	miR-222-3p mimics	miR-222-3p inhibitors
HUVECs	0.40 ± 0.08 p ≤ 0.001	1.02 ± 0.12	0.59 ± 0.18 p = 0.08	1.31 ± 0.62	0.88 ± 0.14	0.72 ± 0.07
SC cells	0.40 ± 0.04 p ≤ 0.001	1.38 ± 0.15 p = 0.06	0.29 ± 0.03 p ≤ 0.001	1.26 ± 0.08 p = 0.09	0.27 ± 0.03 p ≤ 0.001	1.53 ± 0.12 p ≤ 0.001
TM cells	0.71 ± 0.20	1.18 ± 0.20	0.63 ± 0.10	0.84 ± 0.29	0.38 ± 0.03 p ≤ 0.001	1.68 ± 0.14 p ≤ 0.05

Table 39: Summary of transfection effects on the expression of CTGF after miR-222-3p transfection.

CTGF expression after miR-222-3p transfection calculated in relation to appropriate controls. Given are expression changes ± SEM and relevant p-values. Significant changes are highlighted in red.

DCN

DCN is another factor, affected by glaucoma. As shown by literature, DCN is not expressed endogenously by HUVECs (Buraschi et al. 2013). Therefore, it was not investigated here. Since SC and TM do express DCN, its expression profile after miR-222-3p transfection was investigated (**Figure 58**). **Table 40** summarizes the findings.

When SC cells (SC68, SC71, SC74 and SC70, n = 3 each) were transfected with miR-222-3p mimics, DCN expression was significantly and high significantly increased after 48 and 72 hours of transfection, respectively. Transfection with miR-222-3p inhibitors led to the opposite result and significantly reduced the DCN expression after 72 hours.

In TM cells (TM120, n = 3 for 48 hours, n = 6 for 72 hours, n = 3 for 144 hours) no effects on DCN expression was found after transfection with miR-222-3p mimics and inhibitors at all investigated timepoints.

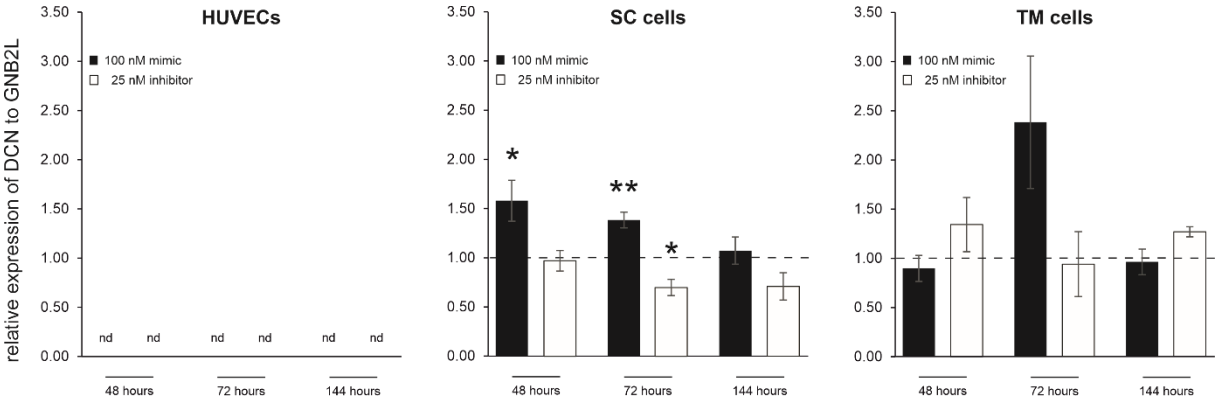

Figure 58: DCN expression was affected by transfection with miR-222-3p mimics and inhibitors in SC cells but not in TM cells, while it was not detectable in HUVECs at all.

Relative mRNA expression of DCN was investigated in HUVECs (nd = not detectable), four SC cell strains (SC68, SC71, SC74 and SC79, n = 3 each) and TM cells (TM120, n = 3 for 48 hours, n = 6 for 72 hours, n = 3 for 144 hours) after transfection with miR-222-3p mimics and inhibitors as well as appropriate controls (set to 1, indicated by the dashed lines) for 48, 72 and 144 hours. GNB2L was used as reference gene.

DCN	48 hours		72 hours		144 hours	
	miR-222-3p mimics	miR-222-3p inhibitors	miR-222-3p mimics	miR-222-3p inhibitors	miR-222-3p mimics	miR-222-3p inhibitors
HUVECs	nd	nd	nd	nd	nd	nd
SC cells	1.63 ± 0.22 p ≤ 0.05	1.01 ± 0.11	1.42 ± 0.08 p ≤ 0.01	0.72 ± 0.08 p ≤ 0.05	1.11 ± 0.14	0.73 ± 0.14
TM cells	0.89 ± 0.13	1.34 ± 0.28	2.38 ± 0.67 p = 0.13	0.94 ± 0.33	0.96 ± 0.13	1.27 ± 0.05 p = 0.06

Table 40: Summary of transfection effects on the expression of DCN after miR-222-3p transfection.

DCN expression after miR-222-3p transfection calculated in relation to appropriate controls. Given are expression changes ± SEM and relevant p-values, nd = not detectable. Significant changes are highlighted in red.

BMP-4

Another member of the TGF-β superfamily is the bone morphogenic protein-4 (BMP-4), that is counteracting the TGF-β2 effects (Fuchshofer et al. 2007; Wordinger et al. 2007). Its mRNA expression was investigated after miR-222-3p alterations (**Figure 59**) and **Table 41** summarizes the findings.

In HUVECs, BMP-4 expression was only affected at one of the investigated timepoints by miR-222-3p alterations. When HUVECs (n = 4 for 48 hours, n = 6 for 72 hours and n = 5 for 144 hours) were transfected with miR-222-3p mimics, BMP-4 expression was highly significantly reduced after 72 hours of treatment.

When SC cells (SC68, SC71, SC74 and SC79, n = 3 each) were transfected with miR-222-3p mimics, BMP-4 expression was high significantly reduced after 72 as well as after 144 hours. Conflictingly, the BMP-4 expression was also significantly reduced by miR-222-3p inhibitors after 48 hours of transfection. Furthermore, no alteration of miR-222-3p were found to lead to an increased BMP-4 expression in SC cells.

In TM cells (TM120, n = 3 for 48 hours, n = 6 for 72 hours, n = 3 for 144 hours), BMP-4 expression was unaffected after transfection with miR-222-3p mimics and inhibitors at all three investigated timepoints.

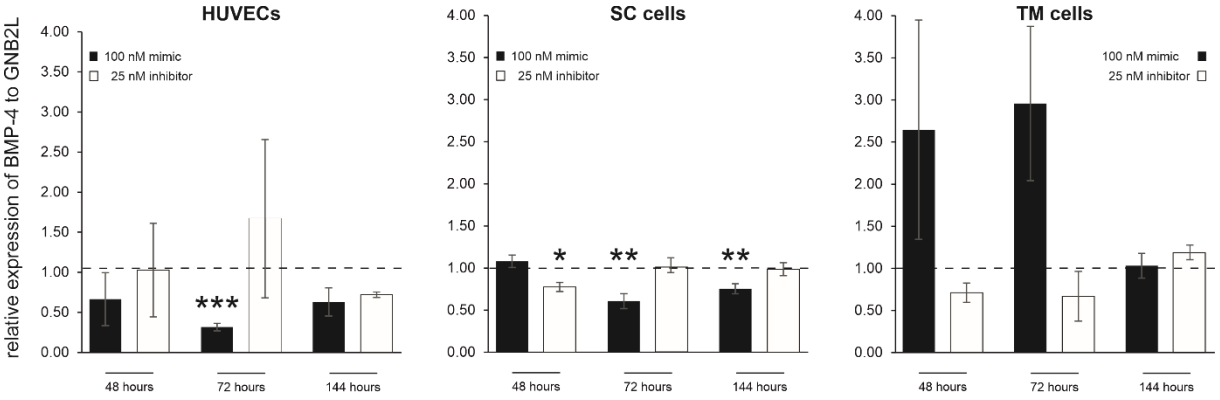

Figure 59: BMP-4 expression was contradictory affected by transfection with miR-222-3p mimics and inhibitors in HUVECs and SC cells, but not in TM cells.

Relative mRNA expression of BMP-4 was investigated in HUVECs (n = 4 for 48 hours, n = 6 for 72 hours, n = 5 for 144 hours), four SC cell strains (SC68, SC71, SC74 and SC79, n = 3 each) and TM cells (TM120, n = 3 for 48 hours, n = 6 for 72 hours, n = 3 for 144 hours) after transfection with miR-222-3p mimics and inhibitors as well as appropriate controls (set to 1, indicated by the dashed lines) for 48, 72 and 144 hours. GNB2L was used as reference gene.

BMP-4	48 hours		72 hours		144 hours	
	miR-222-3p mimics	miR-222-3p inhibitors	miR-222-3p mimics	miR-222-3p inhibitors	miR-222-3p mimics	miR-222-3p inhibitors
HUVECs	0.64 ± 0.32	0.99 ± 0.56	0.30 ± 0.05 p ≤ 0.001	1.61 ± 0.95	0.60 ± 0.17	0.69 ± 0.03 p = 0.07
SC cells	1.09 ± 0.08	0.78 ± 0.05 p ≤ 0.05	0.61 ± 0.09 p ≤ 0.01	1.02 ± 0.09	0.76 ± 0.06 p ≤ 0.01	1.00 ± 0.08
TM cells	2.55 ± 1.26	0.68 ± 0.11	2.85 ± 0.89 p = 0.07	0.64 ± 0.29	0.99 ± 0.14	1.15 ± 0.08

Table 41: Summary of transfection effects on the expression of BMP-4 after miR-222-3p transfection.

BMP-4 expression after miR-222-3p transfection calculated in relation to appropriate controls. Given are expression changes ± SEM and relevant p-values. Significant changes are highlighted in red.

α-SMA

By this study, it has been shown that reduction in cellular stiffness and reduction of α-SMA expression go hand in hand. To further investigate what is affecting α-SMA expression, its expression was analyzed after miR-222-3p transfection (**Figure 60**). In **Table 42**, findings are summarized.

When HUVECs (n = 4 for 48 hours, n = 6 for 72 hours and n = 5 for 144 hours) were transfected with miR-222-3p mimics, α-SMA expression was high significantly reduced already after 48 hours of transfection. By the transfection with miR-222-3p inhibitors, the α-SMA expression was significantly increased after 48 hours of treatment as well.

When SC cells (SC68, SC71, SC74 and SC79, n = 3 each) were transfected with miR-222-3p mimics, α-SMA expression was also highly significantly reduced after 72 as well as 144 hours of transfection. Interestingly, α-SMA expression was also significantly reduced after 72 hours of transfection with miR-222-3p inhibitors. Otherwise, inhibition of miR-222-3p had no effect on α-SMA expression.

In TM cells (TM120, n = 3 for 48 hours, n = 6 for 72 hours, n = 3 for 144 hours), α-SMA expression was highly significantly reduced after 144 hours of transfection. On the other hand, transfection with miR-222-3p inhibitors significantly increased α-SMA expression after the same treatment period.

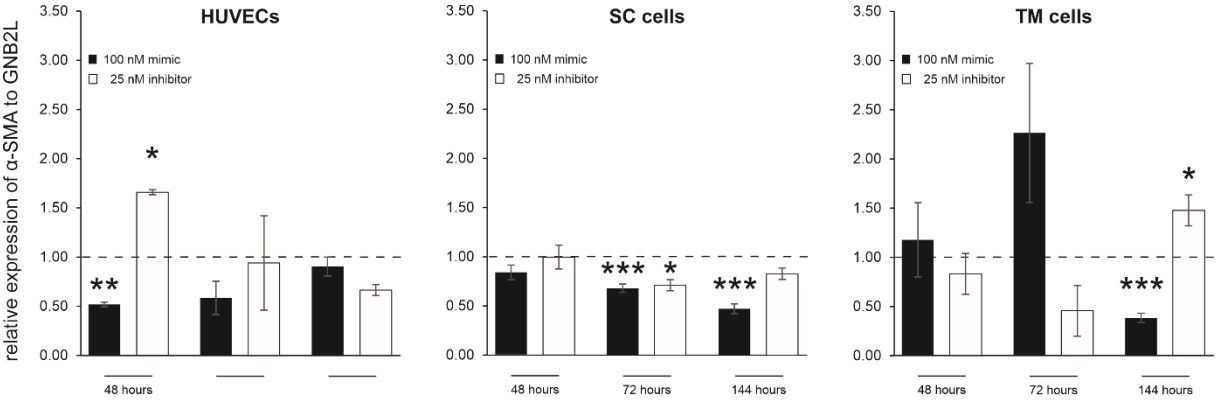

Figure 60: α-SMA expression was affected by transfection with miR-222-3p mimics and inhibitors in HUVECs, SC as well as TM cells.

Relative mRNA expression of α-SMA was investigated in HUVECs (n = 4 for 48 hours, n = 6 for 72 hours, n = 5 for 144 hours), four SC cell strains (SC68, SC71, SC74 and SC79, n = 3 each) and TM cells (TM120, n = 3 for 48 hours, n = 6 for 72 hours, n = 3 for 144 hours) after transfection with miR-222-3p mimics and inhibitors as well as appropriate controls (set to 1, indicated by the dashed lines) for 48, 72 and 144 hours. GNB2L was used as reference gene.

α-SMA	48 hours		72 hours		144 hours	
	miR-222-3p mimics	miR-222-3p inhibitors	miR-222-3p mimics	miR-222-3p inhibitors	miR-222-3p mimics	miR-222-3p inhibitors
HUVECs	0.56 ± 0.02 p ≤ 0.01	1.80 ± 0.03 p ≤ 0.05	0.63 ± 0.18 p = 0.09	1.02 ± 0.52	0.98 ± 0.10	0.72 ± 0.06
SC cells	0.91 ± 0.08	1.08 ± 0.12	0.74 ± 0.05 p ≤ 0.001	0.78 ± 0.06 p ≤ 0.05	0.51 ± 0.05 p ≤ 0.001	0.90 ± 0.06
TM cells	1.21 ± 0.39	0.86 ± 0.21	2.34 ± 0.73 p = 0.14	0.47 ± 0.27 p = 0.09	0.39 ± 0.05 p ≤ 0.001	1.53 ± 0.16 p ≤ 0.05

Table 42: Summary of transfection effects on the expression of α-SMA after miR-222-3p transfection.

α-SMA expression after miR-222-3p transfection calculated in relation to appropriate controls. Given are expression changes ± SEM and relevant p-values. Significant changes are highlighted in red.

eNOS

Since the NO signaling pathway - and thereby its major component eNOS - are of particular interest of the present study, eNOS expression after miR-222-3p transfection was investigated (**Figure 61**). Results are summarized in **Table 42**.

When HUVECs (n = 4 for 48 hours, n = 3 for 72 hours and n = 5 for 144 hours) were transfected with miR-222-3p mimics, eNOS expression was high significantly increased after 48 hours of transfection. On the other hand, the transfection with miR-222-3p inhibitors led to no changes of eNOS expression at any of the investigated timepoints.

To reveal if there is more effect on eNOS expression by higher miRNA concentrations, transfection experiments were not only performed with 100 nM mimics but also with 200 nM mimics. For inhibitors, not only 25 nM, but also 100 nM were used for

transfection experiments. Nevertheless, none of the investigated concentrations could significantly affect eNOS expression in HUVECs at the investigated timepoints (data not shown).

Since the present study was already confronted with detection problems of eNOS, it was of no wonder that eNOS expression was not detectable in SC cells under standard, static cell culture conditions.

Even if eNOS as well as iNOS have been reported to be altered in glaucomatous SC as well as TM cells (Nathanson and McKee 1995a; Fernandez-Durango et al. 2008), none of those NOSs were detectable in transfected TM cells of this present study (data not shown).

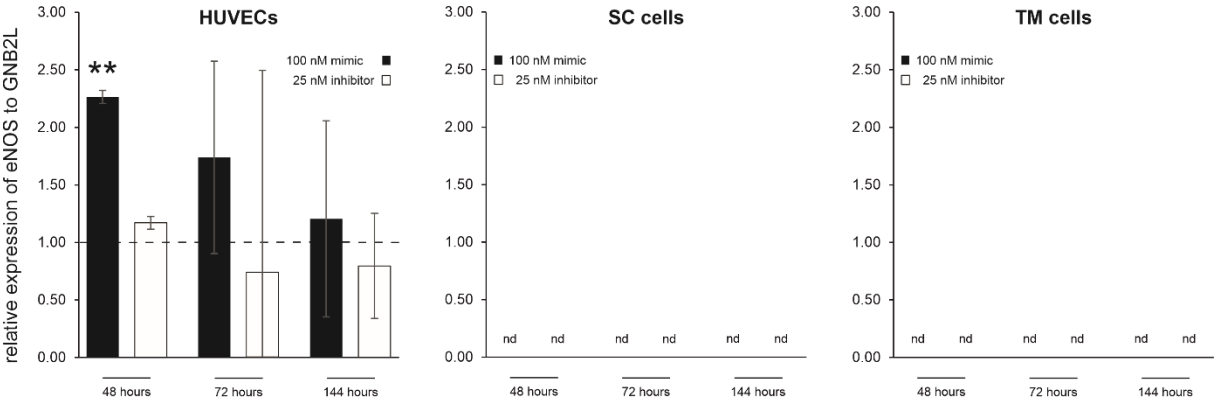

Figure 61: eNOS expression was affected by transfection with miR-222-3p mimics in HUVECs, but not detectable in SC and TM cells.

Relative mRNA expression of α-SMA was investigated in HUVECs (n = 4 for 48 hours, n = 3 for 72 hours, n = 5 for 144 hours), SC cells (nd = not detectable) and TM cells (nd = not detectable) after transfection with miR-222-3p mimics and inhibitors as well as appropriate controls (set to 1, indicated by the dashed lines) for 48, 72 and 144 hours. GNB2L was used as reference gene.

eNOS	48 hours		72 hours		144 hours	
	miR-222-3p mimics	miR-222-3p inhibitors	miR-222-3p mimics	miR-222-3p inhibitors	miR-222-3p mimics	miR-222-3p inhibitors
HUVECs	2.26 ± 0.06 p ≤ 0.01	1.17 ± 0.06	1.73 ± 0.84	0.74 ± 1.75	1.20 ± 0.85	0.80 ± 0.46
SC cells	nd	nd	nd	nd	nd	nd
TM cells	nd	nd	nd	nd	nd	nd

Table 43: Summary of transfection effects on the expression of eNOS after miR-222-3p transfection.

eNOS expression after miR-222-3p transfection calculated in relation to appropriate controls. Given are expression changes ± SEM and relevant p-values, nd = not detectable. Significant changes are highlighted in red.

4.2.13.2 transfection effects of miR-455-3p mimics and inhibitors

TGF-β2

After the transfection with miR-455-3p mimics and inhibitors, the expression of TGF-β2 was investigated (**Figure 62**). **Table 44** summarizes the findings.

In HUVECs (n = 3), the expression of TGF-β2 was not affected by the transfection with miR-455-3p mimics and inhibitors.

When SC cells (SC68, SC71, SC74 and SC79, n=3 each) were transfected with miR-455-3p mimics, TGF-β2 expression was unaffected. By transfection with miR-455-3p inhibitors, TGF-β2 expression was significantly upregulated after 72 hours.

Furthermore, the effect of miR-444-3p transfection was investigated in TM cells. When TM cells (TM120, n = 6 for 48 hours, n = 3 for 72 and 144 hours) were transfected with miR-455-3p mimics, TGF-β2 expression was unaffected at all three investigated timepoints. The transfection with miR-455-3p inhibitors resulted in a highly significant decrease of TGF-β2 expression after 144 hours.

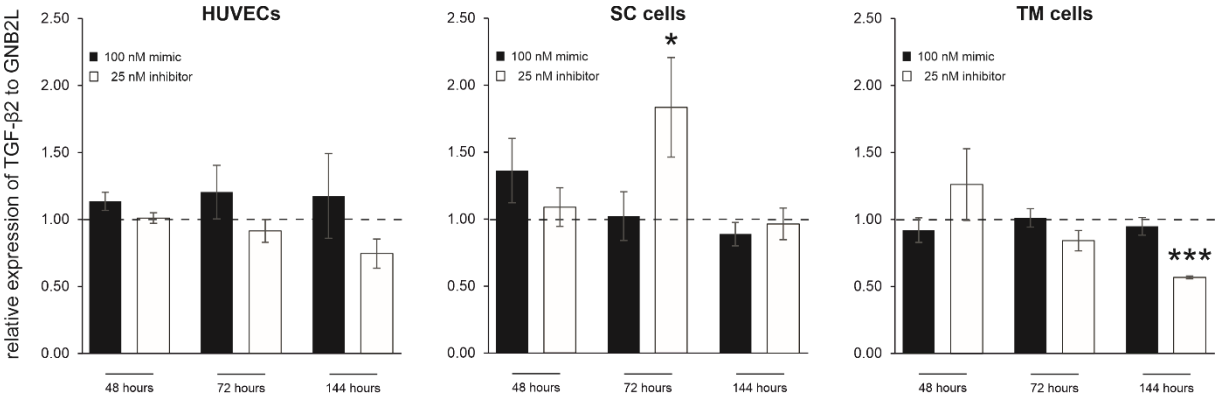

Figure 62: TGF-β2 expression was contradictorily affected by transfection with miR-455-3p mimics in SC and TM cells, but not at all in HUVECs.

Relative mRNA expression of TGF-β2 was investigated in HUVECs (n = 3), four SC cell strains (SC68, SC71, SC74 and SC79, n = 3 each) and TM cells (TM120, n = 6 for 48 hours, n = 3 for 72 and 144 hours) after transfection with miR-455-3p mimics and inhibitors as well as appropriate controls (set to 1, indicated by the dashed lines) for 48, 72 and 144 hours. GNB2L was used as reference gene.

TGF-β2	48 hours		72 hours		144 hours	
	miR-455-3p mimics	miR-455-3p inhibitors	miR-455-3p mimics	miR-455-3p inhibitors	miR-455-3p mimics	miR-455-3p inhibitors
HUVECs	1.21 ± 0.07 p = 0.07	1.08 ± 0.04	1.28 ± 0.21	0.97 ± 0.09	1.25 ± 0.34	0.79 ± 0.12
SC cells	1.35 ± 0.24	1.08 ± 0.14	1.01 ± 0.18	1.82 ± 0.37 p ≤ 0.05	0.88 ± 0.09	0.96 ± 0.12
TM cells	0.98 ± 0.10	1.35 ± 0.29	1.07 ± 0.07	0.90 ± 0.08	1.01 ± 0.07	0.60 ± 0.01 p ≤ 0.001

Table 44: Summary of transfection effects on the expression of TGF-β2 after miR-455-3p transfection.

TGF-β2 expression after miR-455-3p transfection calculated in relation to appropriate controls. Given are expression changes ± SEM and relevant p-values. Significant changes are highlighted in red.

PAI-1

Even if TGF-β2 expression itself is not consistently affected by miR-455-3p transfection, the investigation of the expression profile of its response gene PAI-1 might lighten transfection effects (**Figure 63**). **Table 45** summarizes the findings.

When HUVECs (n = 3) were transfected with miR-455-3p mimics, PAI-1 expression was high significantly increased ($p \leq 0.01$) after 48 hours of transfection. Paradoxically, the same period of transfection with miR-455-3p inhibitors did also high significantly increase the PAI-1 expression.

Furthermore, SC cells (SC68, SC71, SC74 and SC79, n = 3 each) were investigated. There, PAI-1 expression was high significantly increased after 48 hours of transfection but significantly decreased after 144 hours. On the other hand, the transfection with miR-455-3p inhibitors significantly increased the expression of PAI-1 after 48 hours which led to conflicting results.

When TM cells (TM120, n = 6 for 48 hours, n = 3 for 72 and 144 hours) were transfected with miR-455-3p mimics, PAI-1 expression was not affected significantly at any investigated timepoint. On the other hand, the transfection with miR-445-3p inhibitor led to a highly significantly increased PAI-1 expression after 48 hours of transfection.

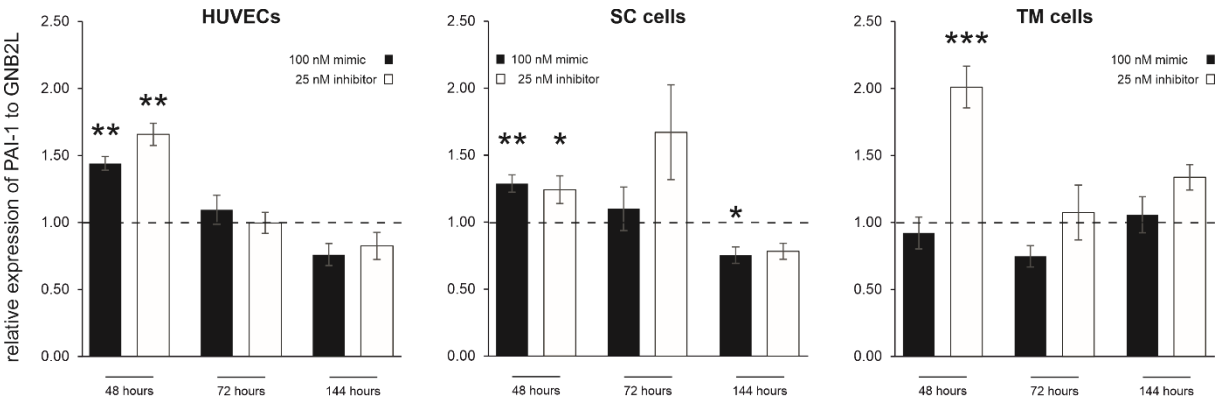

Figure 63: PAI-1 expression was contradictorily affected by transfection with miR-455-3p mimics in HUVECs, SC and TM cells.

Relative mRNA expression of PAI-1 was investigated in HUVECs (n = 3), four SC cell strains (SC68, SC71, SC74 and SC79, n = 3 each) and TM cells (TM120, n = 6 for 48 hours, n = 3 for 72 and 144 hours) after transfection with miR-455-3p mimics and inhibitors as well as appropriate controls (set to 1, indicated by the dashed lines) for 48, 72 and 144 hours. GNB2L was used as reference gene.

PAI-1	48 hours		72 hours		144 hours	
	miR-455-3p mimics	miR-455-3p inhibitors	miR-455-3p mimics	miR-455-3p inhibitors	miR-455-3p mimics	miR-455-3p inhibitors
HUVECs	1.55 ± 0.06 p ≤ 0.01	1.79 ± 0.09 p ≤ 0.01	1.18 ± 0.12	1.08 ± 0.08	0.82 ± 0.09	0.89 ± 0.11
SC cells	1.29 ± 0.07 p ≤ 0.01	1.25 ± 0.10 p ≤ 0.05	1.10 ± 0.16	1.68 ± 0.36 p = 0.05	0.75 ± 0.06 p ≤ 0.05	0.79 ± 0.06
TM cells	0.95 ± 0.12	2.08 ± 0.16 p ≤ 0.001	0.77 ± 0.08	1.11 ± 0.21	1.09 ± 0.14	1.38 ± 0.10

Table 45: Summary of transfection effects on the expression of PAI-1 after miR-455-3p transfection.

PAI-1 expression after miR-455-3p transfection calculated in relation to appropriate controls. Given are expression changes ± SEM and relevant p-values. Significant changes are highlighted in red.

CTGF

Furthermore, the effect of miR-455-3p transfection on CTGF expression was investigated (**Figure 64**). In **Table 46**, results are summarized.

When HUVECs (n = 3) were transfected with miR-455-3p mimics, CTGF expression was also not affected significantly after none of the investigated timepoints. Furthermore, transfection with miR-455-3p inhibitors led to inconsistent results. While the 48-hour treatment high significantly increased the expression of CTGF, the long-term treatment for 144 hours led to a significantly reduced CTGF expression.

On the other hand, SC cells (SC68, SC71, SC74 and SC79, n = 3 each) had no effect of miR-455-3p mimics and inhibitors on CTGF expression.

Furthermore, TM cell (TM120, n = 6 for 48 hours, n = 3 for 72 and 144 hours) also had no changes of CTGF expression after miR-455-3p transfection.

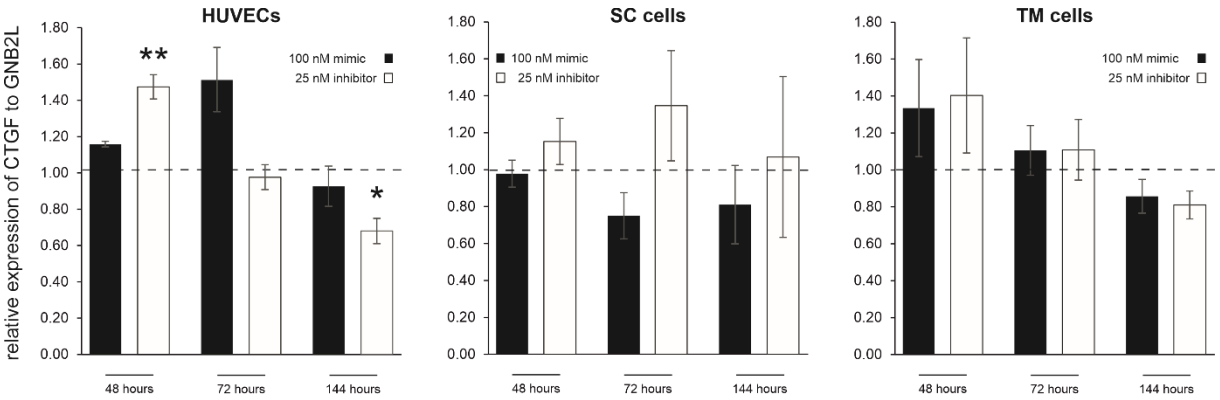

Figure 64: CTGF expression was contradictorily affected by transfection with miR-455-3p mimics in HUVECs, but not at all in SC as well as TM cells.

Relative mRNA expression of CTGF was investigated in HUVECs (n = 3), four SC cell strains (SC68, SC71, SC74 and SC79, n = 3 each) and TM cells (TM120, n = 6 for 48 hours, n = 3 for 72 and 144 hours) after transfection with miR-455-3p mimics and inhibitors as well as appropriate controls (set to 1, indicated by the dashed lines) for 48, 72 and 144 hours. GNB2L was used as reference gene.

CTGF	48 hours		72 hours		144 hours	
	miR-455-3p mimics	miR-455-3p inhibitors	miR-455-3p mimics	miR-455-3p inhibitors	miR-455-3p mimics	miR-455-3p inhibitors
HUVECs	1.16 ± 0.02	1.47 ± 0.07 p ≤ 0.01	1.51 ± 0.18 p = 0.08	0.98 ± 0.07	0.93 ± 0.11	0.68 ± 0.07 p ≤ 0.05
SC cells	0.96 ± 0.07	1.14 ± 0.12	0.74 ± 0.12	1.33 ± 0.29	0.80 ± 0.21	1.05 ± 0.43
TM cells	1.31 ± 0.26	1.38 ± 0.31	1.09 ± 0.13	1.09 ± 0.16	0.84 ± 0.09	0.80 ± 0.07

Table 46: Summary of transfection effects on the expression of CTGF after miR-455-3p transfection.

CTGF expression after miR-455-3p transfection calculated in relation to appropriate controls. Given are expression changes ± SEM and relevant p-values. Significant changes are highlighted in red.

DCN

The glaucoma-associated factor DCN was investigated after miR-455-3p transfection (**Figure 65**). As shown by Buraschi et al., DCN is not expressed in HUVECs. Furthermore, Overby at al. could show that SC cells do express DCN. Here, its expression was investigated after miR-455-3p transfection and results are summarized in **Table 47**.

When SC cells (SC68, SC71, SC74 and SC70, n = 3 each) were transfected with miR-455-3p, DCN expression was not affected at any investigated timepoint, neither with miR-455-3p mimics nor inhibitors.

In TM cells (TM120, n = 6 for 48 hours, n = 3 for 72 and 144 hours), alterations on miR-455-3p did also have no significant effect on DNC expression.

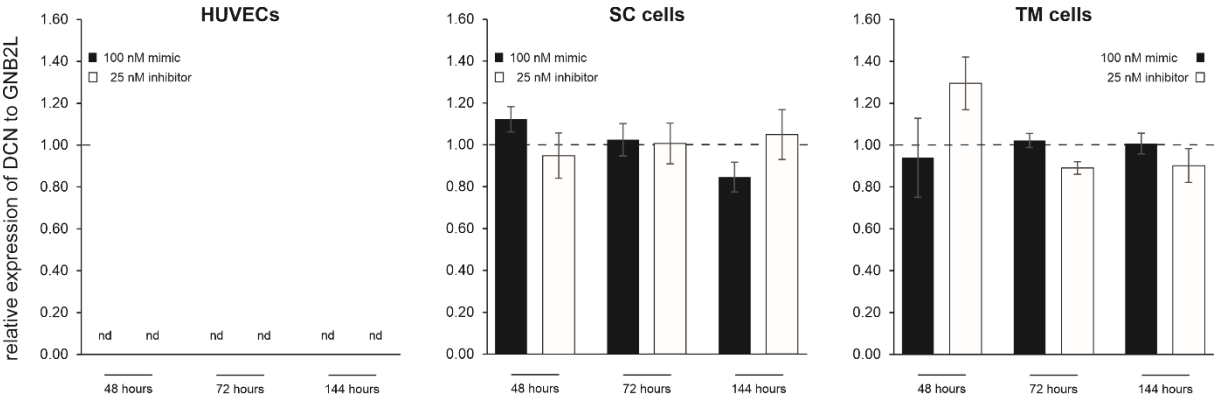

Figure 65: DCN expression was not affected by transfection with miR-455-3p mimics and inhibitors in SC and TM cells, while it was not detectable in HUVECs at all.

Relative mRNA expression of DCN was investigated in HUVECs (nd = not detectable), four SC cell strains (SC68, SC71, SC74 and SC79, n = 3 each) and TM cells (TM120, n = 6 for 48 hours, n = 3 for 72 and 144 hours) after transfection with miR-455-3p mimics and inhibitors as well as appropriate controls (set to 1, indicated by the dashed lines) for 48, 72 and 144 hours. GNB2L was used as reference gene.

DCN	48 hours		72 hours		144 hours	
	miR-455-3p mimics	miR-455-3p inhibitors	miR-455-3p mimics	miR-455-3p inhibitors	miR-455-3p mimics	miR-455-3p inhibitors
HUVECs	nd	nd	nd	nd	nd	nd
SC cells	1.14 ± 0.06	0.97 ± 0.11	1.04 ± 0.08	1.02 ± 0.10	0.86 ± 0.07	1.07 ± 0.12
TM cells	0.94 ± 0.19	1.29 ± 0.13	1.02 ± 0.03	0.89 ± 0.03	1.01 ± 0.05	0.90 ± 0.08

Table 47: Summary of transfection effects on the expression of DCN after miR-455-3p transfection.

DCN expression after miR-455-3p transfection calculated in relation to appropriate controls. Given are expression changes ± SEM and relevant p-values, nd = not detectable. Significant changes are highlighted in red.

BMP-4

As member of the TGF-β superfamily and antagonizing the TGF-β effect (Fuchshofer et al. 2007; Wordinger et al. 2007), BMP-4 expression was investigated after miR-455-3p transfection (**Figure 66**). In **Table 48**, findings are summarized.

When HUVECs (n = 3) were transfected with miR-455-3p mimics, BMP-4 expression was significantly increased after 72 hours. On the other hand, the transfection with miR-455-3p inhibitors led to significant reduction after 144 hours.

In SC cells (SC68, SC71, SC74 and SC79, n = 3 each), results were contradictory to the findings in HUVECs. There, BMP-4 expression was unaffected after the transfection with miR-455-3p mimics and high significantly increased when transfected with miR-455-3p inhibitors for 48 hours.

Furthermore, alterations on miR-455-3p did not significantly affect BMP-4 expression in TM cells (TM120, n = 6 for 48 hours, n = 3 for 72 and 144 hours) at any of the investigated timepoints.

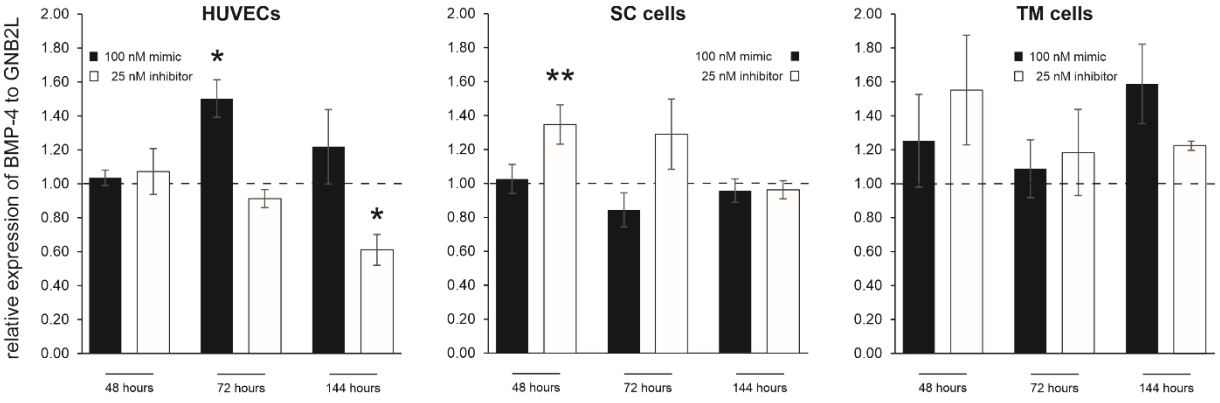

Figure 66: BMP-4 expression was contradictory affected by transfection with miR-455-3p mimics and inhibitors in HUVECs and SC cells, but not affected at all in TM cells.

Relative mRNA expression of BMP-4 was investigated in HUVECs (n = 3), four SC cell strains (SC68, SC71, SC74 and SC79, n = 3 each) and TM cells (TM120, n = 6 for 48 hours, n = 3 for 72 and 144 hours) after transfection with miR-455-3p mimics and inhibitors as well as appropriate controls (set to 1, indicated by the dashed lines) for 48, 72 and 144 hours. GNB2L was used as reference gene.

BMP-4	48 hours		72 hours		144 hours	
	miR-455-3p mimics	miR-455-3p inhibitors	miR-455-3p mimics	miR-455-3p inhibitors	miR-455-3p mimics	miR-455-3p inhibitors
HUVECs	1.08 ± 0.05	1.12 ± 0.14	1.56 ± 0.12 p ≤ 0.05	0.95 ± 0.06	1.27 ± 0.23	0.64 ± 0.09 p ≤ 0.05
SC cells	1.03 ± 0.09	1.35 ± 0.12 p ≤ 0.01	0.84 ± 0.10	1.30 ± 0.21	0.96 ± 0.07	0.97 ± 0.05
TM cells	1.25 ± 0.27	1.55 ± 0.32	1.09 ± 0.17	1.18 ± 0.25	1.59 ± 0.23	1.23 ± 0.03

Table 48: Summary of transfection effects on the expression of BMP-4 after miR-455-3p transfection.

BMP-4 expression after miR-455-3p transfection calculated in relation to appropriate controls. Given are expression changes ± SEM and relevant p-values. Significant changes are highlighted in red.

α-SMA

The effect of miR-455-3p alterations on α-SMA expression was investigated (**Figure 67**). All findings are summarized in **Table 49**.

In HUVECs (n = 3), transfection with miR-455-3p mimics significantly reduced α-SMA expression after 72 hours. The transfection with miR-455-3p inhibitors led to ambiguous results. While the α-SMA expression was high significantly increased after 48 hours, the 144-hour transfection high significantly reduced the α-SMA expression.

When SC cells (SC68, SC71, SC74 and SC79, n = 3 each) were transfected with miR-455-3p mimics, α-SMA expression was highly significantly reduced after 144 hours of transfection while miR-455-3p inhibition had not significant effect.

Interestingly, α-SMA expression was not affected in TM cells (TM120, n = 6 for 48 hours, n = 3 for 72 and 144 hours) by miR-455-3p alterations.

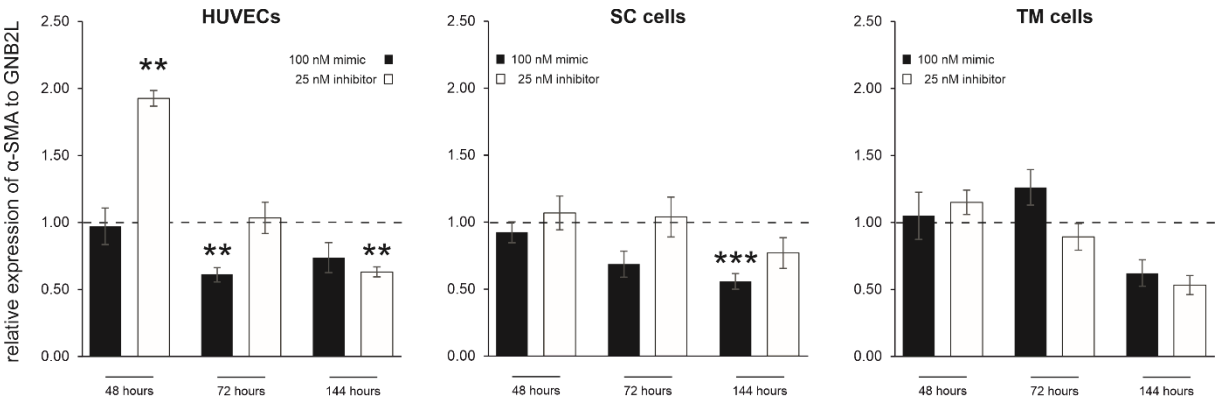

Figure 67: α-SMA expression was affected by transfection with miR-455-3p mimics and inhibitors in HUVECs and SC cells, but not affected at all in TM cells.

Relative mRNA expression of α-SMA was investigated in HUVECs (n = 3), four SC cell strains (SC68, SC71, SC74 and SC79, n = 3 each) and TM cells (TM120, n = 6 for 48 hours, n = 3 for 72 and 144 hours) after transfection with miR-455-3p mimics and inhibitors as well as appropriate controls (set to 1, indicated by the dashed lines) for 48, 72 and 144 hours. GNB2L was used as reference gene.

α-SMA	48 hours		72 hours		144 hours	
	miR-455-3p mimics	miR-455-3p inhibitors	miR-455-3p mimics	miR-455-3p inhibitors	miR-455-3p mimics	miR-455-3p inhibitors
HUVECs	1.00 ± 0.14	1.99 ± 0.06 p ≤ 0.01	0.63 ± 0.06 p ≤ 0.01	1.07 ± 0.12	0.76 ± 0.12	0.65 ± 0.04 p ≤ 0.01
SC cells	0.98 ± 0.08	1.13 ± 0.13	0.72 ± 0.10 p = 0.06	1.10 ± 0.16	0.59 ± 0.06 p ≤ 0.001	0.81 ± 0.12
TM cells	1.13 ± 0.19	1.24 ± 0.10	1.36 ± 0.14	0.96 ± 0.11	0.67 ± 0.11	0.57 ± 0.08

Table 49: Summary of transfection effects on the expression of α-SMA after miR-455-3p transfection.

α-SMA expression after miR-455-3p transfection calculated in relation to appropriate controls. Given are expression changes ± SEM and relevant p-values. Significant changes are highlighted in red.

eNOS

Finally, eNOS expression was also investigated after miR-455-3p transfection (**Figure 68**) and results are summarized in **Table 43**.

When HUVECs (n = 3) were transfected with miR-455-3p mimics, eNOS expression was significantly increased after the inhibition of miR-455-3p for 48 hours. Longer periods of treatment had no impact on eNOS mRNA expression.

In SC and TM cells, eNOS was not detectable as it was shown transfection experiments with miR-222-3p.

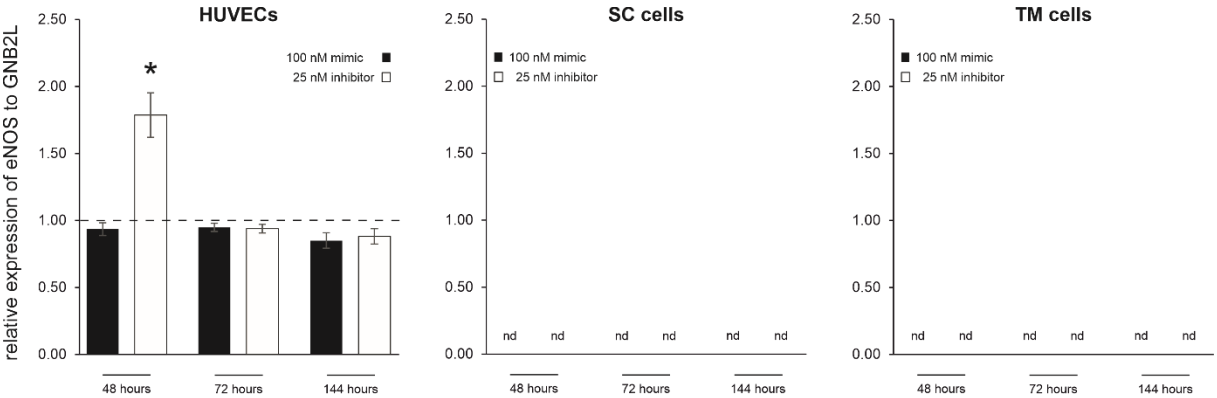

Figure 68: eNOS expression was affected by transfection with miR-455-3p inhibitors in HUVECs, but not detectable in SC and TM cells.

Relative mRNA expression of α-SMA was investigated in HUVECs (n = 3), SC cells (nd = not detectable) and TM cells (nd = not detectable) after transfection with miR-455-3p mimics and inhibitors as well as appropriate controls (set to 1, indicated by the dashed lines) for 48, 72 and 144 hours. GNB2L was used as reference gene.

eNOS	48 hours		72 hours		144 hours	
	miR-455-3p mimics	miR-455-3p inhibitors	miR-455-3p mimics	miR-455-3p inhibitors	miR-455-3p mimics	miR-455-3p inhibitors
HUVECs	0.93 ± 0.05	1.79 ± 0.17 p ≤ 0.05	0.95 ± 0.03	0.94 ± 0.03	0.85 ± 0.06	0.88 ± 0.06
SC cells	nd	nd	nd	nd	nd	nd
TM cells	nd	nd	nd	nd	nd	nd

Table 50: Summary of transfection effects on the expression of eNOS after miR-455-3p transfection.

eNOS expression after miR-455-3p transfection calculated in relation to appropriate controls. Given are expression changes ± SEM and relevant p-values, nd = not detectable. Significant changes are highlighted in red.

4.3 Intracameral delivery of layer-by-layer coated nanoparticles as potential delivery system for miRNA to outflow tissue

Published by Dillinger et al., our working group has proven the ability of NPs to deliver siRNA towards AH outflow cells. Furthermore, HA-decorated NP have been shown to keep their mobility in the ECM and accumulated within the TM (Dillinger et al. 2018).

As long-term goal, this study worked on the development of a delivery system for causative glaucoma therapy with miRNA. So far, this study investigated the distribution of gold-core NP (AuNP) within the anterior chamber of *ex vivo* perfused eyes. Experiments were performed in collaboration with the Department for Pharmaceutical Technology. There, Tobias Sonntag prepared AuNPs and did their quantification.

4.3.1 Characterization of gold-core nanoparticles

Initially, NPs were investigated by TEM. AuNPs from Nanopartz™ with 5, 50, 100 and 150 nm and an additional set of 13 nm AuNPs were visualized. Unlike those purchased from Nanopartz™, the 13 nm cores were processed self-made. With respect to the scale bars, the size of AuNPs fitted manufacturer's information (**Figure 69**).

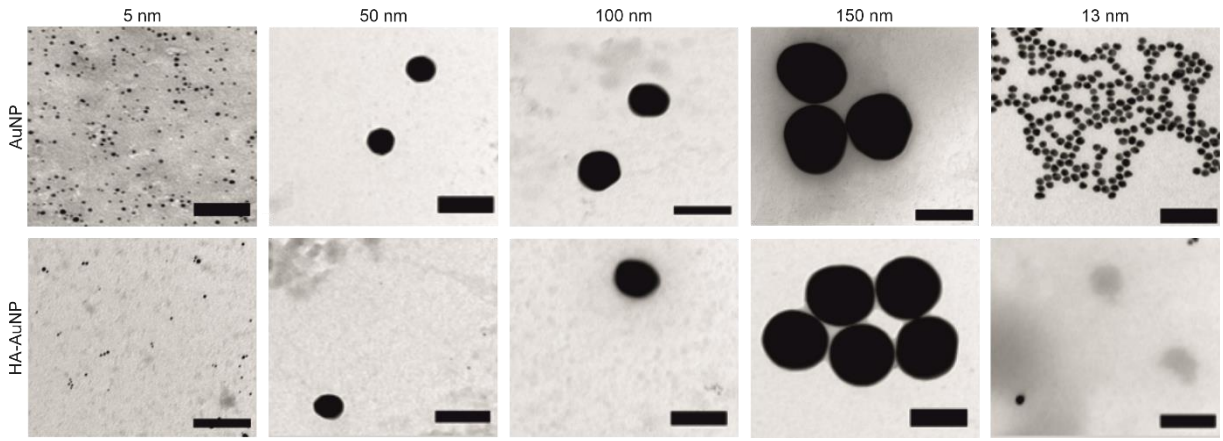

Figure 69: Transmission electron microscopy images of gold nanoparticles.

By this method, gold-cores of 5, 50, 100 and 150 nm small nanoparticles (AuNPs) from Nanopartz™ and 13 nm self-made AuNPs were visualized. If the surface was citrate or hyaluronan was not distinguishable. Nevertheless, the total diameter of the HA-coated NP (HA-AuNP) was expected to be slightly bigger than the core alone. Scale bars: 100 nm.

If the surface was citrate or hyaluronan was not distinguishable by TEM. To investigate whether the total diameter of the HA-AuNP was slightly bigger than that of the AuNP without HA, the hydrodynamic diameter was determined for all investigated AuNPs (**Figure 70**). The size distribution was number weighted, meaning that each particle (but not its volume) counted equally. Thereby, only the 150 nm HA-AuNP were on average slightly smaller than those without the final HA layer. All other NPs showed an increase in diameter after addition of the final HA-layer. Nevertheless, the size increase was about three times and thereby unexpectedly big for the 5 nm AuNP.

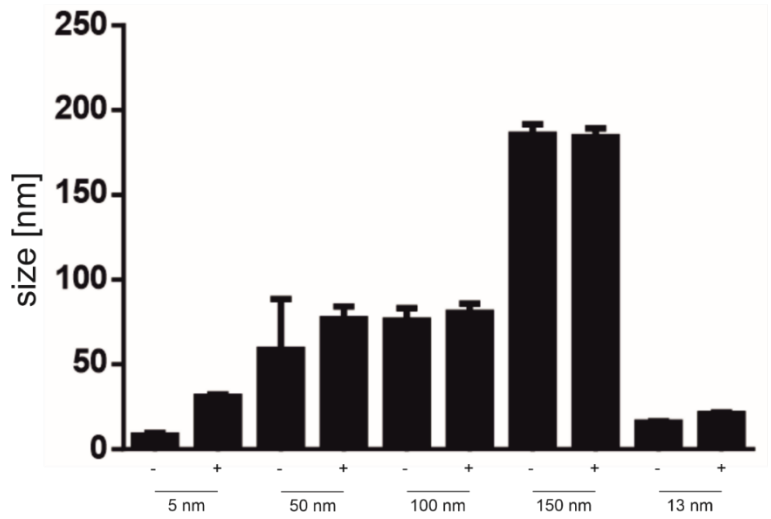

Figure 70: Hydrodynamic diameter of gold-core nanoparticles.

The number weighted size distribution of 5, 50, 100 and 150 nm AuNPs from Nanopartz™ as well as 13 nm self-made AuNPs with (+) or without (-) a final layer of hyaluronan (HA). The total diameter of the HA-AuNPs were expected to be slightly bigger than the AuNP without HA.

In addition, the zeta-potential of AuNPs and HA-AuNPs was determined (data not shown). Thereby, it was proven that the binding of negatively charged HA on the AuNPs surface decreased the zeta-potential for Nanopartz™ NPs. Self-made AuNPs of 13 nm did not change the surface charge by the addition of HA whether it was bindable by an SH-group or not.

Furthermore, the stability of AuNP was proven (data not shown). When incubated in medium with 0.35% FBS - which is the corresponding protein amount of the AH - HA-coating improved colloidal stability. Similar results were reported for fluorescent layer-by-layer NPs with and without HA (Dillinger et al. 2018).

4.3.2 Ex vivo eye perfusion experiments with gold-core nanoparticles

Other than fluorescent NP, the gold cores of AuNPs allow for one by one retrievability of each single NP. To investigate its distribution within the anterior chamber, *ex vivo* perfusion experiments were performed (see 3.6.3). Thereafter, the following distinct tissues were prepared: ciliary body (CI), cornea (CO), iris (IR), lens (LE) and TM. After preparation (n = 6), tissue was weighted (**Figure 71**). Distinct weight, SEM as well as percental aberration are given thereafter in **Table 51**.

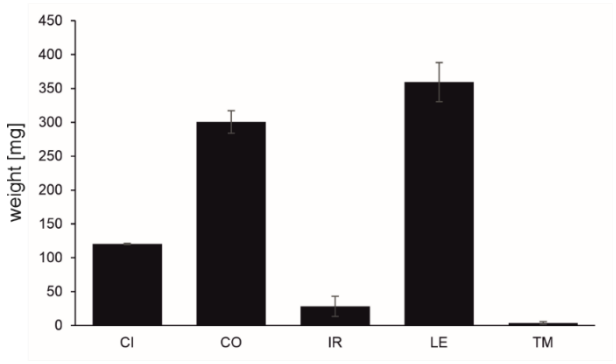

Figure 71: Weight of prepared tissue after ex vivo eye perfusion experiments.

Ciliary body (CI), cornea (CO), iris (IR), lens (LE) as well as trabecular meshwork (TM) were prepared after ex vivo eye perfusion experiments (n = 6). Weight was given in mg and error bars represent SEM.

tissue	weight [mg]	± SEM	aberration [%]
CI	120.47	14.82	12.31
CO	300.48	16.58	5.52
IR	28.27	1.97	6.98
LE	359.50	28.80	8.01
TM	3.83	0.78	20.41

Table 51: Weight of prepared tissue after ex vivo eye perfusion experiments.

Ciliary body (CI), cornea (CO), iris (IR), lens (LE) as well as trabecular meshwork I were prepared after ex vivo eye perfusion experiments. Weight was given in mg and aberration in %.

The aberration of CO, IR and LE was smaller than 10%. Since these tissues have smooth surface, less fluid adhesion occurred. In CI and TM, aberration was the highest. Those tissues have the most rough, fissured surface of all investigated tissues. Thereby, proportionally more fluid - leftover by the preparation process - might lead to weight variations. To avoid these inaccuracies, tissue was freeze-dried for further investigations.

By inductively coupled plasma mass spectroscopy (ICP-MS), gold content of five tissues of the anterior chamber was investigated after *ex vivo* eye perfusion experiments. Perfusion was performed with 5, 50, 100 and 150 nm AuNPs from Nanopartz™ as well as 13 nm self-made AuNPs.

Figure 72 shows the results for AuNP with citrate surface (n = 3, expect the result for TM, perfused with 5 nm AuNPs, there n = 2 due to a significant outlier). For all AuNP sizes, the most gold was found in CI, IR and - moist importantly - in the TM. Almost no gold was found in CO and LE. Form 50 nm over 100 nm to 150 nm, the bigger the AuNPs were, the more gold was found. **Table 52** summarizes the findings.

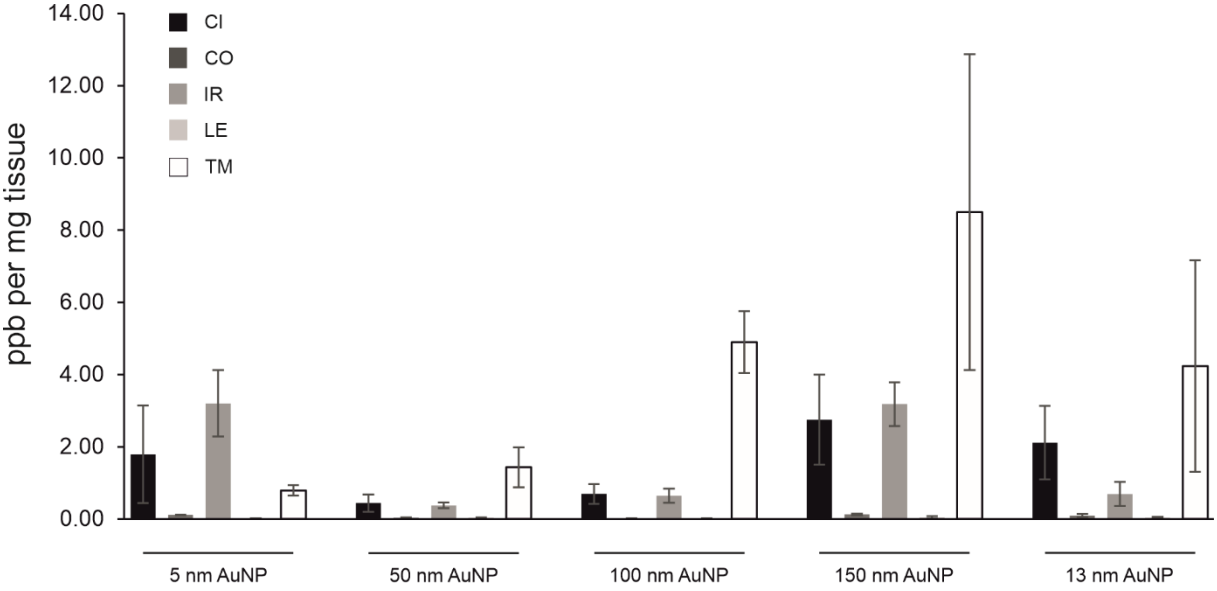

Figure 72: Gold content of eye tissue, especially of the trabecular meshwork, increased by the size of nanoparticles with citrate surface after ex vivo perfusion.

By inductively coupled plasma mass spectroscopy, gold content of five tissues (CI = ciliary body, CO = cornea, IR = iris, LE = lens, TM = trabecular meshwork) of the anterior chamber was investigated after ex vivo eye perfusion experiments (n = 3, expect the result for TM, perfused with 5 nm AuNPs, there n = 2 due to a significant outlier). Perfusion was performed with 5, 50, 100 and 150 nm AuNPs from Nanopartz™ as well as 13 nm self-made AuNPs. Data are presented as mean ± SEM.

AuNP	CI	CO	IR	LE	TM
5 nm	1.79 ± 1.35	0.12 ± 0.01	3.20 ± 0.92	0.02 ± 0.01	0.79 ± 0.15
50 nm	0.44 ± 0.24	0.04 ± 0.01	0.38 ± 0.08	0.04 ± 0.01	1.43 ± 0.56
100 nm	0.70 ± 0.28	0.02 ± 0.00	0.65 ± 0.16	0.02 ± 0.00	4.90 ± 0.85
150 nm	2.75 ± 1.25	0.13 ± 0.02	3.18 ± 0.61	0.05 ± 0.03	8.50 ± 4.37
13 nm	2.12 ± 1.02	0.10 ± 0.05	0.69 ± 0.33	0.04 ± 0.02	4.24 ± 2.93

Table 52: Summary of gold content of eye tissue after ex vivo perfusion with AuNPs.

Gold content of ciliary body (CI), cornea (CO), iris (IR), lens (LE) and trabecular meshwork (TM). Given in ppb per mg tissue ± SEM.

In **Figure 73**, the results for HA-AuNP are presented (n = 3, expect the result for tissues perfused with 150 nm HA-AuNPs, there n = 2). Expect of the 5 nm AuNP, for all AuNP sizes, the moist gold was found in the TM. Again, in CI, IR and TM was more gold per mg tissue found than in CO and LE. Interestingly, 100 nm HA-coated AuNP were found more abundant in all five tissues than the corresponding 100 nm AuNP with citrate surface. For the 150 nm as well as 13 nm sized AuNP, findings were the

other way around. There, less gold was found in the samples perfused with HA-AuNPs than in those with citrate AuNP. Furthermore, the results for the TM perfused with 5 nm HA-AuNP were negative since there, the results for the blank perfused tissue had higher counts than the particle-perfused one. **Table 53** summarizes the findings.

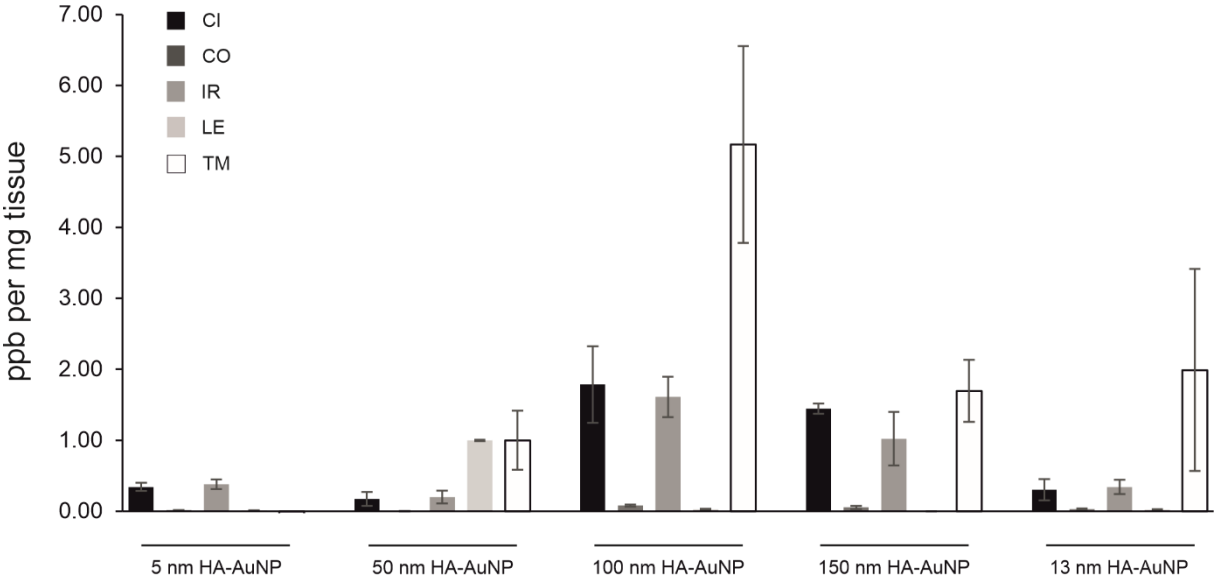

Figure 73: Gold content of eye tissue varied by the size of nanoparticles with hyaluronan surface after ex vivo perfusion.

By inductively coupled plasma mass spectroscopy, gold content of five tissues (CI = ciliary body, CO = cornea, IR = iris, LE = lens, TM = trabecular meshwork) of the anterior chamber was investigated after ex vivo eye perfusion experiments (n = 3, expect the result for TM, perfused with 5 nm AuNPs, there n = 2 due to a significant outlier). Perfusion was performed with 5, 50, 100 and 150 nm AuNPs from Nanopartz™ as well as 13 nm self-made HA-AuNPs. Data are presented as mean ± SEM.

HA-AuNP	CI	CO	IR	LE	TM
5 nm	0.34 ± 0.06	0.02 ± 0.00	0.38 ± 0.07	0.01 ± 0.01	-0.13 ± -0.04
50 nm	0.18 ± 0.10	0.00 ± 0.00	0.20 ± 0.09	1.00 ± 0.01	1.00 ± 0.42
100 nm	1.79 ± 0.54	0.08 ± 0.01	1.61 ± 0.28	0.03 ± 0.01	5.17 ± 1.39
150 nm	1.45 ± 0.07	0.05 ± 0.02	1.02 ± 0.38	0.00 ± 0.00	1.70 ± 0.44
13 nm	0.31 ± 0.15	0.03 ± 0.01	0.34 ± 0.10	0.02 ± 0.01	1.99 ± 1.42

Table 53: Summary of gold content of eye tissue after ex vivo perfusion with HA-AuNPs.

Gold content of ciliary body (CI), cornea (CO), iris (IR), lens (LE) and trabecular meshwork (TM). Given in ppb per mg tissue ± SEM.

To further investigate, how deep the AuNPs perforated into the outflow tissue, TEM images of perfused outflow tissue were investigated. Thereby, AuNP and HA-AuNP were retrievable within the porcine TM. Images of outflow tissue, perfused with 100 nm NPs, are shown in **Figure 74**. Both, AuNP and HA-AuNP were found within the ECM of outflow tissue (indicated by the arrows).

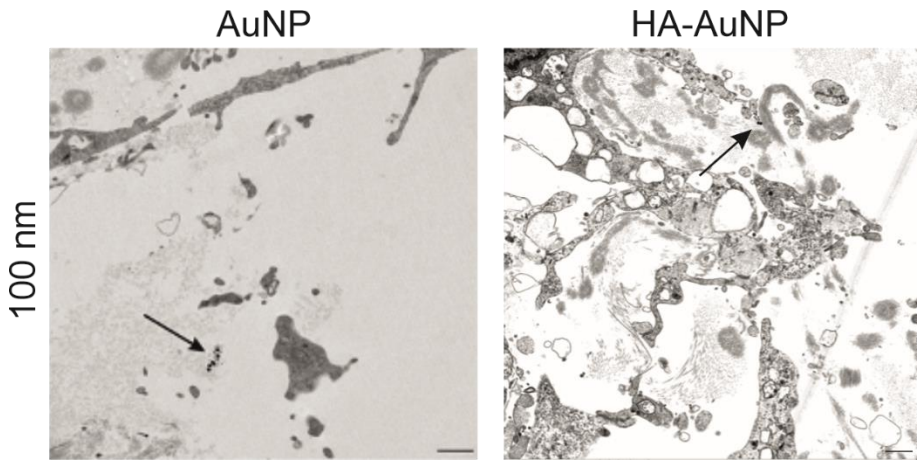

Figure 74: Transmission electron microscopy images of outflow tissue, perfused with 100 nm gold nanoparticles.

By this method, gold-cores of 100 nm NPs were visualized in porcine outflow tissue after ex vivo eye perfusion experiments. AuNP were found within the ECM of outflow tissue, independent on their surface coating (indicated by the arrows). Scale bars: 1,000 nm.

Furthermore, HA-AuNP were spread throughout the whole outflow tissue and even reached the AP, which is the porcine analog of the human SC (**Figure 75**). There, HA-AuNP were also found to be located intracellularly in AP cells.

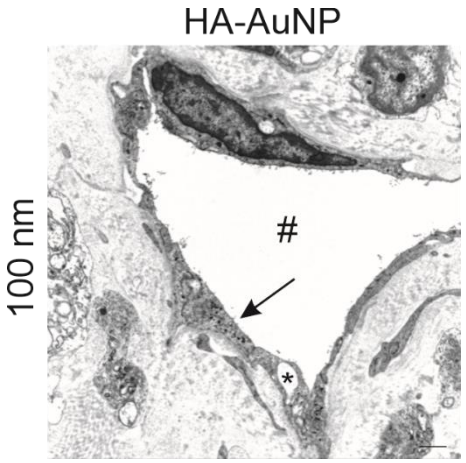

Figure 75: Transmission electron microscopy image of the aqueous plexus of a porcine eye, perfused with 100 nm HA-coated gold nanoparticles.

*By this method, gold-cores of 100 nm HA-AuNPs were visualized after ex vivo eye perfusion experiments. HA-AuNP perforated the outflow tissue deep and reached the aqueous plexus (AP, lumen marked with #, giant vacuole marked with *). Furthermore, HA-AuNPs were found to be located intracellularly in AP cells (indicated by the arrow). Scale bar: 1,000 nm.*

Finally, it was investigated if and how the HA-receptor CD44 abundance varied in SC cells (SC68, SC74 and SC89) under flow conditions *in vitro* (**Figure 76**). Thereby, CD44 mRNA expression was not affected by flow conditions. Neither after one day of incubation nor after one week, CD44 mRNA was affected compared to static controls

(one day: 0 dyn/cm² (n = 11): 1.00 ± 0.19, 10 dyn/cm² (n = 11): 0.99 ± 0.19; one week: 0 dyn/cm² (n = 12): 1.00 ± 0.19, 10 dyn/cm² (n = 11): 0.98 ± 0.21).

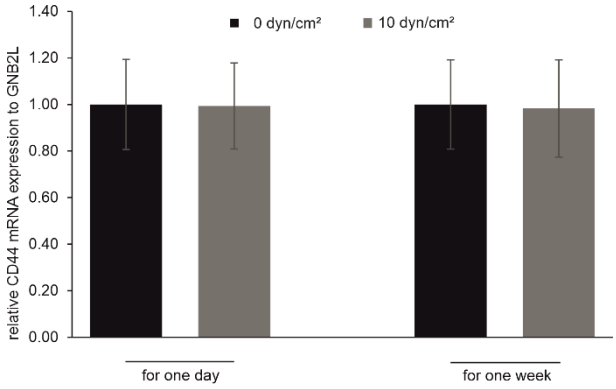

Figure 76: CD44 mRNA expression in SC cells was unaffected by in vitro flow conditions.

CD44 mRNA expression was investigated by RT-qPCR in SC cells (SC68, SC74 and SC89) after one day (n = 11 for 0 dyn/cm² respective n = 11 for 10 dyn/cm² in total) as well as after one week (n = 12 for 0 dyn/cm² respective n = 11 for 10 dyn/cm² in total) under flow conditions. At both time points, flow conditions of 10 dyn/cm² had no impact on CD44 mRNA expression compared to static control (0 dyn/cm²).

With those findings, NP have been shown once again to be a promising tool as potential delivery system for agents towards the area of increased outflow resistance during POAG. Whether it will be NO analogs or miRNAs, manipulating on the expression of glaucoma relevant genes, NP hold the power to deliver both.

5 Discussion

5.1 Summary

The aim of the present study was to gain a better understanding of the molecular mechanisms underlying glaucoma.

Initially, a glaucoma mouse model, overexpressing CTGF under a lens-specific promotor, was investigated. It was found that macroglia activation and IOP increase are specific for the transgenic βB1-CTGF mice, independent on their genetic background.

Thereafter, we identified a potential antagonist to the CTGF effects by treating human SC cells with an exogenous NO donor. DETA-NO treatment not only reduced the expression of the TGF-β response genes PAI-1 and CTGF but also caused significant reduction of cell stiffness and α-SMA expression. Furthermore, the expression of ECM components, including NID-1, COL2A2 and FN, was reduced.

Additionally, the endogenous NO production of SC cells was investigated. By *in vitro* flow conditions, NO production of SC cells was induced. An incubation for 24 hours at 10 dyn/cm² was sufficient to increase NO production towards detectable amounts while one week of incubation significantly increased this induction. Interestingly, the expression or synthesis of eNOS was neither affected by exogenous NO treatment nor by flow conditions.

By a miRNA-microarray, 39 miRNAs associated to the NO signaling pathway were differentially expressed in healthy and glaucomatous SC cell strains. 4 miRNAs were found to have a positive correlation of miRNA expression and the stiffness of the corresponding SC cell strains. With TaqMan technique, miR-222-3p and miR-455-3p were confirmed to be more abundant in glaucomatous SC cell strains in comparison to healthy donors. In turn, DETA-NO treatment led to a reduced expression of these two miRNAs.

The transfection with miR-222-3p caused a significant down-regulation of PAI-1, CTGF and α-SMA in SC cells while DCN expression was significantly increased. On the other hand, the inhibition of miR-222-3p significantly up-regulated the expression of CTGF. Nevertheless, transfection studies with miR-455-3p led to time-dependent effects. Additionally, HUVECs and TM cells were included in the transfection studies.

To investigate a potential delivery system for miRNAs, the distribution of AuNPs within the anterior chamber was assessed after *ex vivo* perfusion of porcine eyes. NP can function as intracameral delivery system for glaucoma therapy and can carry siRNA, miRNA (mimics or inhibitors) or NO donors as agents. Therefore, they must be addressed specifically towards outflow tissue.

Here, the gold content of ciliary body, cornea, iris, lens, and the TM was analyzed after perfusion with AuNP. ICP-MS analysis had shown that independent on AuNP size and surface, almost no gold was detected in cornea and lens. Instead, gold was found in ciliary body, iris and - with the highest amount - in the TM.

5.2 CTGF causes glaucoma, independent on the genetic background

According to the gene expression profile of the human TM, CTGF belongs to the 50 most abundant genes (Tomarev et al. 2003). In the AH of POAG patients, a significant increased amount of CTGF have been reported (Fahmy et al. 2008; Browne et al. 2011). Furthermore, CTGF expression is elevated in glaucomatous SC cells compared to healthy strains (Overby et al. 2014). With its ability to induce ECM deposition and increasing the cell contraction in TM cells (Junglas et al. 2009), CTGF is suggested to be a potential glaucoma-causing factor.

Our group established a transgenic mouse line that overexpresses CTGF under a lens-specific promotor. While no structural changes of the iridocorneal angle were obvious, transgenic mice develop an elevated IOP and a progressive loss of axons in the optic nerve head, which is the main characteristic for glaucoma (Junglas et al. 2012).

The present study investigated this mouse model in a Black6/J background and observed a significant increased IOP in transgenic mice at the age of 8 and 12 weeks. Black6/J is an inbreeding mouse strain with increased homozygosity as far as individuals are considered to be genetically identical (Wang et al. 1999). Although parameter as IOP or axon numbers investigated in these strains may be particularly consistent within a group, findings might be influenced by hidden genetic abnormalities. For example, Black6 mice from the NIH subline (Black6/N) were found to carry the rd8 mutation in the *Crb1* gene, coding for retinal degeneration, while the Black6/J strain from the Jackson Laboratory does not (Mattapallil et al. 2012; Simon et al. 2013). Since homozygous animals develop phenotypical changes, those mice should be excluded, and only Black6/J mice were used.

The present study focused further on the investigation of the mouse model in a pure CD1 background. CD1 is an outbred strain with a diverse gene pool and have been shown to be very sensitive regarding IOP with higher axon loss than other strains (Cone et al. 2010). We found the IOP of transgenic βB1-CTGF mice with a CD1 background to be elevated not until the age of 15 weeks. This was diverging from initial findings, where transgenic mice developed an increased IOP already after 4 weeks (Junglas et al. 2012). This finding might be explained since experiments were performed in two different laboratories and this circumstance has been reported to be potential to lead to discrepancies in the results (Crabbe et al. 1999; Wahlsten et al. 2006).

Furthermore, different mouse strains were investigated. While mice in the original paper were analyzed as first generation of a mixed FVBN/CD1 background, the present study investigated them in a pure CD1 background. Since there, the macroglia activating and IOP increasing effect of the CTGF overexpression was sustained (Reinehr et al. 2019), the glaucoma-causing effect of CTGF and thereby the power of the corresponding mouse model were underlined.

5.3 Endogenous NO signaling is weak in SC cells under standard *in vitro* conditions

eNOS protein was reported to be detectable in cell cultures of TM and SC cells (Perkumas and Stamer 2012). In the present study, we could not reproduce these data by Western Blot which was likely due to the unavailability of the Santa Cruz antibody used by Perkumas and Stamer. Nevertheless, we could detect eNOS protein by ELISA, a more sensitive method. However, *in vitro* conditions always have been a model for the *in vivo* situation that was confronted with restrictions and limitations as differentiation processes and the lack of signals from neighboring cells. In histological sections of the murine iridocorneal angle, eNOS protein can be easily stained in the SC endothelium (data not shown).

In vivo, SC cells are confronted with an incessant flow of AH passing by and through the cells. Perfusion experiments with inverted flow direction have shown that pore forming ability - an essential feature of creating outflow resistance within the SC cells endothelium *in vivo* - was severely impaired (Overby et al. 2014). In the present study, experiments were performed under flow conditions, where SC cells were exposed to

shear stress applied by passing medium. By this setup, NO production was induced and increased over time as it was shown by Ashpole et al. in 2014.

Furthermore, shear stress has been shown to post-transcriptionally regulate eNOS activity. The recruitment of HSP-90 protein to eNOS enhances its activation (García-Cardeña et al. 1998). Thereby, NO production can be increased even if eNOS synthesis remains unaffected. If eNOS gets phosphorylated at Ser(1177) by Akt kinase, Ca^{2+} sensitivity of eNOS is altered towards an enzyme activity maximum below physiological Ca^{2+} concentrations. Thereby, an Akt-dependent, but Ca^{2+}-independent regulatory mechanism of eNOS activity might also contribute to an increased NO production beside alterations of eNOS synthesis (Dimmeler et al. 1999; Fisslthaler et al. 2000). Even if the Ser(1177) phosphorylation leads to a low NO production, subsequent phosphorylation at Thr(495) and high intracellular Ca^{2+} recruit CALM-1 to the complex and further enhances NO production (Fleming et al. 2001). Hence, NO production can be enhanced even if eNOS protein amount itself is unaffected.

The expression of both eNOS enhancers, HSP-90 and CALM-1, has been shown to be significantly reduced by DETA-NO treatment. One might assume that high NO level could function as negative feedback loop to avoid persistent NO production. Nevertheless, CAV-1 as an eNOS inhibitor has been shown to be also significantly reduced by the same treatment. CAV-1 was the first protein being described to be associated to eNOS (García-Cardeña et al. 1996). Back then, authors found that the above mentioned Thr-phosphorylation goes hand in hand with a 50% decrease in enzyme activity at low intracellular Ca^{2+} conditions. By external stimuli, a Ca^{2+} influx can promote the dissociation of CAV-1 from eNOS, allowing for the binding of the enhancer CALM-1 (Michel et al. 1997). Therefore, an increasing intracellular Ca^{2+} concentration is a promoter of NO production by eNOS, while high NO concentrations from the exogenous donor did not consistently affect components of the NO signaling pathway.

CAV-1 knockout mice have a decreased outflow facility and therefore develop increased IOP (Lei et al. 2016). Interestingly, an increased eNOS activity was found in those mice due to increased tyrosine nitration. A mislocalization of the enzyme is thought to cause the reduction of flow-dependent signaling (Yu et al. 2006), but further studies are necessary to address the underlying mechanisms.

5.4 DETA-NO treatment reduces SC cell stiffness and actin stress fibers

The effect of NO donors on the AH outflow facility has been investigated over decades. Exogenous NO has been proven to decrease outflow resistance and thereby IOP in various species (Johnson and Kamm 1983; Nathanson and McKee 1995b; Schneemann et al. 2002; Dismuke et al. 2008; Ellis et al. 2009; Borghi et al. 2010; Stamer et al. 2011; Chang et al. 2015; Ge et al. 2016). On the other hand, SC cell stiffness has been widely investigated and its dynamic range of contractility has been found to be like that of smooth muscle cells. Despite donor-specific variability in baseline stiffness and responsiveness, SC cells stiffen in response to agents that are known to increase outflow resistance and soften in response to agents that are known to decrease outflow resistance (Zhou et al. 2012; Stack et al. 2018).

The present study investigated the response of SC cells after DETA-NO treatment for the first time. While DETA-NO treatment has been known to lead to the relaxation of TM cells (Dismuke et al. 2014), AFM measurements revealed significantly reduced stiffness of HUVECs and SC cells. Together with the finding, that α-SMA expression was also significantly reduced by DETA-NO treatment, the softening of SC cells in response to DETA-NO might be beneficial since it was shown that cortical as well as subcortical stiffness of glaucomatous SC cells are increased compared to those from healthy donors while pore formation has been found to be decreased (Overby et al. 2014).

However, these findings underline the potential of NO to reduce SC cell stiffness which further has been shown to go hand in hand with a decreased outflow resistance, increased outflow facility and reduced IOP. By investigating eNOS overexpressing mice, a first model was described with reduced IOP, elevated outflow facility but with anatomically normal iridocorneal angle (Stamer et al. 2011; Chang et al. 2015). In transgenic mice, an outflow regulating mechanism was found to be continually present while it was pressure-dependent in WT mice and only seen above 35 mmHg. They hypothesize, that the mechanosensitivity of eNOS activity postulated in systemic vasculature (Topper et al. 1996; Go et al. 2001; van Haperen et al. 2003) is transmissible to SC endothelium. Functioning as “barostat”, SC cells are thought to sense changes in the IOP and regulate outflow facility to restore IOP homeostasis (Stamer et al. 2011). This assumption becomes even more substantial since three polymorphisms in the NOS3 gene, coding for eNOS, have been found to be associated

to POAG (Tunny et al. 1998; Logan et al. 2005; Kang et al. 2010). Furthermore, the glaucomatous TM and SC have a decreased reactivity of the NO-indicator marker NADPH-d (Nathanson and McKee 1995a) and eNOS knockout mice have been shown to develop elevated IOP and decrease AH outflow (Lei et al. 2015).

5.5 Exogenous NO reduced expression of glaucoma-associated factors

Even if the involvement of impaired NO production in the pathogenesis of POAG is very likely, there are other factors that have been shown to be associated to POAG. CTGF has been proven to be a glaucoma-causing factor (Junglas et al. 2009; Junglas et al. 2012; Reinehr et al. 2019) and is furthermore associated to disorders with a pathological increase in ECM deposition (Ito et al. 1998; Schneemann et al. 2002; Sato et al. 2000; Di Mola et al. 2004; Cicha et al. 2005; Yamamoto et al. 2005). CTGF has been shown to induce the expression of ECM components as COL4 and FN (Junglas et al. 2009). In the present study, we identified the potential of exogenous NO to significantly reduce CTGF expression and synthesis in SC cells. Furthermore, this reduction went hand in hand with a significant decrease of the expression of the ECM components NID-1, COL4A4 and FN.

In the pathogenesis of POAG, the CTGF effect is thought to be induced by the abnormal high TGF-β2 level in the AH (Fuchshofer and Tamm 2009). In the present study, we could not show an impact of DETA-NO treatment on TGF-β2 expression. However, expression itself does not allow for any assumptions regarding TGF-β2 activity. This could only be done by studying TGF-β2 activity at protein level. So far, the reduced expression of the TGF-β downstream effectors PAI-1 and CTGF hints for reduced TGF-β signaling. In HUVECs, an endothelial cell line used as a model cell line within this study, the downregulation of TGF-β2 mRNA has been shown and further confirmed a significant down-regulation of PAI-1 and CTGF mRNA expression after DETA-NO treatment in another endothelial cell line.

The flow experiments on cultured SC cells showed no change in CTGF mRNA expression. The present study applied constant flow and thereby reproduced data from HUVECs which have been reported to show no alterations in CTGF expression under constant shear stress (Eskin et al. 2004).

In summary, NO has not only an effect on cell stiffness but also on the expression profile of some glaucoma relevant genes, which are associated with an increased formation of stress fibers and thereby an increased cell stiffness (Overby et al. 2014).

5.6 miR-222-3p mimics also positively affect the expression of glaucoma-associated genes

MiRNAs are strong post-transcriptional regulators of mRNA abundance by complementary sequence paring to the 3’ UTR of the target mRNA (Krol et al. 2010; Huntzinger and Izaurralde 2011). This paring leads either to the cleavage of the bound mRNA or to less efficient translation into protein. Thereby, miRNA alterations have been linked to many diseases. (Esteller 2011)

Since small RNA sequencing revealed altered miRNA expression profiles for glaucomatous and healthy SC cell strains, the investigation of those miRNAs might give an insight to yet unknown regulation of the disease. In the present study, miR-222-3p and miR-455-3p have been confirmed to be significantly elevated in glaucomatous SC cells. Furthermore, both miRNAs have been shown to be significantly reduced by DETA-NO treatment.

miR-222-3p has been shown to target STAT5A, being involved in inflammation-mediated vascular remodeling (Dentelli et al. 2010), iNOS (Brown and Yin 2013) and eNOS (Suárez et al. 2007), eventually via the transcription factor ets-1 (Evangelista et al. 2013). Evangelista proclaimed that the inhibition of miR-222-3p does induce the expression of eNOS of about 25%. Even if such an induction might take place in SC cells, the present study was confronted with still undetectable eNOS mRNA amounts. Furthermore, eNOS protein and its activation (determined by Ser(1177) phosphorylation) has been shown to be lower in aged human aortic endothelial cells with corresponding increased amount of eNOS-suppressing miR-222-3p amounts (Rippe et al. 2012). Our experiments were performed in SC cells with less than 10 passages. Therefore, an influence of aging in our cells is unlikely since Rippe et al. defined their primary endothelial cells with passage 27 ± 1 as non-senescent controls and those with passage 44 ± 1 as senescent. However, the finding that exogenous NO efficiently reduced the miRNA abundance might provide a regulatory mechanism to reduce miRNAs, which we have reported here to be elevated in the pathogenesis of POAG.

By transfection experiments, miR-222-3p alterations have been shown to affect the expression of glaucoma-relevant genes in SC cells. Even if one could have expected the opposite, transfection with miR-222-3p mimics significantly down-regulated CTGF, PAI-1 and α-SMA expression. Since no direct interaction of miR-222-3p with CTGF, PAI-1, etc. was found by evaluation with the TargetScan software, further studies are needed to confirm if there are other transcription factors that are targeted by the miRNA which then might have an impact on those genes. However, the finding that miR-222-3p mimics significantly reduced CTGF expression, while miR-222-3p inhibition led to the opposite result, was consistent in HUVECs and TM cells and therefore deserves further investigations.

The miR-221-3p/222-3p family has been found to have inhibitory effects on TGF-β signaling (Verjans et al. 2018). In biopsies from fibrotic myocards, a negative correlation of miRNA level was reported with the extent of fibrosis and ventricular stiffness. By *in vitro* TGF-β treatment of cardiac fibroblasts, miR-222-3p expression was downregulated and by inhibition of miR-222-3p, the pro-fibrotic signaling was induced. If this counteracting effect of miR-222-3p and TGF-β signaling can be transferred to cells of the outflow tissue is worth to be addressed by further investigations.

That the transfection results for HUVECs and TM cells did not cover every finding made in SC cells might suggest for a cell type specific effect. Furthermore, there might be some other limitations: So far, only one TM cell and one HUVEC line were investigated. Since they derive from one single donor each, donor-specific aberrations might influence findings. Additionally, other timepoints might reveal changes in different cell types. Since HUVECs often reacted fast - with pronounced changes already after 48 hours - earlier time points might benefit the quality of these results. Besides, only one mimic and one inhibitor concentration were tested so far. For miR-455-3p, other concentrations might be more suitable since that miRNA has been found to be less abundant than miR-222-3p.

5.7 AuNPs specifically accumulate within the outflow tissue and can be addressed towards the TM by functionalization with HA

Since transfection with miRNA has been shown to positively affect the expression of some glaucoma-relevant genes, their potential as glaucoma treatment deserves

investigation. In recent years, NP were developed to deliver sufficient therapeutic concentrations of drugs specifically towards target tissue. Furthermore, they can be designed to release drugs over prolonged time. Therefore, their administration might not only increase drug's effectiveness but also patient's compliance by reduced application frequency.

Concerning eye diseases, intracameral injection of NP-associated drugs would avoid side effects of topical applications. Commonly, POAG drugs are applied as eye drops but are accompanied by off-target effects as conjunctival hyperemia (Chandrawati et al. 2017) and low bioavailability of active agents in the AH (Janagam et al. 2017; Mietzner and Breunig 2019; Subrizi et al. 2019).

Our group in cooperation with Prof. Dr. Breunig had developed layer-by-layer coated NPs with a biodegradable PLGA core and a final coating of HA. Thereby, the NP's mobility was improved in the ECM of outflow tissue and NPs reached JCT and SC endothelium in *ex vivo* perfusion experiments. Furthermore, HA is a natural ligand of the CD44 receptor, which leads to an improved cellular uptake of HA-NPs by cells of the outflow pathway. Coated with siRNA against CTGF, our HA-coated NPs effectively transfected TM cells and significantly reduced CTGF synthesis. (Dillinger et al. 2018)

Since the NPs used for the experiments published by Dillinger et al. had a fluorescent core for tracking, the detection of single NPs and their quantification was not possible. Hence, the present study performed *ex vivo* perfusion experiments with Au-NP. Thereby, we were able to recover gold as ppb per mg tissue in five tissues of the anterior chamber. Convincingly, the greatest amount of gold was recovered in the TM for NPs ranging from 13 to 150 nm in size. Only 5 nm small NPs did not accumulate within the TM which might be due to their small size and an increased likelihood to pass the outflow tissue with flow. However, particles with a size from 200 to 500 nm can pass the inner wall pores (Abu-Hassan et al. 2014), therefore all of our investigated AuNPs were suitable, not to clog the outflow pathway. If our NP get functionalized with siRNA, miRNA (mimics or inhibitors) or even NO donating components in further approaches, they are proven by this study to reach their target site in the outflow tissue.

That there was in general less gold detected for HA-AuNP compared to AuNP might be due to an additional dialysis step. In the process of HA-coating, dialysis became necessary to eliminate unbound HA. Therefore, the molecular cut-off of the selectively

permeable membrane was chosen to be 2.5-times bigger than HA but smaller than the particles. It has to be clarified in future studies, whether the dialysis has an impact.

5.8 Further directions

The βB1-CTGF overexpressing mouse line will be further investigated in different genetic backgrounds. Beside IOP evaluation at different ages, the ultrastructure of the iridocorneal angle as well as axon numbers must be investigated. Furthermore, crossbreeding with DCN knockout mice will allow an insight in the interaction of two glaucoma-causing factors.

In vivo and *ex vivo* studies with NO donors will reveal their potential to treat glaucomatous changes. Ideally, the administration will be combined with NPs, developed to specifically target outflow tissue.

Concerning miRNA, the mechanisms and targets must be investigated further. *In vitro* TGF-β2- and CTGF-treated TM and SC cells as well as corneoscleral rings from murine glaucoma models can be evaluated regarding their miRNA expression profile. With gain-of-function and loss-of-function experiments, miRNA interaction partner should be identified. At protein level, their physiological effect must be proven. Furthermore, miR-222-3p had shown a high potential to reduce CTGF expression when abundant. Therefore, its influence on SC cell stiffness can be investigated by AFM. *In vivo*, miRNA mimics and inhibitors could be applied, embedded in a NP transport system, to target outflow tissue. Thereafter, IOP and outflow facility measurements could give an insight on their impact on factors, relevant for the pathogenesis of POAG.

So far, the interaction of miRNAs with eNOS has not been tested in the present study since eNOS was hardly detectable under static cell culture conditions. By a transcellular perfusion setup, this limitation might be overcome and an *in vitro* situation that better mimics the *in vivo* situation might allow for further studies of the NO signaling pathway in SC cells.

6 Conclusion

The present study reports the glaucoma-causing effects of CTGF overexpression in a murine mouse model to be regardless of the genetic background. Beside minor variations in the temporal sequence of the appearance of changes, the power of the corresponding βB1-CTGF mouse model was underlined.

By *in vitro* treatment with exogenous NO, not only CTGF but also the expression of ECM components was reduced. Thereby, it provides potential to positively intercept glaucomatous changes beside reducing cell stiffness, which also was proven within this study. Furthermore, the influence of miRNA abundance on the expression profile of SC cells has been argued. Even if their impairment on eNOS could not be addressed, this study exhibited stunning impact on the expression profile of CTGF and other glaucoma-associated factors.

With the tracking of AuNPs in tissues of the anterior chamber after *ex vivo* perfusion experiments, we finally underlined their potential to specifically accumulate in the TM. Thereby, undesired side effects on other tissues are expected to be negligible when NP will be functionalized with siRNA or miRNA (mimics or inhibitors) coating in future experiments.

7 Publication bibliography

Abu-Hassan, Diala W.; Acott, Ted S.; Kelley, Mary J. (2014): The Trabecular Meshwork. A Basic Review of Form and Function. In *Journal of ocular biology* 2 (1). DOI: 10.13188/2334-2838.1000017.

Agarwal, Puneet; Daher, Aqil Mohammad; Agarwal, Renu (2015): Aqueous humor TGF-β2 levels in patients with open-angle glaucoma. A meta-analysis. In *Molecular Vision* 21, pp. 612–620.

Allingham, R. Rand; Liu, Yutao; Rhee, Douglas J. (2009): The genetics of primary open-angle glaucoma. A review. In *Experimental eye research* 88 (4), pp. 837–844. DOI: 10.1016/j.exer.2008.11.003.

Alward, Wallace L. M. (2003): Biomedicine. A new angle on ocular development. In *Science* 299 (5612), pp. 1527–1528. DOI: 10.1126/science.1082933.

Ashpole, Nicole E.; Overby, Darryl R.; Ethier, C. Ross; Stamer, W. Daniel (2014): Shear stress-triggered nitric oxide release from Schlemm's canal cells. In *Investigative ophthalmology & visual science* 55 (12), pp. 8067–8076. DOI: 10.1167/iovs.14-14722.

Bachmann, Bjoern; Birke, Marco; Kook, Daniel; Eichhorn, Michael; Lütjen-Drecoll, Elke (2006): Ultrastructural and biochemical evaluation of the porcine anterior chamber perfusion model. In *Investigative ophthalmology & visual science* 47 (5), pp. 2011–2020. DOI: 10.1167/iovs.05-1393.

Baskerville, Scott; Bartel, David P. (2005): Microarray profiling of microRNAs reveals frequent coexpression with neighboring miRNAs and host genes. In *RNA* 11 (3), pp. 241–247. DOI: 10.1261/rna.7240905.

Bhattacharya, Sanjoy K.; Gabelt, B'Ann T.; Ruiz, Jose; Picciani, Renata; Kaufman, Paul L. (2009): Cochlin expression in anterior segment organ culture models after TGFbeta2 treatment. In *Investigative ophthalmology & visual science* 50 (2), pp. 551–559. DOI: 10.1167/iovs.08-2632.

Borghi, Valentina; Bastia, Elena; Guzzetta, Massimiliano; Chiroli, Valerio; Toris, Carol B.; Batugo, Minerva R. et al. (2010): A novel nitric oxide releasing prostaglandin analog, NCX 125, reduces intraocular pressure in rabbit, dog, and primate models of glaucoma. In *Journal of ocular pharmacology and therapeutics* 26 (2), pp. 125–132. DOI: 10.1089/jop.2009.0120.

Brown, Peter N.; Yin, Hang (2013): PNA-based microRNA inhibitors elicit anti-inflammatory effects in microglia cells. In *Chemical communications* 49 (39), pp. 4415–4417. DOI: 10.1039/C2CC36540E.

Browne, John G.; Ho, Su Ling; Kane, Rosemary; Oliver, Noelynn; Clark, Abbot F.; O'Brien, Colm J.; Crean, John K. (2011): Connective tissue growth factor is increased in pseudoexfoliation glaucoma. In *Investigative ophthalmology & visual science* 52 (6), pp. 3660–3666. DOI: 10.1167/iovs.10-5209.

Buraschi, S.; Neill, T.; Goyal, A.; Poluzzi, C.; Smythies, J.; Owens, R. T. et al. (2013): Decorin causes autophagy in endothelial cells via Peg3. In *Proceedings of the National Academy of Sciences* 110 (28), E2582-E2591. DOI: 10.1073/pnas.1305732110.

Buys, Emmanuel S.; Potter, Lincoln R.; Pasquale, Louis R.; Ksander, Bruce R. (2014): Regulation of intraocular pressure by soluble and membrane guanylate cyclases and their role in glaucoma. In *Frontiers in molecular neuroscience* 7, p. 38. DOI: 10.3389/fnmol.2014.00038.

Chandrawati, Rona; Chang, Jason Y. H.; Reina-Torres, Ester; Jumeaux, Coline; Sherwood, Joseph M.; Stamer, W. Daniel et al. (2017): Localized and Controlled Delivery of Nitric Oxide to the Conventional Outflow Pathway via Enzyme Biocatalysis. Toward Therapy for Glaucoma. In *Advanced materials* 29 (16). DOI: 10.1002/adma.201604932.

Chang, C. J.; Chiang, C. H.; Chow, J. C.; Lu, D. W. (2000): Aqueous humor nitric oxide levels differ in patients with different types of glaucoma. In *Journal of ocular pharmacology and therapeutics* 16 (5), pp. 399–406. DOI: 10.1089/jop.2000.16.399.

Chang, Jason Y. H.; Stamer, W. Daniel; Bertrand, Jacques; Read, A. Thomas; Marando, Catherine M.; Ethier, C. Ross; Overby, Darryl R. (2015): Role of nitric oxide in murine conventional outflow physiology. In *American journal of physiology. Cell physiology* 309 (4), C205-14. DOI: 10.1152/ajpcell.00347.2014.

Cicha, Iwona; Yilmaz, Atilla; Klein, Michael; Raithel, Dieter; Brigstock, David R.; Daniel, Werner G. et al. (2005): Connective tissue growth factor is overexpressed in complicated atherosclerotic plaques and induces mononuclear cell chemotaxis in vitro. In *Arteriosclerosis, thrombosis, and vascular biology* 25 (5), pp. 1008–1013. DOI: 10.1161/01.ATV.0000162173.27682.7b.

Collaborative Normal-Tension Glaucoma Study Group (1998a): Comparison of glaucomatous progression between untreated patients with normal-tension glaucoma and patients with therapeutically reduced intraocular pressures. In *American Journal of Ophthalmology* 126 (4), pp. 487–497. DOI: 10.1016/S0002-9394(98)00223-2.

Collaborative Normal-Tension Glaucoma Study Group (1998b): The effectiveness of intraocular pressure reduction in the treatment of normal-tension glaucoma. In *American Journal of Ophthalmology* 126 (4), pp. 498–505. DOI: 10.1016/S0002-9394(98)00272-4.

Cone, Frances E.; Gelman, Scott E.; Son, Janice L.; Pease, Mary E.; Quigley, Harry A. (2010): Differential susceptibility to experimental glaucoma among 3 mouse strains using bead and viscoelastic injection. In *Experimental eye research* 91 (3), pp. 415–424. DOI: 10.1016/j.exer.2010.06.018.

Crabbe, J. C.; Wahlsten, D.; Dudek, B. C. (1999): Genetics of mouse behavior. Interactions with laboratory environment. In *Science* 284 (5420), pp. 1670–1672. DOI: 10.1126/science.284.5420.1670.

Danielson, Keith G.; Baribault, Helene; Holmes, David F.; Graham, Helen; Kadler, Karl E.; Iozzo, Renato V. (1997): Targeted Disruption of Decorin Leads to Abnormal Collagen Fibril Morphology and Skin Fragility. In *Journal of Cell Biology* 136 (3), pp. 729–743. DOI: 10.1083/jcb.136.3.729.

Dentelli, Patrizia; Rosso, Arturo; Orso, Francesca; Olgasi, Cristina; Taverna, Daniela; Brizzi, Maria Felice (2010): microRNA-222 controls neovascularization by regulating signal transducer and activator of transcription 5A expression. In *Arteriosclerosis, thrombosis, and vascular biology* 30 (8), pp. 1562–1568. DOI: 10.1161/ATVBAHA.110.206201.

Di Mola, Fabio F.; Di Sebastiano, Pierluigi; Gardini, Andrea; Innocenti, Paolo; Zimmermann, Arthur; Büchler, Markus W.; Friess, Helmut (2004): Differential expression of connective tissue growth factor in inflammatory bowel disease. In *Digestion* 69 (4), pp. 245–253. DOI: 10.1159/000079845.

Dickie, M. M. (1975): Keeping Records. Biology of the Laboratory Mouse. In *Dover Publications*, p. 706.

Dillinger, Andrea E.; Guter, Michaela; Froemel, Franziska; Weber, Gregor R.; Perkumas, Kristin; Stamer, W. Daniel et al. (2018): Intracameral Delivery of Layer-by-

Layer Coated siRNA Nanoparticles for Glaucoma Therapy. In *Small* 14 (50), e1803239. DOI: 10.1002/smll.201803239.

Dimmeler, S.; Fleming, I.; Fisslthaler, B.; Hermann, C.; Busse, R.; Zeiher, A. M. (1999): Activation of nitric oxide synthase in endothelial cells by Akt-dependent phosphorylation. In *Nature* 399 (6736), pp. 601–605. DOI: 10.1038/21224.

Dismuke, W. Michael; Liang, Jin; Overby, Darryl R.; Stamer, W. Daniel (2014): Concentration-related effects of nitric oxide and endothelin-1 on human trabecular meshwork cell contractility. In *Experimental eye research* 120, pp. 28–35. DOI: 10.1016/j.exer.2013.12.012.

Dismuke, William M.; Mbadugha, Chigozirim C.; Ellis, Dorette Z. (2008): NO-induced regulation of human trabecular meshwork cell volume and aqueous humor outflow facility involve the BKCa ion channel. In *American journal of physiology. Cell physiology* 294 (6), C1378-86. DOI: 10.1152/ajpcell.00363.2007.

Eacker, Stephen M.; Dawson, Ted M.; Dawson, Valina L. (2009): Understanding microRNAs in neurodegeneration. In *Nature reviews. Neuroscience* 10 (12), pp. 837–841. DOI: 10.1038/nrn2726.

Ellis, Dorette Z.; Dismuke, William M.; Chokshi, Binna M. (2009): Characterization of soluble guanylate cyclase in NO-induced increases in aqueous humor outflow facility and in the trabecular meshwork. In *Investigative ophthalmology & visual science* 50 (4), pp. 1808–1813. DOI: 10.1167/iovs.08-2750.

Emam, Wafaa A.; Zidan, Haidy E.; Abdulhalim Bahaa-Eldin H.; Dabour Sherif A.; Ghali, Manar A.; Kamal, Aliaa T. (2014): Endothelial nitric oxide synthase polymorphisms and susceptibility to high-tension primary open-angle glaucoma in an Egyptian cohort. In *Molecular Vision* (20), pp. 804–811, checked on 1/29/2018.

Eskin, Suzanne G.; Turner, Nancy A.; McIntire, Larry V. (2004): Endothelial cell cytochrome P450 1A1 and 1B1. Up-regulation by shear stress. In *Endothelium* 11 (1), pp. 1–10. DOI: 10.1080/10623320490432434.

Esteller, Manel (2011): Non-coding RNAs in human disease. In *Nature reviews. Genetics* 12 (12), pp. 861–874. DOI: 10.1038/nrg3074.

Ethier, C. Ross; Read, A. Thomas; Chan, Darren (2004): Biomechanics of Schlemm's canal endothelial cells. Influence on F-actin architecture. In *Biophysical journal* 87 (4), pp. 2828–2837. DOI: 10.1529/biophysj.103.038133.

Evangelista, Alicia M.; Deschamps, Anne M.; Liu, Delong; Raghavachari, Nalini; Murphy, Elizabeth (2013): miR-222 contributes to sex-dimorphic cardiac eNOS expression via ets-1. In *Physiological genomics* 45 (12), pp. 493–498. DOI: 10.1152/physiolgenomics.00008.2013.

Fahmy, I. A.; Ismail, S. A. M.; Abd-EL-Hamid, M. (2008): Role of Aqueous Humor Matrix Metalloproteinase-2 and Its Inhibitor and Connective Tissue Growth Factor in the Pathogenesis of Primary Open Angle Glaucoma and pseudoexfoliative glaucoma. In *Rawal Medical Journal* 33 (2), pp. 179–182.

Fernandez-Durango, Raquel; Fernandez-Martinez, Amalia; Garcia-Feijoo, Julian; Castillo, Alfredo; La Casa, Jose Martinez de; Garcia-Bueno, Borja et al. (2008): Expression of nitrotyrosine and oxidative consequences in the trabecular meshwork of patients with primary open-angle glaucoma. In *Investigative ophthalmology & visual science* 49 (6), pp. 2506–2511. DOI: 10.1167/iovs.07-1363.

Ferrarelli, Leslie K. (2015): Focus issue. Noncoding RNAs in cancer. In *Science signaling* 8 (368), eg3. DOI: 10.1126/scisignal.aaa9789.

Fisslthaler, B.; Dimmeler, S.; Hermann, C.; Busse, R.; Fleming, I. (2000): Phosphorylation and activation of the endothelial nitric oxide synthase by fluid shear stress. In *Acta physiologica Scandinavica* 168 (1), pp. 81–88. DOI: 10.1046/j.1365-201x.2000.00627.x.

Fleenor, Debra L.; Shepard, Allan R.; Hellberg, Peggy E.; Jacobson, Nasreen; Pang, Iok-Hou; Clark, Abbot F. (2006): TGFbeta2-induced changes in human trabecular meshwork. Implications for intraocular pressure. In *Investigative ophthalmology & visual science* 47 (1), pp. 226–234. DOI: 10.1167/iovs.05-1060.

Fleming, I.; Fisslthaler, B.; Dimmeler, S.; Kemp, B. E.; Busse, R. (2001): Phosphorylation of Thr(495) regulates Ca(2+)/calmodulin-dependent endothelial nitric oxide synthase activity. In *Circulation research* 88 (11), E68-75. DOI: 10.1161/hh1101.092677.

Fuchshofer, Rudolf; Tamm, Ernst R. (2009): Modulation of extracellular matrix turnover in the trabecular meshwork. In *Experimental eye research* 88 (4), pp. 683–688. DOI: 10.1016/j.exer.2009.01.005.

Fuchshofer, Rudolf; Welge-Lussen, Ulrich; Lütjen-Drecoll, Elke (2003): The effect of TGF-β2 on human trabecular meshwork extracellular proteolytic system. In

Experimental eye research 77 (6), pp. 757–765. DOI: 10.1016/s0014-4835(03)00220-3.

Fuchshofer, Rudolf; Yu, Alice H. L.; Welge-Lüssen, Ulrich; Tamm, Ernst R. (2007): Bone morphogenetic protein-7 is an antagonist of transforming growth factor-beta2 in human trabecular meshwork cells. In *Investigative ophthalmology & visual science* 48 (2), pp. 715–726. DOI: 10.1167/iovs.06-0226.

García-Cardeña, G.; Fan, R.; Shah, V.; Sorrentino, R.; Cirino, G.; Papapetropoulos, A.; Sessa, W. C. (1998): Dynamic activation of endothelial nitric oxide synthase by Hsp90. In *Nature* 392 (6678), pp. 821–824. DOI: 10.1038/33934.

García-Cardeña, G.; Fan, R.; Stern, D. F.; Liu, J.; Sessa, W. C. (1996): Endothelial nitric oxide synthase is regulated by tyrosine phosphorylation and interacts with caveolin-1. In *The Journal of Biological Chemistry* 271 (44), pp. 27237–27240. DOI: 10.1074/jbc.271.44.27237.

Ge, Pei; Navarro, Iris; Kessler, Marco; Bernier, Silvie; Perl, Nicholas; Sarno, Renee et al. (2016): The Soluble Guanylate Cyclase Stimulator IWP-953 Increases Conventional Outflow Facility in Mouse Eyes. In *Investigative ophthalmology & visual science* (57), p. 3010.

Go, Y. M.; Boo, Y. C.; Park, H.; Maland, M. C.; Patel, R.; Pritchard, K. A. et al. (2001): Protein kinase B/Akt activates c-Jun NH(2)-terminal kinase by increasing NO production in response to shear stress. In *Journal of applied physiology* 91 (4), pp. 1574–1581. DOI: 10.1152/jappl.2001.91.4.1574.

Gordon, Mae O.; Beiser, Julia A.; Brandt, James D.; Heuer, Dale K.; Higginbotham, Eve J.; Johnson, Chris A. et al. (2002): The Ocular Hypertension Treatment Study. Baseline factors that predict the onset of primary open-angle glaucoma. In *Archives of ophthalmology* 120 (6), 714-20; discussion 829-30. DOI: 10.1001/archopht.120.6.714.

Gottanka, Johannes; Chan, Darren; Eichhorn, Michael; Lütjen-Drecoll, Elke; Ethier, C. Ross (2004): Effects of TGF-beta2 in perfused human eyes. In *Investigative ophthalmology & visual science* 45 (1), pp. 153–158. DOI: 10.1167/iovs.03-0796.

Grant, W. M. (1963): Experimental aqueous perfusion in enucleated human eyes. In *Archives of ophthalmology* 69, pp. 783–801. DOI: 10.1001/archopht.1963.00960040789022.

Grisanti, Salvatore; Szurman, Peter; Warga, Max; Kaczmarek, Radoslaw; Ziemssen, Focke; Tatar, Olcay; Bartz-Schmidt, Karl Ulrich (2005): Decorin Modulates Wound Healing in Experimental Glaucoma Filtration Surgery. A Pilot Study. In *Investigative ophthalmology & visual science* 46 (1), p. 191. DOI: 10.1167/iovs.04-0902.

Guo, Tao; Guo, Li; Fan, Yuchen; Fang, Li; Wei, Jiahong; Tan, Ye et al. (2019): Aqueous humor levels of TGFβ2 and SFRP1 in different types of glaucoma. In *BMC ophthalmology* 19 (1), p. 170. DOI: 10.1186/s12886-019-1183-1.

Gutschner, Tony; Diederichs, Sven (2012): The hallmarks of cancer. A long non-coding RNA point of view. In *RNA biology* 9 (6), pp. 703–719. DOI: 10.4161/rna.20481.

Hemish, Jill; Nakaya, Naoki; Mittal, Vivek; Enikolopov, Grigori (2003): Nitric Oxide Activates Diverse Signaling Pathways to Regulate Gene Expression. In *The Journal of Biological Chemistry* 278 (43), pp. 42321–42329. DOI: 10.1074/jbc.M308192200.

Higginbotham, Eve J.; Gordon, Mae O.; Beiser, Julia A.; Drake, Michael V.; Bennett, G. Richard; Wilson, M. Roy; Kass, Michael A. (2004): The Ocular Hypertension Treatment Study. Topical medication delays or prevents primary open-angle glaucoma in African American individuals. In *Archives of ophthalmology* 122 (6), pp. 813–820. DOI: 10.1001/archopht.122.6.813.

Hill, Lisa J.; Mead, Ben; Blanch, Richard J.; Ahmed, Zubair; Cogan, Felicity de; Morgan-Warren, Peter J. et al. (2015): Decorin Reduces Intraocular Pressure and Retinal Ganglion Cell Loss in Rodents Through Fibrolysis of the Scarred Trabecular Meshwork. In *Investigative ophthalmology & visual science* 56 (6), pp. 3743–3757. DOI: 10.1167/iovs.14-15622.

Hill, LisaJ; Ahmed, Zubair; Logan, Ann (2016): Decorin treatment for reversing trabecular meshwork fibrosis in open-angle glaucoma. In *Neural Regeneration Research* 11 (6), p. 0. DOI: 10.4103/1673-5374.184489.

Huntzinger, Eric; Izaurralde, Elisa (2011): Gene silencing by microRNAs. Contributions of translational repression and mRNA decay. In *Nature reviews. Genetics* 12 (2), pp. 99–110. DOI: 10.1038/nrg2936.

Ihn, Hironobu (2002): Pathogenesis of fibrosis. Role of TGF-beta and CTGF. In *Current opinion in rheumatology* 14 (6), pp. 681–685. DOI: 10.1097/00002281-200211000-00009.

Inatani, M.; Tanihara, H.; Katsuta, H.; Honjo, M.; Kido, N.; Honda, Y. (2001): Transforming growth factor-beta 2 levels in aqueous humor of glaucomatous eyes. In *Graefe's archive for clinical and experimental ophthalmology* 239 (2), pp. 109–113. DOI: 10.1007/s004170000241.

Ito, Y.; Aten, J.; Bende, R. J.; Oemar, B. S.; Rabelink, T. J.; Weening, J. J.; Goldschmeding, R. (1998): Expression of connective tissue growth factor in human renal fibrosis. In *Kidney international* 53 (4), pp. 853–861. DOI: 10.1111/j.1523-1755.1998.00820.x.

Jampel, H. D.; Roche, N.; Stark, W. J.; Roberts, A. B. (1990): Transforming growth factor-beta in human aqueous humor. In *Current eye research* 9 (10), pp. 963–969. DOI: 10.3109/02713689009069932.

Janagam, Dileep R.; Wu, Linfeng; Lowe, Tao L. (2017): Nanoparticles for drug delivery to the anterior segment of the eye. In *Advanced drug delivery reviews* 122, pp. 31–64. DOI: 10.1016/j.addr.2017.04.001.

Jayaram, Hari; Phillips, Jay I.; Lozano, Diana C.; Choe, Tiffany E.; Cepurna, William O.; Johnson, Elaine C. et al. (2017): Comparison of MicroRNA Expression in Aqueous Humor of Normal and Primary Open-Angle Glaucoma Patients Using PCR Arrays. A Pilot Study. In *Investigative ophthalmology & visual science* 58 (12), p. 4988. DOI: 10.1167/iovs.17-22568.

Johnson, M. C.; Kamm, R. D. (1983): The Role of Schlemm's Canal in Aqueous Outflow from the Human Eye. In *Investigative ophthalmology & visual science* 24 (3), pp. 320–325.

Johnson, Mark (2006): 'What controls aqueous humour outflow resistance?'. In *Experimental eye research* 82 (4), pp. 545–557. DOI: 10.1016/j.exer.2005.10.011.

Junglas, Benjamin; Kuespert, Sabrina; Seleem, Amin A.; Struller, Tobias; Ullmann, Sabrina; Bösl, Michael et al. (2012): Connective Tissue Growth Factor Causes Glaucoma by Modifying the Actin Cytoskeleton of the Trabecular Meshwork. In *The American Journal of Pathology* 180 (6), pp. 2386–2403. DOI: 10.1016/j.ajpath.2012.02.030.

Junglas, Benjamin; Yu, Alice H.L.; Welge-Lüssen, Ulrich; Tamm, Ernst R.; Fuchshofer, Rudolf (2009): Connective tissue growth factor induces extracellular matrix deposition

in human trabecular meshwork cells. In *Experimental eye research* 88 (6), pp. 1065–1075. DOI: 10.1016/j.exer.2009.01.008.

Kang, Jae Hee; Wiggs, Janey L.; Rosner, Bernard A.; Hankinson, Susan E.; Abdrabou, Wael; Fan, Bao Jian et al. (2010): Endothelial nitric oxide synthase gene variants and primary open-angle glaucoma. Interactions with sex and postmenopausal hormone use. In *Investigative ophthalmology & visual science* 51 (2), pp. 971–979. DOI: 10.1167/iovs.09-4266.

Keller, Kate E.; Acott, Ted S. (2013): The Juxtacanalicular Region of Ocular Trabecular Meshwork. A Tissue with a Unique Extracellular Matrix and Specialized Function. In *Journal of ocular biology* 1 (1), p. 3.

Kosior-Jarecka, Ewa; Gerkowicz, Marek; Latalska, Małgorzata; Kozioł-Montewka, Maria; Szczepanik, Agnieszka (2004): Poziom tlenku azotu w cieczy wodnistej u pacjentów z jaskra. In *Klinika oczna* 106 (1-2 Suppl), pp. 158–159.

Krol, Jacek; Loedige, Inga; Filipowicz, Witold (2010): The widespread regulation of microRNA biogenesis, function and decay. In *Nature reviews. Genetics* 11 (9), pp. 597–610. DOI: 10.1038/nrg2843.

Kwon, Young H.; Fingert, John H.; Kuehn, Markus H.; Alward, Wallace L. M. (2009): Primary open-angle glaucoma. In *The New England journal of medicine* 360 (11), pp. 1113–1124. DOI: 10.1056/NEJMra0804630.

Leask, Andrew; Abraham, David J. (2004): TGF-beta signaling and the fibrotic response. In *Federation of American Societies for Experimental Biology* 18 (7), pp. 816–827. DOI: 10.1096/fj.03-1273rev.

Lei, Yuan; Song, Maomao; Wu, Jihong; Xing, Chao; Sun, Xinghuai (2016): eNOS Activity in CAV1 Knockout Mouse Eyes. In *Investigative ophthalmology & visual science* 57 (6), pp. 2805–2813. DOI: 10.1167/iovs.15-18841.

Lei, Yuan; Zhang, Xuejin; Song, Maomao; Wu, Jihong; Sun, Xinghuai (2015): Aqueous Humor Outflow Physiology in NOS3 Knockout Mice. In *Investigative ophthalmology & visual science* 56 (8), pp. 4891–4898. DOI: 10.1167/iovs.15-16564.

Logan, Joanne F. J.; Chakravarthy, Usha; Hughes, Anne E.; Patterson, Chris C.; Jackson, Jonathan A.; Rankin, Simon J. A. (2005): Evidence for association of endothelial nitric oxide synthase gene in subjects with glaucoma and a history of

migraine. In *Investigative ophthalmology & visual science* 46 (9), pp. 3221–3226. DOI: 10.1167/iovs.05-0368.

Luna, Coralia; Li, Guorong; Qiu, Jianming; Epstein, David L.; Gonzalez, Pedro (2011): Cross-talk between miR-29 and transforming growth factor-betas in trabecular meshwork cells. In *Investigative ophthalmology & visual science* 52 (6), pp. 3567–3572. DOI: 10.1167/iovs.10-6448.

Lütjen-Drecoll, E.; Shimizu, T.; Rohrbach, M.; Rohen, J. W. (1986): Quantitative analysis of ‘plaque material’ in the inner- and outer wall of Schlemm's canal in normal- and glaucomatous eyes. In *Experimental eye research* 42 (5), pp. 443–455. DOI: 10.1016/0014-4835(86)90004-7.

Mattapallil, Mary J.; Wawrousek, Eric F.; Chan, Chi-Chao; Zhao, Hui; Roychoudhury, Jayeeta; Ferguson, Thomas A.; Caspi, Rachel R. (2012): The Rd8 mutation of the Crb1 gene is present in vendor lines of C57BL/6N mice and embryonic stem cells, and confounds ocular induced mutant phenotypes. In *Investigative ophthalmology & visual science* 53 (6), pp. 2921–2927. DOI: 10.1167/iovs.12-9662.

Meister, Gunter; Landthaler, Marcus; Dorsett, Yair; Tuschl, Thomas (2004): Sequence-specific inhibition of microRNA- and siRNA-induced RNA silencing. In *RNA* 10 (3), pp. 544–550. DOI: 10.1261/rna.5235104.

Michel, J. B.; Feron, O.; Sase, K.; Prabhakar, P.; Michel, T. (1997): Caveolin versus calmodulin. Counterbalancing allosteric modulators of endothelial nitric oxide synthase. In *The Journal of Biological Chemistry.* 272 (41), pp. 25907–25912. DOI: 10.1074/jbc.272.41.25907.

Mietzner, Raphael; Breunig, Miriam (2019): Causative glaucoma treatment. Promising targets and delivery systems. In *Drug discovery today* 24 (8), pp. 1606–1613. DOI: 10.1016/j.drudis.2019.03.017.

Min, Seong Hee; Lee, Tong-Il; Chung, Yun Seok; Kim, Hwang Ki (2006): Transforming growth factor-beta levels in human aqueous humor of glaucomatous, diabetic and uveitic eyes. In *Korean journal of ophthalmology: KJO* 20 (3), pp. 162–165. DOI: 10.3341/kjo.2006.20.3.162.

Nathanson, J. A.; McKee, M. (1995a): Alterations of ocular nitric oxide synthase in human glaucoma. In *Investigative ophthalmology & visual science* 36 (9), pp. 1774–1784.

Nathanson, J. A.; McKee, M. (1995b): Identification of an extensive system of nitric oxide-producing cells in the ciliary muscle and outflow pathway of the human eye. In *Investigative ophthalmology & visual science* 36 (9), pp. 1765–1773.

NikhalaShree, Sampath; Karthikkeyan, Gayathree; George, Ronnie; Shantha, Balekudaru; Vijaya, Lingam; Ratra, Vineet et al. (2019): Lowered Decorin With Aberrant Extracellular Matrix Remodeling in Aqueous Humor and Tenon's Tissue From Primary Glaucoma Patients. In *Investigative ophthalmology & visual science* 60 (14), p. 4661. DOI: 10.1167/iovs.19-27091.

Ochiai, Y.; Ochiai, H. (2002): Higher Concentration of Transforming Growth Factor-β in Aqueous Humor of Glaucomatous Eyes and Diabetic Eyes. In *Japanese Journal of Ophthalmology* 46 (3), pp. 249–253. DOI: 10.1016/s0021-5155(01)00523-8.

Overby, Darryl R.; Zhou, Enhua H.; Vargas-Pinto, Rocio; Pedrigi, Ryan M.; Fuchshofer, Rudolf; Braakman, Sietse T. et al. (2014): Altered mechanobiology of Schlemm's canal endothelial cells in glaucoma. In *Proceedings of the National Academy of Sciences of the United States of America* 111 (38), pp. 13876–13881. DOI: 10.1073/pnas.1410602111.

Ozcan, Altan Atakan; Ozdemir, Nusret; Canataroglu, Abdullah (2004): The aqueous levels of TGF-beta2 in patients with glaucoma. In *International ophthalmology* 25 (1), pp. 19–22. DOI: 10.1023/b:inte.0000018524.48581.79.

Perkumas, K. M.; Stamer, W. D. (2012): Protein markers and differentiation in culture for Schlemm’s canal endothelial cells. In *Experimental eye research* 96 (1), pp. 82–87. DOI: 10.1016/j.exer.2011.12.017.

Picht, G.; Welge-Luessen, U.; Grehn, F.; Lütjen-Drecoll, E. (2001): Transforming growth factor β2 levels in the aqueous humor in different types of glaucoma and the relation to filtering bleb development. In *Graefe's Arch Clin Exp Ophthalmol* 239 (3), pp. 199–207. DOI: 10.1007/s004170000252.

Pritchard, K. A.; Ackerman, A. W.; Gross, E. R.; Stepp, D. W.; Shi, Y.; Fontana, J. T. et al. (2001): Heat shock protein 90 mediates the balance of nitric oxide and superoxide anion from endothelial nitric-oxide synthase. In *The Journal of Biological Chemistry* 276 (21), pp. 17621–17624. DOI: 10.1074/jbc.C100084200.

Quigley, H. A. (1996): Number of people with glaucoma worldwide. In *British Journal of Ophthalmology* 80 (5), pp. 389–393. DOI: 10.1136/bjo.80.5.389.

Quigley, H. A. (2011): Glaucoma. In *Lancet* (377), pp. 1367–1377.

Reinehr, Sabrina; Koch, Dennis; Weiss, Maximilian; Froemel, Franziska; Voss, Christina; Dick, H. Burkhard et al. (2019): Loss of retinal ganglion cells in a new genetic mouse model for primary open-angle glaucoma. In *Journal of cellular and molecular medicine. DOI:* 10.1111/jcmm.14433.

Resnikoff, Serge; Pascolini, Donatella; Etya'ale, Daniel; Kocur, Ivo; Pararajasegaram, Ramachandra; Pokharel, Gopal P., Mariotti, Silvio P. (2004): Global data on visual impairment in the year 2002. In *Bulletin of the World Health Organization* (82), pp. 844–851, checked on 8/17/2020.

Rippe, Catarina; Blimline, Mark; Magerko, Katherine A.; Lawson, Brooke R.; LaRocca, Thomas J.; Donato, Anthony J.; Seals, Douglas R. (2012): MicroRNA changes in human arterial endothelial cells with senescence. Relation to apoptosis, eNOS and inflammation. In *Experimental gerontology* 47 (1), pp. 45–51. DOI: 10.1016/j.exger.2011.10.004.

Rohen, J. W.; Lütjen-Drecoll, E.; Flügel, C.; Meyer, M.; Grierson, I. (1993): Ultrastructure of the Trabecular Meshwork 10in Untreated Cases of Primary Open-Angle Glaucoma (POAG). In *Experimental eye research* 56 (6), pp. 683–692. DOI: 10.1006/exer.1993.1085.

Sato, S.; Nagaoka, T.; Hasegawa, M.; Tamatani, T.; Nakanishi, T.; Takigawa, M.; Takehara, K. (2000): Serum levels of connective tissue growth factor are elevated in patients with systemic sclerosis. Association with extent of skin sclerosis and severity of pulmonary fibrosis. In *The Journal of rheumatology* 27 (1), pp. 149–154.

Schneemann, Andrea; Dijkstra, Berlinde G.; van den Berg, Thomas J.; Kamphuis, Willem; Hoyng, Philip F. J. (2002): Nitric oxide/guanylate cyclase pathways and flow in anterior segment perfusion. In *Graefe's archive for clinical and experimental ophthalmology* 240 (11), pp. 936–941. DOI: 10.1007/s00417-002-0559-7.

Simon, Michelle M.; Greenaway, Simon; White, Jacqueline K.; Fuchs, Helmut; Gailus-Durner, Valérie; Wells, Sara et al. (2013): A comparative phenotypic and genomic analysis of C57BL/6J and C57BL/6N mouse strains. In *Genome biology* 14 (7), R82. DOI: 10.1186/gb-2013-14-7-r82.

Sriram, Krishna; Laughlin, Justin G.; Rangamani, Padmini; Tartakovsky, Daniel M. (2016): Shear-Induced Nitric Oxide Production by Endothelial Cells. In *Biophysical journal* 111 (1), pp. 208–221. DOI: 10.1016/j.bpj.2016.05.034.

Stack, Trevor; Vahabikashi, Amir; Johnson, Mark; Scott, Evan (2018): Modulation of Schlemm's canal endothelial cell stiffness via latrunculin loaded block copolymer micelles. In *Journal of biomedical materials research. Part A* 106 (7), pp. 1771–1779. DOI: 10.1002/jbm.a.36376.

Stamer, D. W.; Roberts, B. C.; Epstein, D. L.; Allingham, R. R. (2000): Isolation of primary open-angle glaucomatous trabecular meshwork cells from whole eye tissue. In *Current eye research* 20 (5), pp. 347–350.

Stamer, W. D.; Roberts, B. C.; Howell, D. N.; Epstein, D. L. (1998): Isolation, culture, and characterization of endothelial cells from Schlemm's canal. In *Investigative ophthalmology & visual science* 39 (10), pp. 1804–1812.

Stamer, W. D.; Seftor, R. E.; Williams, S. K.; Samaha, H. A.; Snyder, R. W. (1995): Isolation and culture of human trabecular meshwork cells by extracellular matrix digestion. In *Current eye research* 14 (7), pp. 611–617. DOI: 10.3109/02713689508998409.

Stamer, W. Daniel; Braakman, Sietse T.; Zhou, Enhua H.; Ethier, C. Ross; Fredberg, Jeffrey J.; Overby, Darryl R.; Johnson, Mark (2015): Biomechanics of Schlemm's canal endothelium and intraocular pressure reduction. In *Progress in retinal and eye research* 44, pp. 86–98. DOI: 10.1016/j.preteyeres.2014.08.002.

Stamer, W. Daniel; Lei, Yuan; Boussommier-Calleja, Alexandra; Overby, Darryl R.; Ethier, C. Ross (2011): eNOS, a pressure-dependent regulator of intraocular pressure. In *Investigative ophthalmology & visual science* 52 (13), pp. 9438–9444. DOI: 10.1167/iovs.11-7839.

Suárez, Yajaira; Fernández-Hernando, Carlos; Pober, Jordan S.; Sessa, William C. (2007): Dicer dependent microRNAs regulate gene expression and functions in human endothelial cells. In *Circulation research* 100 (8), pp. 1164–1173. DOI: 10.1161/01.RES.0000265065.26744.17.

Subrizi, Astrid; Del Amo, Eva M.; Korzhikov-Vlakh, Viktor; Tennikova, Tatiana; Ruponen, Marika; Urtti, Arto (2019): Design principles of ocular drug delivery systems.

Importance of drug payload, release rate, and material properties. In *Drug discovery today* 24 (8), pp. 1446–1457. DOI: 10.1016/j.drudis.2019.02.001.

Tham, Yih-Chung; Li, Xiang; Wong, Tien Y.; Quigley, Harry A.; Aung, Tin; Cheng, Ching-Yu (2014): Global prevalence of glaucoma and projections of glaucoma burden through 2040. A systematic review and meta-analysis. In *Ophthalmology* 121 (11), pp. 2081–2090. DOI: 10.1016/j.ophtha.2014.05.013.

Tomarev, Stanislav I.; Wistow, Graeme; Raymond, Vincent; Dubois, Stéphane; Malyukova, Irina (2003): Gene expression profile of the human trabecular meshwork. NEIBank sequence tag analysis. In *Investigative ophthalmology & visual science* 44 (6), pp. 2588–2596. DOI: 10.1167/iovs.02-1099.

Topper, J. N.; Cai, J.; Falb, D.; Gimbrone, M. A. (1996): Identification of vascular endothelial genes differentially responsive to fluid mechanical stimuli. Cyclooxygenase-2, manganese superoxide dismutase, and endothelial cell nitric oxide synthase are selectively up-regulated by steady laminar shear stress. In *Proceedings of the National Academy of Sciences* 93 (19), pp. 10417–10422. DOI: 10.1073/pnas.93.19.10417.

Tripathi, R. C.; Li, J.; Chan, W. F.; Tripathi, B. J. (1994): Aqueous humor in glaucomatous eyes contains an increased level of TGF-beta 2. In *Experimental eye research* 59 (6), pp. 723–727. DOI: 10.1006/exer.1994.1158.

Trivedi, Rupal H.; Nutaitis, Matthew; Vroman, David; Crosson, Craig E. (2011): Influence of race and age on aqueous humor levels of transforming growth factor-beta 2 in glaucomatous and nonglaucomatous eyes. In *Journal of ocular pharmacology and therapeutics* 27 (5), pp. 477–480. DOI: 10.1089/jop.2010.0100.

Tsai, Der-Chong; Hsu, Wen-Ming; Chou, Ching-Kuang; Chen, Shih-Jen; Peng, Chi-Hsien; Chi, Chin-Wen et al. (2002): Significant Variation of the Elevated Nitric Oxide Levels in Aqueous Humor from Patients with Different Types of Glaucoma. In *Ophthalmologica* 216 (5), pp. 346–350. DOI: 10.1159/000066187.

Tunny, T. J.; Richardson, K. A.; Clark, C. V. (1998): Association study of the 5' flanking regions of endothelial-nitric oxide synthase and endothelin-1 genes in familial primary open-angle glaucoma. In *Clinical and experimental pharmacology & physiology* 25 (1), pp. 26–29. DOI: 10.1111/j.1440-1681.1998.tb02138.x.

van Haperen, Rien; Cheng, Caroline; Mees, Barend M.E.; van Deel, Elza; Waard, Monique de; van Damme, Luc C.A. et al. (2003): Functional Expression of Endothelial Nitric Oxide Synthase Fused to Green Fluorescent Protein in Transgenic Mice. In *The American Journal of Pathology* 163 (4), pp. 1677–1686. DOI: 10.1016/s0002-9440(10)63524-9.

Vargas-Pinto, R.; Gong, H.; Vahabikashi, A.; Johnson, M. (2013): The effect of the endothelial cell cortex on atomic force microscopy measurements. In *Biophysical journal* 105 (2), pp. 300–309. DOI: 10.1016/j.bpj.2013.05.034.

Verjans, Robin; Peters, Tim; Beaumont, Francisco Javier; van Leeuwen, Rick; van Herwaarden, Tessa; Verhesen, Wouter et al. (2018): MicroRNA-221/222 Family Counteracts Myocardial Fibrosis in Pressure Overload-Induced Heart Failure. In *Hypertension* 71 (2), pp. 280–288. DOI: 10.1161/HYPERTENSIONAHA.117.10094.

Vermeulen, A.; Robertson, B.; Dalby, A. B.; Marshall, W. S.; Karpilow, J.; Leake, D. et al. (2007): Double-stranded regions are essential design components of potent inhibitors of RISC function. In *RNA* 13 (5), pp. 723–730. DOI: 10.1261/rna.448107.

Wahlsten, Douglas; Bachmanov, Alexander; Finn, Deborah A.; Crabbe, John C. (2006): Stability of inbred mouse strain differences in behavior and brain size between laboratories and across decades. In *Proceedings of the National Academy of Sciences* 103 (44), pp. 16364–16369. DOI: 10.1073/pnas.0605342103.

Wang, J.; Hill, W. G.; Charlesworth, D.; Charlesworth, B. (1999): Dynamics of inbreeding depression due to deleterious mutations in small populations. Mutation parameters and inbreeding rate. In *Genetical research* 74 (2), pp. 165–178. DOI: 10.1017/s0016672399003900.

Wienholds, Erno; Plasterk, Ronald H. A. (2005): MicroRNA function in animal development. In *FEBS letters* 579 (26), pp. 5911–5922. DOI: 10.1016/j.febslet.2005.07.070.

Wordinger, Robert J.; Fleenor, Debra L.; Hellberg, Peggy E.; Pang, Iok-Hou; Tovar, Tara O.; Zode, Gulab S. et al. (2007): Effects of TGF-beta2, BMP-4, and gremlin in the trabecular meshwork. Implications for glaucoma. In *Investigative ophthalmology & visual science* 48 (3), pp. 1191–1200. DOI: 10.1167/iovs.06-0296.

Yamamoto, Toshiyuki; Sawada, Yasuyuki; Katayama, Ichiro; Nishioka, Kiyoshi (2005): Nodular scleroderma. Increased expression of connective tissue growth factor. In *Dermatology (Basel, Switzerland)* 211 (3), pp. 218–223. DOI: 10.1159/000087015.

Yu, Jun; Bergaya, Sonia; Murata, Takahisa; Alp, Ilkay F.; Bauer, Michael P.; Lin, Michelle I. et al. (2006): Direct evidence for the role of caveolin-1 and caveolae in mechanotransduction and remodeling of blood vessels. In *The Journal of clinical investigation* 116 (5), pp. 1284–1291. DOI: 10.1172/JCI27100.

Zhou, E. H.; Krishnan, R.; Stamer, W. D.; Perkumas, K. M.; Rajendran, K.; Nabhan, J. F. et al. (2012): Mechanical responsiveness of the endothelial cell of Schlemm's canal. Scope, variability and its potential role in controlling aqueous humour outflow. In *Journal of the Royal Society, Interface* 9 (71), pp. 1144–1155. DOI: 10.1098/rsif.2011.0733.

8 Figures

9 Tables

10 Abbreviations

abbreviation	meaning
3’-UTR	3-prime untranslated region
AFM	atomic force microscopy
AH	aqueous humor
AP	alkaline phosphatase
AP	aqueous plexus
APS	ammonium persulfate
AuNP	gold-core nanoparticle
BL6	Black6/J
BMP-4	bone morphogenic protein-4
bp	base pair
BSA	bovine serum albumin
c(t)	cycle threshold
CA	California
cDNA	complementary deoxyribonucleic acid
CI	ciliary body
CO	cornea
CO	Colorado
CTGF	Connective Tissue Growth Factor
CWFG	cold water fish gelatine
DAPI	4’,6-diamidino-2-phenylindole
DCN	decorin
DETA-NO	diethylenetriamine/nitric oxide adduct
DNA	deoxyribonucleic acid
DTT	dithiothreitol
EBM-2	endothelial cell basal medium-2
EGM-2	endothelial cell growth medium-2
EM	electron microscopy
eNOS	endothelial nitric oxide synthase
ets-1	V-ets erythroblastosis virus E26 oncogene homolog-1
fwd	forward
GFAP	glial fibrillary acidic protein
GS	glutamine synthetase
HA	hyaluronan acid
HA-AuNP	hyaluronan acid coated, gold -core nanoparticle
HRP	horseradish peroxidase
HUVEC	human umbilical vein endothelial cell
ICP-MS	inductively coupled plasma mass spectroscopy
iNOS	inducible nitric oxide synthase
IOP	intraocular pressure
IR	iris
JCT	juxtacanalicular tissue
kDa	kilodalton
KO	knockout
LE	lens
L-NAME	N-nitro-L-arginine methyl ester hydrochloride
MA	Massachusetts
min	minute
miRNA	micro ribonucleic acid
ml	milliliter

mM	millimolar
mmHg	millimeter of mercury
MN	Minnesota
MO	Missouri
MP	milk powder
mRNA	messenger ribonucleic acid
µCI	microcurie
µl	microliter
µM	micromolar
n/a	not applicable
na	not available
NC	North Carolina
nd	not detectable
NJ	New Jersey
nm	nanometer
nM	nanomolar
nNOS	neuronal nitric oxide synthase
NO	nitric oxide
NOS	nitric oxide synthase
NP	nanoparticle
ns	not statistically significant
NY	New York
OR	Oregon
PA	Pennsylvania
PBS	phosphate buffered saline
PCR	polymerase chain reaction
PFA	paraformaldehyde
Php	phosphate buffer
POAG	Primary Open Angle Glaucoma
ppb	parts per billion
PVDF	polyvinylidene difluoride
rev	reverse
RGCs	retinal ganglion cells
RISC	RNA-induced silencing complex
RNA	ribonucleic acid
RPM	reads per million
RT	room temperature
RT	reverse transcriptase
RT-qPCR	quantitative, real-time polymerase chain reaction
SC	Schlemm’s Canal
SDS	sodium dodecyl sulfate
sec	second
SEM	standard error of the mean
Ser	serine
siRNA	small interfering ribonucleic acid
SNAP	S-nitroso-N-acetyl penicillamine
TEM	transmission electron microscopy
TEMED	tetramethylethylenediamine
TG	transgenic
TGF-β	Transforming Growth Factor-β
TGF-β2	Transforming Growth Factor-β2
Thr	threonine
TM	trabecular meshwork
TX	Texas

UK	United Kingdom
USA	United States of America
UV	ultraviolet
V	voltage
VI	Virginia
VIM	vimentin
WA	Washington
WI	Wisconsin
WT	wildtype

11 Acknowledgement

Mein Dank gilt Prof. Dr. Ernst Tamm für die Möglichkeit, meine Doktorarbeit an seinem Lehrstuhl durchführen zu dürfen. Außerdem möchte ich Ihnen für die Übernahme des Vorsitzes bei meiner Promotionsprüfung danken.

Ich danke Prof. Dr. Miriam Breunig für die Übernahme des Zweitgutachtens sowie Prof. Dr. Frank Schweda und Prof. Dr. Stephan Schneuwly für die Übernahme des Amts des Drittprüfers bzw. des Ersatzprüfers. Meinen Mentoren Prof. Dr. Mark Johnson und Prof. Dr. Markus Kretz danke ich für die inhaltliche Betreuung meiner Doktorarbeit.

Mein herzlichster Dank geht an Prof. Dr. Rudolf Fuchshofer, der mich während der vergangenen vier Jahre hervorragend betreut und das Erstgutachten für diese Arbeit übernommen hat. Vielen Dank für all die Antworten auf meine Fragen sowie die Unterstützung bei der Erstellung der schriftlichen Arbeit: alle kommenden Chefs werden sich an dir messen lassen müssen! Du hast mich aber nicht nur beruflich beeinflusst, dein Einfluss hat mich auch persönlich geprägt und beim Erwachsen werden begleitet. Du bist der beste Doktorvater, den ich mir wünschen konnte!

Mein besonderer Dank gilt Ramona Pawlak, die mich bereits seit ihrer Masterarbeit begleitet. Mit ihr die AG Fuchshofer zu rocken, hat großen Spaß gemacht! Dass man immer und bedingungslos auf sie zählen kann, ist ein unschätzbares Gut. Danke dir dafür!

Des Weiteren möchte ich Andrea Dillinger danken, die mir wiederum seit meiner Masterarbeit mütterlich zur Seite stand. Ihrem Vorbild nachzustreben hat mir einige Mühe bereitet, aber auch viel Inspiration geliefert. Danke!

Außerdem möchte ich der gesamten Sammlung danken. Ihr wart mir über all die Jahre ein kollegialer und freundschaftlicher Haufen, der die Höhen und Tiefen des Laboralltags begleitet, abgefangen oder gepuscht hat, wie es gerade nötig war. Ohne Sabrina Schmitt, Christina Bielmeier, Kristina Elsner, Johanna Heimbucher, Reza Naghibi und Sabrina Habel wäre die Zeit meiner Promotion nicht halb so schön gewesen…

Ohne die Unterstützung von Silvia Babl, Angelika Pach, Margit Schimmel, Elke Stauber, Eva Wirkert und Renate Liebl wäre wiederum meine Arbeit nicht halb so gut gelungen. Eure Expertise ist unentbehrlich! Vielen Dank dafür!

Mein Dank gilt auch allen weiteren Lehrstuhlmitgliedern, den Präparatoren und Post Docs sowie Miriam Breunig, Tobias Sonntag, Raphael Mietzner, Jo Wegener und Christian Kade für die Zusammenarbeit im Nano-Projekt.

Von ganzem Herzen danke ich auch meinen Eltern, die mir diesen Weg ermöglicht und mir immer zur Seite gestanden haben. Meinem Mann Adrian gebührt besonderer Dank für das geduldige Ertragen meiner stressbedingten Launen und der selbstauferlegten Arbeitszeiten. Danke für deinen bedingungslosen Rückhalt! Ich liebe dich, Mann von Frau Doktor!